AN ABSTRACT OF THE THESIS OF

Engelene t. H. Chrysostom for the degree of Doctor of Philosophy in Chemistry presented on May 2, 2001. Title: Applications of High Resolution Coherent Anti-Stokes Raman Scattering Spectroscopy.

Abstract approved:

Signature redacted for privacy.

Joseph W. Nibler

The high resolution Coherent Anti-Stokes Raman spectrometer at OSU has been used to investigate the ν_1 symmetric stretching mode of sulfur trioxide and its ^{32}S, ^{34}S, ^{16}O, ^{18}O isotopomers. Q-branch structure of this mode was observed at 0.001 cm^{-1} resolution and a complex band structure was seen for the first time. The modeling of this has required consideration of a subtle combination of Fermi resonance and indirect Coriolis interactions with nearby hidden states; $2\nu_4(\ell = 0,\pm2)$, $\nu_2+\nu_4(\ell = \pm1)$, and $2\nu_2(\ell = 0)$ as well as direct coupling between ν_1 and $2\nu_4$ $(\ell = \pm2)$. The analysis of the perturbed ν_1 spectrum was made possible by locating some of these states via concurrent infrared hot-band studies in a collaboration with Pacific Northwest National Laboratories. Details are presented in this thesis and resultant molecular parameters for $^{32}S^{16}O_3$ include: $\nu_1 = 1064.59(1)$ cm^{-1}; $\alpha_1^{B} = 0.000818(2)$ cm^{-1}; $\alpha_1^{C} = 0.000329(5)$ cm^{-1}; $r_e= 1.41768(12)$ Å.

In a second application of high-resolution CARS spectroscopy, the linewidths of the Q-branch of the ν_2 (C≡C symmetric stretching) mode of acetylene were investigated.

The line broadening and shifts for odd lines J = 7 - 15 of the Q-branch in the pressure range of 5 to 160 Torr were determined. It was found that the precision of these measurements was limited due to saturation broadening at low pressures. However at higher pressures there was a characteristic linear dependence of linewidth with pressure and hence the broadening coefficients in the range of (122 – 166) x 10^{-3} cm^{-1}/amagat were determined. These results have been published in Journal of Raman Spectroscopy, vol. 31, 719-723 (2000).

Applications of High Resolution Coherent Anti-Stokes Raman Scattering Spectroscopy

by

Engelene t. H. Chrysostom

A THESIS

Submitted to

Oregon State University

in partial fulfillment of
the requirements for the
degree of

Doctor of Philosophy

Presented May 2, 2001
Commencement June 2001

Doctor of Philosophy thesis of Engelene t. H. Chrysostom presented on May 2, 2001

APPROVED:

Signature redacted for privacy.
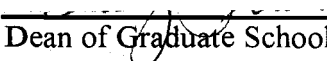
Major Professor, representing Chemistry

Signature redacted for privacy.

Chair of Department of Chemistry

Signature redacted for privacy.

Dean of Graduate School

I understand that my thesis will become part of the permanent collection of Oregon State University libraries. My signature below authorizes release of my thesis to any reader upon request.

Signature redacted for privacy.

Engelene t. H. Chrysostom, Author

ACKNOWLEDGEMENTS

cultures with a myriad of personalities into a cohesive team without us losing our individualities. Joe, your kindness will always be remembered.

The Nibler group, past and present, a wonderful group of guys whose teasing over the years taught me how to laugh at myself. I am grateful to all the former members, however in particular I would like to express my gratitude to Matthias, Marshall, and Darren. Of course not to be forgotten are the current members, Nicu, Tony, Jeff and Stéphanie. Your company, support and encouragement made the whole PhD process very enjoyable.

Throughout my career at Oregon State University I had the unique opportunity to collaborate with many different scientists. Each one was unique and I learned a lot from them all. Thank you Drs. Blake, Maki, Smirnov, Vereschagin and Weber.

I wish to also thank the Department of Chemistry and all its members for the financial support over the years and making my stay at OSU a pleasant and certainly memorable experience.

Thanks to my very special friends Julia, Sherry, and Annabelle. Last and by no means least I want to thank my fiancé Georg for his support in particular over the last couple of months.

TABLE OF CONTENTS

LIST OF FIGURES

LIST OF FIGURES (continued)

LIST OF TABLES

LIST OF APPENDICES

LIST OF APPENDIX TABLES

Dedication

This thesis is dedicated to my grandparents, Gerhard ter Heersche, Johanna Hendrina ter Heersche Gunneman, Audrich Chrysostom and Phredestina Hernandez Chrysostom.

It is also dedicated to a special friend and colleague, Nicolae "Nicu" Vulpanovici. Your courageous life, though short, has touched us all. You will always be remembered.

1. INTRODUCTION

1.1 Overview of Thesis

Coherent anti-Stokes Raman Scattering spectroscopy (CARS) has been actively developed both theoretically (*1-2*) and experimentally (*3-8*) over the last two decades. The technique has proven quite powerful, and a number of applications have been made in the CARS facility at Oregon State University. In this thesis, two applications will be presented that emphasize the aspect of high resolution CARS spectroscopy.

In the first of these, CARS has been used to investigate the ν_1 symmetric stretching mode of the various isotopomers of sulfur trioxide ($^{32}S^{16}O_3$, $^{32}S^{18}O_3$, $^{34}S^{16}O_3$ and $^{34}S^{18}O_3$). This infrared inactive vibration had been examined previously by conventional Raman spectroscopy (*9*) but only at 5 cm^{-1} resolution, with no Q-branch structure discernable. In this work, this band was examined using CARS at an instrumental resolution of 0.001cm^{-1}(*10*), revealing a remarkably complex spectrum whose explanation has proven a challenging task.

As part of this effort to understand the spectra of SO_3, collaboration with Pacific Northwest National Laboratories was undertaken, and we were able to investigate at high resolution the ($\nu_1 + \nu_2$) infrared active mode. This yielded molecular parameters for this combination band. Using this information along with the parameters from the

complete analysis of the ν_2, ν_3, and ν_4 modes (done by others in our laboratory), we were able to extract accurate molecular parameters for ν_1 from the CARS data analysis.

CARS is also being increasingly used to probe *in situ* gases in hostile combusting media *(11-12)*, discharge media, and plasmas *(13, 8)*. It is often employed to deduce the local temperature and concentration of gases *(14)*. In order to correctly interpret the experimental results in such diagnostic applications of CARS, there is a need for accurate linewidth data *(15)* and a proper understanding of the factors that influence lineshapes, such as collisional, Doppler, and instrumental broadening. Thus the second application of high resolution CARS, in chapter 5 of this thesis, involves the use of CARS in a study of linewidths of acetylene. There is presented an investigation of linewidths and particularly of the collisional broadening of the ν_2 C≡C stretching mode of the Q-branch of acetylene. The results of this study have already been published *(16)*; this thesis section is a slightly expanded version of the article.

1.2 Brief Overview of CARS Spectroscopy

The field of Raman spectroscopy began with the discovery of the Raman effect in 1928 by the Indian physicist, Sir Chandrasekharan V. Raman (17). The Raman effect can be described as the inelastic scattering of incident light by a medium, as was first predicted by A. Smekal in 1923 *(18)*. Raman scattering is very weak so its application was essentially limited to studies of relatively pure liquids and solids of high number density. It was not until the development of lasers that the field began to rapidly expand due to the increased brightness and power of the excitation sources. Today, using

continuous wave (cw) lasers and sensitive multichannel detectors, Raman spectroscopy has become a more common tool, offering distinct advantages over IR methods in some cases.

The advent of **pulsed** lasers with extremely high peak powers allowed observation of effects due to the nonlinear response of molecules to high optical fields *(1)*. In these nonlinear optical interactions, the scattering process is coherent and can be viewed as a collective, phase-correlated property of a molecular ensemble. Scattering derives from an induced dielectric polarization of the bulk medium (dipole moment per unit volume) that is related to the field via the molecular susceptibility $\chi^{(m)}$ *(19)*. The polarization (*P*) induced can be expressed as a power series in the electric field strength E,

$$P = \chi^{(1)}\,\mathrm{E} + \chi^{(2)}\,\mathrm{EE} + \chi^{(3)}\,\mathrm{EEE} + \ldots. \qquad (1.1)$$

where the $\chi^{(m)}$ are tensors of rank (m+1). These bulk susceptibility terms can be connected to the microscopic properties of the molecules such as Raman cross sections *(1)*. The first susceptibility term gives rise to linear, spontaneous Raman scattering and the second to hyper-Raleigh and hyper-Raman scattering. $\chi^{(2)}$ is also responsible for frequency mixing and doubling processes in certain crystals. The third term $\chi^{(3)}$ is the key term for this work since it is responsible for CARS. For completeness it should be noted that this term is also responsible for Stimulated Raman Scattering SRS (of which Stimulated Raman Gain Scattering (SRGS) and Stimulated Raman Loss Scattering (SRLS) are two special variants) and Photo Acoustic Raman Scattering (PARS). In

these cases, energy is actually transferred to the molecule and the process is said to be non-parametric.

1.3 Theory of CARS Spectroscopy

CARS is a four-wave mixing process which is termed parametric since the molecule serves only to mix the light waves and does not take up energy. In it three incident frequencies, two at a pump frequency ω_1 and one at a Stokes frequency ω_2, are mixed in a sample to produce a new coherent beam at the anti-Stokes frequency, ω_3, where $\omega_3 = 2\omega_1 - \omega_2$. Figure 1-1 represents the CARS nonlinear mixing process.
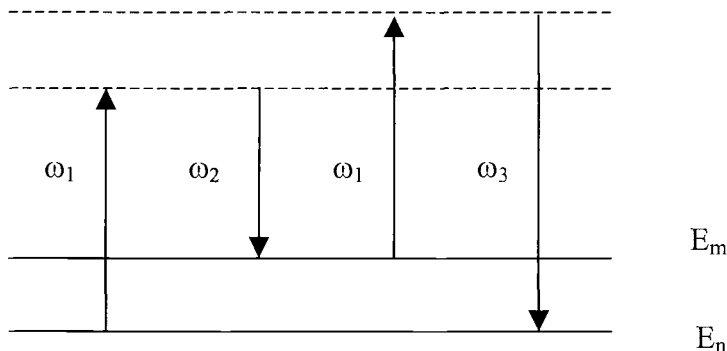
Figure 1-1 Energy level diagram representing the CARS nonlinear mixing process.

Dashed and solid lines represent virtual and real states respectively. Usually the pump frequency is kept constant and the Stokes frequency is scanned. At resonance, the difference between the pump and Stokes beams, $\omega_1-\omega_2$, is equal to a transition frequency of the molecule, ω_{mn}, and the CARS signal has a maximum intensity. Thus

by scanning the frequency of the Stokes beam and monitoring the intensity of the CARS signal, information about the energy levels of the molecule can be determined.

The intensity of the CARS signal, I_3, is given by the following relation,

$$I_3 \propto \left|\chi^{(3)}\right|^2 I_1^2 I_2 \left(\frac{\sin\left(\Delta k \ell/2\right)}{\Delta k \ell/2}\right)^2 \qquad (1.2)$$

where I_1 and I_2 are the intensities of the pump and Stokes beams and ℓ is the interaction length. Δk is the absolute value of the phase mismatch vector and is determined using the relationship, $\Delta k = 2k_1 - k_2 - k_3$. k_1, k_2 and k_3 are the wave vectors of the pump, Stokes and CARS signal beams and their magnitudes are given by the following relation, $k = 2\pi\omega/n$ where ω is the frequency of the light beam and n is the index of refraction of the medium. The phase matching condition means that the incident beams should be aligned such that momentum is conserved so that efficient growth (coherent generation) of the CARS signal can occur. In our experiment the so-called folded BOXCARS *(20)* setup was used and Figure 1-2 shows the phase matching conditions employed here.
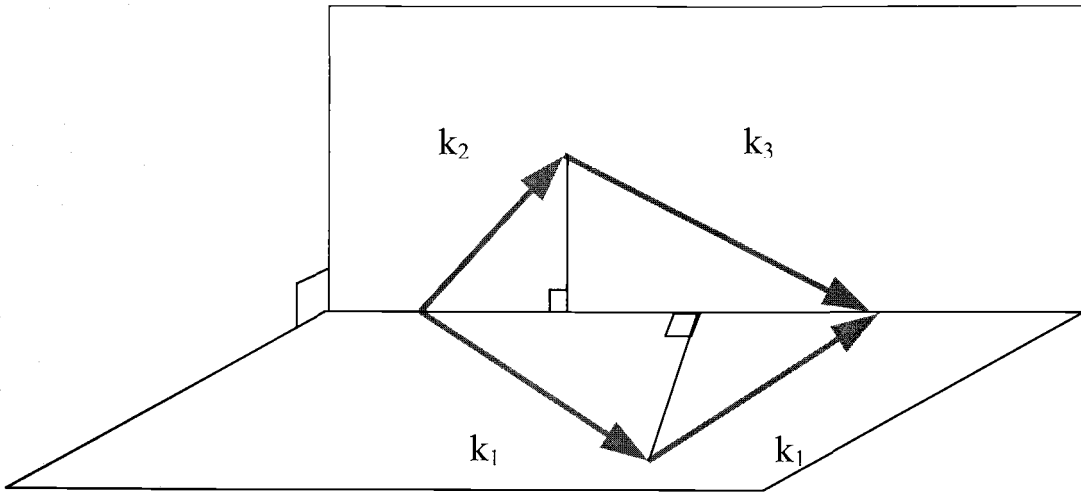
Figure 1-2 Diagram representing the folded BOXCARS phase matching geometry.

The advantages of this folded BOXCARS setup are that the signal generation occurs only at the focus of the beams (i.e. a well defined region), there is a low level of nonresonant background (χ_{nr}) contribution to the CARS signal, and, most important, the latter is spatially separated from the input beams.

The $\chi^{(3)}$ term, which is responsible for the CARS process, can be represented by the following relation,

$$\chi^{(3)} \propto \frac{N_n - N_m}{\omega_{mn} - (\omega_1 - \omega_2) - i\Gamma_{mn}} \left(\frac{d\sigma}{d\Omega} \right) + \chi_{nr} \qquad (1.3)$$

where $N_n - N_m$ is the population difference between lower and upper states of the transition; ω_{mn} and Γ_{mn} are the frequency and the damping constant (linewidth) of the transition; $(d\sigma/d\Omega)$ is the Raman cross section of the molecule; χ_{nr} is the nonresonant

contribution to the bulk susceptibility due to distant electronic resonances. Γ_{mn} determines the line shape of a transition and this is discussed further in chapter 5 where the CARS linewidths of acetylene were investigated.

Mention should be made that CARS experiments are not trivial and are very dependent on the reproducible performance of the pump (ω_1) and tunable (ω_2) lasers. Also due to the nonlinear nature of the CARS process, amplitude, frequency, and spatial fluctuations in ω_1 and ω_2 beams can yield substantial shot to shot fluctuations in the CARS signal. The very high peak powers, which are necessary for this effect, can not only cause optical damage of mirrors and other components but can also complicate the spectra obtained due to power saturation and Stark broadening effects. However by far the major complication to CARS spectra is that the quadratic dependence of the CARS signal intensity on $\chi^{(3)}$ (Equation 1.2) leads to interference distortions in the lineshapes due to the cross terms of nearby resonant transitions with each other and with the χ_{nr}. Hence the direct interpretation of observed CARS spectra requires a more involved analysis procedure than in ordinary linear forms of spectroscopy, as will be discussed in chapters 4 and 5.

2. STUDIES ON SULFUR TRIOXIDE

2.1 Introduction

Sulfur trioxide, SO_3, is an important and interesting molecule. It is prepared industrially on a large scale by the catalytic oxidation of sulfur dioxide (SO_2), via the Contact Process, and is the primary intermediate in the production of sulfuric acid. This Contact Process involves passing a mixture of pure dry sulfur dioxide and air over a catalyst of vanadium (V) oxide (V_2O_5) at about 500 °C. The resultant SO_3 product is then dissolved in water to form fuming sulfuric acid (oleum). This is a violent exothermic reaction since SO_3 is a strong Lewis acid and reacts immediately with water (ΔH_{solv} = -880 kJ/mol). Pure SO_3 boils at 44.5 °C and is obtained commercially as a liquid, containing additives to prevent polymerization. It is also available as oleum.

Sulfur trioxide is also produced as a by product in the environment from the combustion of sulfur containing fuels and is often found in the flue gases from coal and oil power plants. Due to its reactivity with water and its long lifetime in the upper stratosphere (a few months), it is considered a significant contributor to acid rain and as such it has become one of the many toxic chemicals that are regulated by the EPA under the national Toxic Release Inventory (TRI).

Aside from its industrial and environmental importance, the study of SO_3 provides a unique opportunity for the investigation of the spectroscopy of a classic example of an oblate symmetric top. In the vapor phase SO_3 exists primarily as the monomer and is planar with D_{3h} symmetry. The vibration-rotation theory of such molecules is well developed *(21-25)* but has not been applied to this simple molecule

due to lack of accurate spectroscopic data. This study serves to fill the aforementioned gap in the body of knowledge, particularly regarding the ν_1 mode of SO_3.

2.2 Physical Properties of Sulfur Trioxide

SO_3 exists in the solid phase in at least three polymorphic states, termed α, β and γ forms *(26)*. γ-SO_3 consists primarily of cyclic trimers with the possible presence of momomeric SO_3. γ-SO_3 has a melting point of 16.8 °C and exists with the monomer in a reversible equilibrium described by the following equation.

$$S_3O_9 \leftrightharpoons 3\ SO_3 \tag{2.1}$$

About twenty percent of liquid SO_3 is made up of the trimer. The equilibrium lies far to the right in the gas phase, however it is worth noting that the presence of the trimer did lead to incorrect assignments of the fundamentals of SO_3 in earlier infrared studies. β-SO_3 consists of polymeric molecules of varying length with a helical chain structure in an asbestos type structure. Its melting point, or rather its depolymerization to liquid SO_3, occurs between 32 - 45 °C. The presence of water in liquid SO_3 initiates the polymerization process to form β-SO_3. α-SO_3 is a polymer like the β-form but in view of its higher melting point of 62 °C and lower vapor pressure, it is probably a higher polymer with a layer structure. *(26-27)*

2.3 Literature Review

As early as the 1930's, infrared and Raman studies were performed on gaseous and liquid SO_3 *(28-29)*. It should be noted that all the studies thus far on SO_3 refer to $^{32}S^{16}O_3$ isotopomer, except for two papers *(30-31)*. Our current investigations have been expanded to include all the other ^{32}S, ^{34}S, ^{16}O, ^{18}O isotopomers of SO_3.

ν_1, A_1', 1065 cm^{-1}

ν_2, A_2'', 497 cm^{-1}

ν_3, E', 1390 cm^{-1} antisymmetric stretch

ν_4, E', 530 cm^{-1} in-plane asym. bend
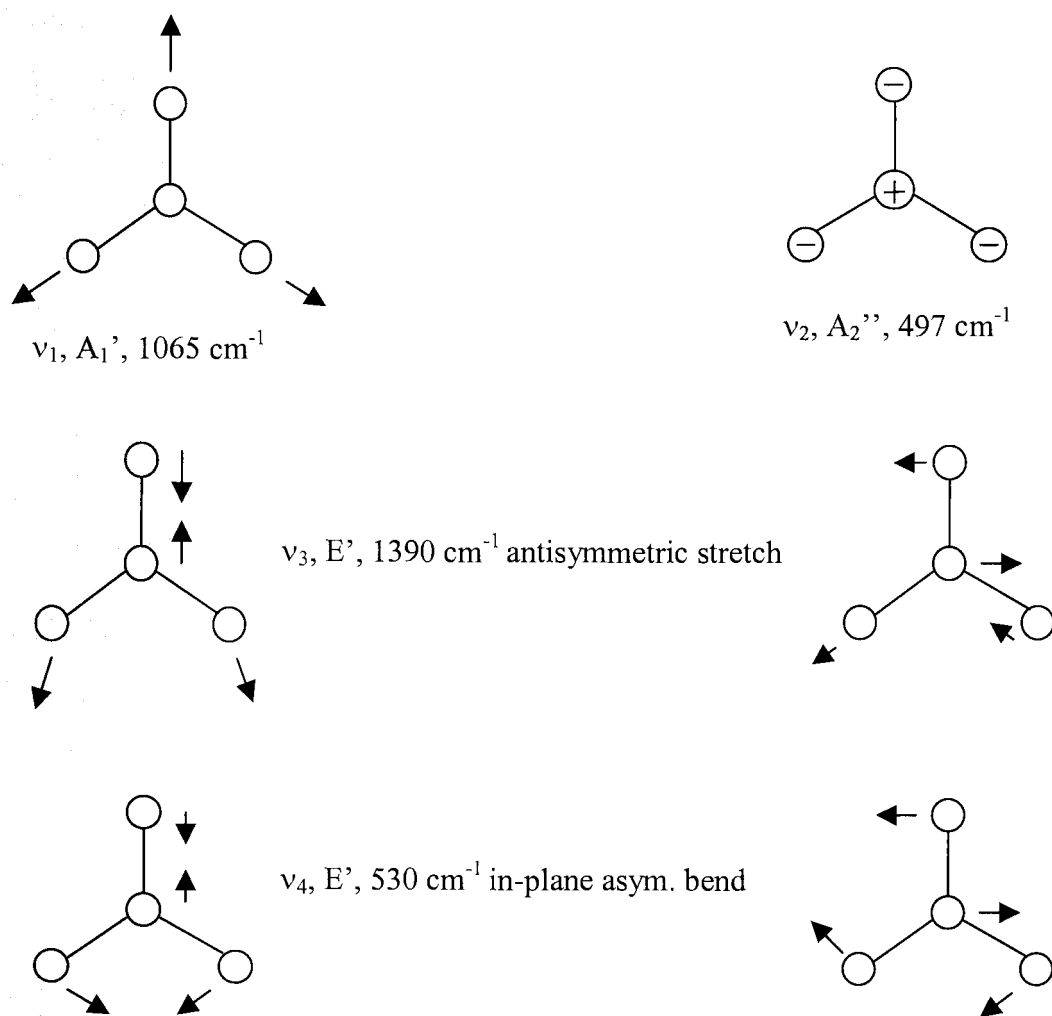
Figure 2-1 Diagram indicating the four vibrational modes of SO_3 and their symmetries.

Gaseous monomeric SO_3, has a planar D_{3h} structure with four vibrational modes, as indicated in Figure 2-1. Of these four vibrational fundamentals, ν_1 (A_1') is Raman active only, ν_2 (A_2'') is infrared active only, and the two degenerate E' modes, ν_3 and ν_4, are both Raman and infrared active.

2.3.1. Infrared Studies of SO_3

SO_3 has been the subject of many infrared studies *(29-32)*. Due to its reactivity and tendency to form trimers (S_3O_9) in the liquid and gas phases *(32-35)* there was some ambiguity in the initial vibrational assignments of ν_2 and ν_4 modes of gaseous monomeric SO_3. In 1930, von Gerding *et al.* *(29)* assigned ν_2 and ν_4 to bands at 530 and 650 cm^{-1} respectively. Further investigations in the early 1960's by Lovejoy *et al.* *(32)*, Stopperka *et al.* *(33)*, and Bent *et al.* *(35)* lead to the assignments of ν_2 and ν_4 to bands at 490 cm^{-1} and 530 cm^{-1} respectively. The band at 650 cm^{-1} was assigned to a trimer vibration. In 1966, Krakow *et al* *(36)* suggested the possibility that maybe the assignment of ν_2 and ν_4 should be interchanged due to the observed band contours. This interpretation found support in 1970, when Thomas *et al.* *(37)*, studied all the IR active modes of SO_3 and proposed that the assignments should be $\nu_2 = 530$ cm^{-1} and $\nu_4= 490$ cm^{-1}. The basis for this reversal of the assignment was the observation of a sharp central Q-branch feature at 530 cm^{-1} and a wide spread of R-branch structure to the high wavenumber side of this feature. These two features were said to be consistent with a parallel band ν_2 rather than a perpendicular band ν_4. The problem of this interpretation was that the 530 cm^{-1} band was observed in Raman spectra of liquid SO_3, suggesting

that this could not be the forbidden mode ν_2. Thomas *et al.(37)* reconciled this difficulty by suggesting that in the liquid phase, molecular distortion might relax the Raman selection rules. In 1973, Kaldor *et al. (38)* resolved the uncertainty in the assignment by performing higher resolution experiments on gaseous SO_3 at lower pressures where neither polymer bands nor intermolecular effects were likely to give rise to false peaks. They also performed some more sophisticated contour band calculations of ν_2 and ν_4, taking into account a strong Coriolis resonance between the two bands and the effects of a Coriolis ℓ-doubling effect in the perpendicular band. They unambiguously determined that the assignments of ν_2 and ν_4 should be 490 cm^{-1} and 530 cm^{-1} respectively. This was later confirmed by a detailed higher resolution (0.005 cm^{-1}) infrared band analysis of ν_2 and ν_4 by Ortigoso *et al.* in 1989 *(39)*.

A number of these experimental gas phase infrared studies had sufficient resolution to yield rovibrational parameters for the ground state of $^{32}S^{16}O_3$. Milne *et al. (40)* examined the ν_3 mode as well as the ν_4 mode of SO_3 as early as 1967 with a spectral resolution of 0.35 cm^{-1}. Kaldor *et al.(41)* in 1973 recorded the $2\nu_3$ and $\nu_3+\nu_4$ bands of SO_3 at 0.03 and 0.04 cm^{-1} resolution respectively. Henfrey *et al. (42)* studied the ν_3 mode at a resolution of 0.01 cm^{-1} in 1983. The highest resolution infrared work performed on SO_3 thus far was the experimental analysis of the ν_2 and ν_4 modes by Ortigoso *et al.(43)*, mentioned above, and this has lead to the most accurate molecular constants for the ground state. These molecular parameters have been used as the initial starting parameters for the improved IR studies being performed in our laboratory.

Relatively little infrared work has been done on the isotopomers of SO_3. One recent IR experimental investigation was performed by Laptev *et al. (31)* in 1998.

These workers observed the ν_1 fundamental in sulfur trioxide induced by symmetry breaking upon ^{18}O substitution; $S^{16}O_2^{18}O$ was observed in the IR spectrum at 1040 cm^{-1}, yielding an isotopic shift of 28 ± 2 cm^{-1} relative to the ν_1 IR inactive mode for $^{32}S^{16}O_3$. In another study infrared spectra of matrix isolated SO$_3$, its polymers and isotopomers were obtained in different rare gas matrices *(30,32,34)*. As expected, the rotational structure is lost in a frozen matrix and the bands collapse to form sharp lines. Unfortunately, while the spectrum is thereby simplified, the matrix transitions are shifted in frequency from the corresponding gas phase frequencies and hence are not representative of the true isolated molecule values. The relative isotopic shift values are expected to be transferable however, and lead to useful predictions of the band origins of the isotopomer transitions.

2.3.2. Raman Studies of SO$_3$

The two earliest Raman spectroscopic investigations of liquid SO$_3$ were done in 1937 by Gerding *et al. (28, 43)*. Walrafen *(44)* also performed some Raman spectral studies on various stoichiometric mole fractions of sulfur trioxide and sulfuric acid compositions (oleums) in 1964. Here assignments were made for the various species present in the vapor phase, such as SO$_3$, its trimers and its complexes with H$_2$SO$_4$.

As mentioned earlier in Chapter 1, the ν_1 mode of gaseous SO$_3$ was studied by S.-Y. Tang *et al.(9)* using conventional Raman spectroscopy. The ν_1 position was determined to be 1065 ± 5 cm^{-1}, with no Q-branch structure discernible at the 5 cm^{-1} resolution used. The other Raman active modes, ν_3 and ν_4, were observed as well.

The pure rotational Raman spectrum of gaseous SO_3 was analyzed by Brassington et al. (45) in 1978 and the rotational constants for the ground state were obtained. These were comparable to results obtained from the vibrational-rotational IR analyses available at that time (36,40). Microwave spectra were also reported, a surprise since a nonpolar molecule such as SO_3 cannot normally be seen by microwave rotational spectroscopy. However a molecule that is rotating rapidly can distort, thereby producing a small dipole moment. Thus, approximately 10 years ago, Meyer et al. (46) used a special microwave Fourier Transform (MWFT) apparatus to obtain such a centrifugally induced pure rotational spectrum of SO_3. These rotational transitions have an intensity that depends on the dipole derivatives and on the displacements in the normal coordinates produced by centrifugal distortion. The theory of these transitions has been discussed at length by Aliev et al. (47) and Watson (48). Aside from the normal selection rule of $\Delta K = 0$ for SO_3 (K is the quantum number for angular momentum about the symmetry axis), an additional selection rule of $\Delta K = \pm 3$ is allowed due to centrifugal distortion. This added selection rule is important since it allows normally "forbidden" transitions to be observed. These give accurate ground state rotational constants, particularly for C, a constant not determined in ordinary vibrational-rotational studies.

SO_3 has also been the subject of several theoretical studies. Ab initio quantum calculations have been performed at different levels of approximation for SO_3, yielding both harmonic (49) and anharmonic (50-51) force fields. In the most recent theoretical study by Martin (57), a fully ab initio quartic force field for SO_3 was calculated and the

results were used to predict several spectroscopic parameters for all of the fundamental modes.

Despite the experimental and theoretical work described above, there exists virtually no good experimental data for the ν_1 mode for $^{32}S^{16}O_3$ or any of the other isotopomers. Since this ν_1 information is absent, no accurate determination of the equilibrium bond length can be made. In this thesis, we have measured the Raman spectra of all the isotopomers of SO_3 and determined the molecular parameters for the ν_1 mode. This has proven an interesting but challenging task, since it has required detailed consideration of subtle aspects of spectroscopy such as symmetry, nuclear spin statistics, Fermi resonance, and direct and indirect Coriolis couplings. The theory for such interactions is presented in the following sections.

2.4 Theory of Oblate Symmetric Tops

An oblate symmetric top such as SO_3 is defined as one in which the three principal moments of inertia are related by the following equation, $I_A = I_B < I_C$. The vibrational-rotational spectrum of such a top can be explained using a simple molecular model in which point masses are assumed to be moving through a potential field provided by the averaged motion of the electrons. The atoms can be thought of as being held together by rather rigid springs giving rise to molecules that can be described mathematically as a semi-rigid bodies*(24)*.

The energy levels of such a model are the eigenvalues of the Schrödinger equation

$$(\hat{H} - E)\Psi = 0 \tag{2.2}$$

where $\hat{H}$ is the quantum mechanical operator for the rotating-vibrating model.

Wilson and Howard *(52)* derived the vibration-rotation Hamiltonian for a semi-rigid top molecule and later it was simplified by Watson *(53)* to the form given below.

$$H = \sum_{\alpha,\beta} \tfrac{1}{2}\mu_{\alpha\beta}\hbar^2 (J_\alpha - \pi_\alpha)(J_\beta - \pi_\beta) + \tfrac{1}{2}\sum_r P_r^2 + V(Q_r) + U \tag{2.3}$$

J_α and J_β are the components of the total angular momentum and P_r and Q_r are momentum and coordinate of the rth normal mode. α and β refer to a summation over x, y, z. There are two kinds of vibration-rotation interaction coefficients appearing as parameters in the Hamiltonian. The first kind occurs in the vector operator π_α and the second kind in the tensor μ, where $\mu_{\alpha\beta}$ are elements that are related to the instantaneous moments of inertia. π_α and π_β are the components of the vibrational angular momentum. U represents a very small, mass–dependent correction to the vibrational potential energy $V(Q_r)$ that can be ignored in further discussions.

The expanded form of the vibrational-rotational Hamiltonian is obtained by expanding $\mu_{\alpha\beta}$ and the potential energy $V(Q_r)$ in powers of the vibrational operators p_r and q_r. These are the dimensionless equivalents of P_r and Q_r which are related by the

following equations, $q_r = \gamma_r^{1/2} Q_r$ and $p_r = P_r / \gamma_r^{1/2}\hbar$, where $\gamma_r = 2\pi c\omega_r / \hbar$ and ω_r is the harmonic frequency of the rth normal mode. The expanded form can be arranged as shown below following the format by Mills *(54)*. Here κ is the Born-Oppenheimer expansion parameter $(m/M)^{1/4}$, $\approx 1/10$, m being the electron mass, and M a typical nuclear mass. The columns in Table 2-1 are arranged in increasing powers of the rotational angular momenta J_α.

Order of Magnitude	Terms in H/hc involving J^0	J^1	J^2
$\kappa^0 v_{vib}$	$\Sigma_r \frac{1}{2}\omega_r(p_r^2 + q_r^2)$	—	—
$\kappa^1 v_{vib}$	$+ \Sigma_{rst}(1/6)\phi_{rst}q_rq_sq_t$	—	—
$\kappa^2 v_{vib}$	$+ \Sigma_{rstu}(1/24)\phi_{rstu}q_rq_sq_tq_u + \Sigma_\alpha B_e^{(\alpha)}[\pi_\alpha^2$	$- 2\pi_\alpha J_\alpha$	$+ J_\alpha^2]$
$\kappa^3 v_{vib}$	$+ \text{quintic anh} + \Sigma_{\alpha\beta r}(\hbar^2/2hc)\mu_{\alpha\beta}^{(r)}q_r[\pi_\alpha\pi_\beta$	$- (\pi_\alpha J_\beta + \pi_\beta J_\alpha)$	$+ J_\alpha J_\beta]$
$\kappa^4 v_{vib}$	$+ \text{sextic anh} + \Sigma_{\alpha\beta rs}(\hbar^2/2hc)\mu_{\alpha\beta}^{(r,s)}q_rq_s[\pi_\alpha\pi_\beta$	$- (\pi_\alpha J_\beta + \pi_\beta J_\alpha)$	$+ J_\alpha J_\beta]$

Table 2-1 The rovibrational Hamitoninan, H/hc, arranged by order of magnitude and power of J.

In this table ϕ_{rst} and ϕ_{rstu} are the cubic and quartic anharmonic force constants represented by the expansion of the potential.

$$V / hc = \frac{1}{2}\sum_r \omega_r q_r^2 + \frac{1}{6}\sum_{rst}\phi_{rst}q_rq_sq_t + \frac{1}{24}\sum_{rst}\phi_{rstu}q_rq_sq_tq_u + ... \qquad (2.4)$$

The vibrational angular momentum is given by

$$\pi_\alpha = \sum_{rs} \zeta_{r,s}^{(\alpha)} Q_r P_s / \hbar = \sum_{rs} \zeta_{r,s}^{(\alpha)} q_r q_s (\omega_s / \omega_r)^{\frac{1}{2}} \qquad (2.5)$$

where $\zeta_{r,s}^{(\alpha)}$ is the Coriolis zeta coupling Q_r to Q_s through rotation about the α axis.

A convenient representation of Table 2-2 by Watson is given below where the terms in the Hamiltonian are written in simplified form using the symbol, $h_{n,m}$ which represents a term in the Hamiltonian involving operators $(q_r, p_r)^n J_\alpha^m$.

Order of Magnitude	Powers of (q_r, p_r) and J_α		
	J^0	J^1	J^2
$\kappa^1 \nu_{vib}$	$+ h_{3,0}$		
$\kappa^0 \nu_{vib}$	$+ h_{2,0}$		
$\kappa^2 \nu_{vib}$	$+ h_{4,0}$	$+ h_{2,1}$	$+ h_{0,2}$
$\kappa^3 \nu_{vib}$	$+ h_{5,0}$	$+ h_{3,1}$	$+ h_{1,2}$
$\kappa^4 \nu_{vib}$	$+ h_{6,0}$	$+ h_{4,1}$	$+ h_{2,2}$

Table 2-2 Terms in the rovibrational Hamiltonian classified by order of magnitude and powers of (q_r, p_r) and J_α.

A simple physical meaning can be assigned to the individual $h_{m,n}$. For example $h_{0,2}$ is the rigid rotor approximation, $h_{1,2}$ and $h_{2,2}$ are the centrifugal distortion operators, $h_{2,1}$ describes Coriolis interaction between rotation and vibration, h_{20} is the harmonic

oscillator operator, and $h_{3,0}$ and $h_{4,0}$ describe the anharmonicity of molecular vibrations. (25).

The energy of vibrational-rotational states can be determined via perturbation theory. The most convenient way to perform the higher-order perturbation treatment of the vibrational-rotational Hamiltonian is based on the method of contact transformations. The method of transformations is based on the replacement of the original vibrational-rotational Hamiltonian by an effective but simpler Hamiltonian. A contact transformation is applied to the complete rovibrational Hamiltonian to obtain a transformed Hamiltonian.

$$\widetilde{H} = U^{-1}HU \qquad (2.6)$$

Here U is unitary such that the harmonic oscillator basis functions are the eigenfunctions of H to the desired degree of approximation. The eigenvalues of $\widetilde{H}$ are the same as those of H. This complete Hamiltonian is transformed using perturbation theory to remove terms, which are vibrationally off-diagonal in the harmonic oscillator basis functions. Then $\widetilde{H}$ is averaged over the appropriate vibrational basis function to obtain the effective rotational Hamiltonian in each vibrational state. This operation corresponds to the adiabatic Born-Oppenheimer separation of vibration from rotation and gives coefficients in the rotational Hamiltonian which show a dependence on the vibrational quantum numbers (such as the rotational constants). This procedure is possible so long as there are no accidental degeneracies (Fermi or Coriolis) between different vibrational states.

2.4.1 Basis Functions

The effective rotational Hamiltonian for an oblate symmetric top in the rigid rotor approximation is given by

$$H_{rot}/hc = C_v J_z^2 + B_v (J_x^2 + J_y^2) + ... \qquad (2.7)$$

where the components of angular momenta are given Cartesian labels according to the convention that z is the molecular axis of symmetry. The eigenvalues given by the zero order effective rotational Hamiltonian are

$$F_v^0(J, k) = C_v k^2 + B_v [J(J+1) - k^2] \qquad (2.8)$$

Here J is the quantum number of total angular momentum, and k is its projection along the molecular z-axis. The values of k are integral values such that $-J \leq k \leq +J$. The quantum number k is the signed component of the angular momentum in the top axis and $K = |k|$. m is the component of J in a space-fixed axis and takes similar values such that $M = |m|$. The energy levels do not depend on m unless in the presence of an electric or magnetic field. The rotational energy levels show a $(2-\delta_{k,0})(2J+1)$-fold degeneracy. The rigid rotor symmetric top rotational wavefunctions are fully specified by the quantum numbers J ,K and M and are written in Dirac notation as |J, K, M> . C_v and B_v are the effective rotational constants.

The zeroth-order vibrational Hamiltonian for a top can be written as,

$$H_{vib}^0 = \sum_r \tfrac{1}{2}(P_r^2 + \lambda_r Q_r^2) \qquad (2.9)$$

Here Q_r and P_r denote the rth normal coordinate and its conjugate momentum, $P_r = -i\hbar\, \partial/\partial Q_r$ and $\tfrac{1}{2}\lambda_r Q_r^2$ are the quadratic terms from the potential V(Q). Since the molecule is a symmetric top, equation 2.9 can be rewritten in terms of nondegenerate (s) and degenerate (t) modes and r is defined as an index over both types of modes. Thus equation 2.9 becomes

$$H_{vib}^0 = \tfrac{1}{2}\sum_s (P_s^2 + \lambda_s Q_s^2) + \tfrac{1}{2}\sum_t [P_{t1}^2 + P_{t2}^2 + \lambda_s (Q_{t1}^2 + Q_{t2}^2)] \qquad (2.10)$$

The eigenvalues of Equation 2.10 gives the zeroth-order vibrational energy levels:

$$G^0(v) = \sum_s \omega_s (v_s + \tfrac{1}{2}) + \sum_t \omega_t (v_t + 1) \qquad (2.11)$$

where ω_s and ω_t are the harmonic vibrational frequencies of the single and degenerate modes of the molecule and v_s and v_t are the vibrational quantum numbers of these modes respectively.

The eigenfunctions of H_{vib}^0 may be chosen to be simultaneous eigenfunctions of the vibrational angular momentum operators.

$$L_t = (Q_{t1}P_{t2} - P_{t1}Q_{t2})/\hbar = (q_{t1}p_{t2} - p_{t1}q_{t2}) \tag{2.12}$$

For each degenerate mode, they can be written

$$\Psi_v^0 = \prod_s \psi_{vs}(Q_s)\prod_t \psi_{vt,\ell t}(Q_{t1},Q_{t2})$$

$$= \prod_s |v_s\rangle \prod_t |v_t,\ell_t\rangle \tag{2.13}$$

and satisfy the equations 2.11 and 2.12.

$$H_{vib}^0 \Psi_v^0 = hcG^0(v)\Psi_v^0 \tag{2.14}$$

$$L_t \Psi_{vt,\ell t}^0 = \ell_t \Psi_{vt,\ell t}^0 \tag{2.15}$$

where ℓ_t is an integer of the same parity as v_t, $-v_t \leq \ell \leq +v_t$. The eigenfunction $\psi_{vt,\ell t} = |v_t,\ell_t\rangle$ has a (v_t+1)-fold degeneracy.

2.4.2 Empirical Term Formula

The simplest empirical relation for the total energy of the molecule *(T)* consists of independent sums of its zeroth-order vibration, $G(v)$, and its rotation, $F_v(J)$, energy:

$$T(v, J) = G(v) + F_v(J) \tag{2.16}$$

G(v) involves only the vibrational quantum numbers and the rotational terms $F_v(J)$ are eigenvalues of the effective rotational Hamiltonian for the appropriate vibrational state.

As a result one would expect the vibration-rotation terms to be given by a power series expansion in the various quantum numbers, with all terms included that are allowed by symmetry restrictions of the molecule. The higher-power terms generally have successively smaller coefficients so that the series converges rapidly. As a result the relative importance of these terms and the relationship of these coefficients to the parameters in the original Hamiltonian must be assessed.

The vibrational term formula is given by

$$G(v) = G(v_s, \ldots, v_t, \ell_t \ldots)$$

$$= \sum_s \omega_s (v_s + \tfrac{1}{2}) + \sum_t \omega_t (v_t + 1)$$

$$+ \sum_{s \geq s'} x_{ss'} (v_s + \tfrac{1}{2})(v_{s'} + \tfrac{1}{2}) + \sum_{s,t} x_{st} (v_s + \tfrac{1}{2})(v_t + \tfrac{1}{2})$$

$$+ \sum_{t \geq t'} x_{tt'} (v_t + 1)(v_{t'} + 1) + \sum_{t \geq t'} g_{tt'} \ell_t \ell_{t'} + \ldots \tag{2.17}$$

where x_{rr} are anharmonicity constants, ℓ_t and $\ell_{t'}$ represent the quantum numbers of degenerate vibrations, and $g_{tt'}$ are added anharmonicity constants for degenerate vibrations. The magnitudes of the anharmonicity constants x_{rr} and g_{tt} are smaller than ω by a factor of about 10^{-2}. One consequence of the anharmonic terms is that overtone

frequencies are not exactly integral multiples of the fundamental frequencies and combination frequencies are not exactly equal to the sum of the fundamental frequencies.

The rotational terms $F_v(J)$ may be fitted to the following formula.

$$F_v(J,k) = B_v[J(J+1) - K^2] + C_v K^2 - \sum_t 2C(\zeta_t)_v kl_t$$

$$- (D_J)_v J^2(J+1)^2 - (D_{JK})_v J(J+1)K^2 - (D_K)_v K^4$$

$$+ \sum_t (\eta_{tJ})_v J(J+1)kl_t + \sum_t (\eta_{tK})_v k^3 l_t + ... \qquad (2.18)$$

where B and C are rotational constants, $\zeta_{r,s}^{(\alpha)}$ is the Coriolis zeta constant coupling Q_r to Q_s through rotation about the α axis and D_J, D_{JK}, D_K, $(\eta_{tJ})_v$ and $(\eta_{tK})_v$ are centrifugal distortion terms. They are typically smaller than the rotational constants by factors of the order of 10^{-4}. $(C\zeta_t)_v = (C\zeta_{zz}^z)$ may be thought of as an effective rotational constant which is only present when $\ell_t \neq 0$ and is more often described as a first-order Coriolis splitting of the zeroth- order degeneracy associated with ℓ_t. Analysis of rotational spectra of molecules shows a vibrational dependence of the rotational constants. This means that for each state there is an effective rotational constant, B_v, C_v, $(C\zeta_t)_v$ which differs from the equilibrium values, $B_e = h/8\pi^2 I_{Be}$, $C_e = h/8\pi^2 I_{Ce}$ and $(C\zeta_t)_e$. The vibrational dependence takes the form

$$B_v = B_e - \sum_r \alpha_r^B \left(v_r + \frac{d_r}{2} \right) + \ldots \tag{2.19}$$

$$C_v = C_e - \sum \alpha_r^C \left(v_r + \frac{d_r}{2} \right) + \ldots \tag{2.20}$$

$$(C\zeta_t)_v = (C\zeta_t)_e - \sum \alpha_r^{C\zeta_t} \left(v_r + \frac{d_r}{2} \right) + \ldots \tag{2.21}$$

where the α's are the vibration-rotation constants and d_r is the degree of degeneracy of the rth vibration.

2.4.3 Perturbation Treatment

Thus far, the results from the contact transformation have yielded purely diagonal terms in the Hamiltonian matrix. Below is a discussion of some of these terms in detail and as well as some terms, which are off-diagonal in the Hamiltonian matrix. All of these were essential to the modeling of the v_1 spectra.

2.4.3.1 First-Order Coriolis Term

Physically it is well known that if the motion of a particle is referred to a uniformly rotating coordinate system, apart from the acceleration produced by the acting forces, two additional accelerations appear, the centrifugal acceleration and the Coriolis acceleration. These may be thought of as due to two apparent forces, the centrifugal force and the Coriolis force. The magnitude of these forces are given by

$F_{centrifugal} = mr\omega^2$ and $F_{Coriolis} = 2mv_a\omega\sin\varphi$ where m is the mass of the particle, v_a its apparent velocity with respect to the moving coordinate system, r its distance from the axis of rotation, ω the angular velocity of the coordinate system with respect to a fixed coordinate system and φ the angle between the axis of rotation and the direction of v_a. The Coriolis force occurs only for a moving particle and is directed at right angles to the direction of motion and at right angles to the axis of rotation *(21)*. The introduction of the Coriolis force leads to an additional coupling between rotation and vibration, which can be explained taking into account the relevant term in the complete Hamiltonian.

The complete Hamiltonian contains the $h_{2,1}$ term $-2C_e\pi_z J_z$. The terms from π_z which connect the two components of a doubly degenerate vibration can be written simply as

$$\pi_z = \sum_t \zeta_{t1,t2}^{(z)}[(Q_{t1}P_{t2} - Q_{t2}P_{t1})/\hbar] + \text{ other terms} \tag{2.22}$$

Equation 2.22 reduces to

$$= \sum_t \zeta_t L_t + \text{other terms} \tag{2.23}$$

where $\zeta_{t1,t2}^{(z)}$ is abbreviated to ζ_t. The corresponding term in the Hamiltonian is

$$-\sum_t 2C_e\zeta_t L_t J_z \tag{2.24}$$

This is diagonal in both vibrational and rotational basis functions, giving a first-order term in the energy

$$-\sum_t 2C_e \zeta_t \ell_t k \tag{2.25}$$

The other terms give rise to interaction between nondegenerate mode v_s and the degenerate mode v_t due to rotation about the x and y axes. Relevant here is Jahn's rule, which states that if the product of the symmetry species of two vibrational modes contains the species of rotation, $\Gamma(Q_s) \times \Gamma(Q_t) \in \Gamma(J_z)$, Coriolis interaction takes place between the modes ω_s and ω_t. This interaction arises from the term

$$h_{2,1} = -2B(\pi_x J_x + \pi_y J_y) \tag{2.26}$$

which leads to the following off-diagonal matrix elements (25),

$$\left\langle v_s - 1, v_t^{\ell_t}; J, k \left| h_{2,1} \right| v_s, (v_t - 1)^{\ell_t \pm 1}; J, k \pm 1 \right\rangle$$

$$= \mp \Omega_{st} \zeta_{st} B[v_s(v_t \mp \ell_t)]^{\frac{1}{2}} [(J(J+1) - k(k \pm 1)]^{\frac{1}{2}} \tag{2.27}$$

where

$$\Omega_{st} = [(\omega_s + \omega_t)/2(\omega_s \omega_t)^{\frac{1}{2}}] \tag{2.28}$$

For simplicity, combining Ω_{st}, ζ_{st}, B, and the J, k dependence together, Equation (2.27) can be written as

$$\left\langle v_s - 1, v_t^{\ell_t}; J, k \left| h_{2,1} \right| v_s, (v_t - 1)^{\ell_t \pm 1}; J, k \pm 1 \right\rangle = \mp W_{1,1} [v_s (v_t \mp \ell_t)]^{\frac{1}{2}} \qquad (2.29)$$

2.4.3.2 Centrifugal Distortion Constants

Physically, as a molecule rotates it also distorts under the effects of centrifugal forces, resulting in the need for additional terms in the energy level expression, which are called centrifugal distortion constants. The centrifugal distortion constants D_J, D_{JK}, and D_K arise from $\tilde{h}_{4,0}$ terms in the transformed Hamiltonian. The other centrifugal distortion constants η_{tJ} and η_{tK} which occur in the rotational term formulas for excited degenerate vibrational states arise from $\tilde{h}_{2,3}$ terms in the transformed Hamiltonian. All these centrifugal distortion constants contribute to the diagonal energy expression (2.18).

2.4.3.3 ℓ-Doubling Constants

The diagonal matrix elements of the operator $h_{2,0}$ and $h_{4,0}$ in the harmonic oscillator approximation yield the vibrational energy level expression for a symmetric top as Equation 2.17. There are a few elements in the transformed Hamiltonian in the rigid, symmetric rotor basis functions, which are off-diagonal in the rotational quantum

numbers and which must be considered. An earlier example of an off-diagonal matrix element was that due to Coriolis coupling about x and y-axes. The most important additional term is that associated with ℓ-doubling.

There are three types of rotational ℓ-doubling interactions, which can arise in an excited degenerate vibrational state of a symmetric top. The difference between them is related to the selection rules in k and ℓ_t which govern the nonzero off-diagonal matrix. For completion they are all mentioned below *(56)* but only the first case (a) is relevant to SO_3 and hence will be the only one discussed in some detail.

(a) $\Delta\ell_t = \pm 2, \Delta k = \pm 2$, denoted $q_t^{(+)}$-type interactions.

(b) $\Delta\ell_t = \pm 2, \Delta k = \mp 2$, denoted $q_t^{(-)}$-type interactions.

(c) $\Delta\ell_t = \pm 2, \Delta k = \mp 1$, denoted r_t-type interactions.

The effect (a) is the most common type of interaction and the ℓ-doubling constant $q_t^{(+)}$ can be written simply as q_t. It defines the magnitude of the off-diagonal matrix elements according to the equation 2.30 below. Here $\widetilde{H}$ includes terms such as the operator $\widetilde{h}_{2,2}$ of type $(q_{t1} \pm iq_{t2})^2$ and $(J_x \pm iJ_y)^2$ which produce elements off-diagonal in the quantum numbers ℓ and k that split and shift the zeroth-order levels.

$$\langle v_t, \ell_t + 1; J, k+1 | \widetilde{H} | v_t, \ell_t - 1; J, k-1 \rangle$$

$$= (\rho/4)q_t^{(+)}[(v_t + 1)^2 - \ell_t^2]^{1/2}\{[J(J+1) - k(k+1)][J(J+1) - k(k-1)]\}^{1/2} \qquad (2.30)$$

Here ρ is equal to either $+1$ or -1, depending on the phase conventions used for the basis functions. For the rotational and vibrational basis functions described earlier,

Mills has shown that $\rho = -1$ in Equation 2.30 (*54*). Using a similar simplification procedure as described before for the off-diagonal term in equation 2.29, the relation 2.30 simplifies to

$$\langle v_t, \ell_t + 1; J, k + 1 | \tilde{H} | v_t, \ell_t - 1; J, k - 1 \rangle = (\tfrac{1}{2}) W_{2,2} [(v_t + 1)^2 - \ell_t^2]^{\frac{1}{2}} \qquad (2.31)$$

There are some symmetry restrictions on the species of the degenerate vibrations (Q_{t1}, Q_{t2}) for which each type of interaction can occur. The $q_t^{(+)}$ interactions occur for all E species vibrations in all symmetric top point groups. In the $v_t = 1$ fundamental levels of such vibrations the matrix element in equation 2.29 gives rise to a doubling of the $k = \ell_t = \pm 1$ pair of levels which is the ℓ-type doubling effect described above. For other values of k, the effect of the element is small, unless the coupled levels are close in energy, in which case the effect is called an ℓ-resonance. Finally, this type of interaction can also occur between a nondegenerate mode of vibration and a degenerate mode as well. It is expected that such a coupling would be significantly reduced compared to a coupling within a degenerate mode, but, for completeness, the off diagonal for such an interaction is

$$\langle v_s, v_t, \ell_t = 0, k | \tilde{H} | v_s - 1, v_t + 2, \ell_t \pm 2, k \pm 1 \rangle$$

$$= w_{2,2} = C_{22} \{ [J(J+1) - k(k+1)][J(J+1) - k(k-1)] \}^{\frac{1}{2}} \qquad (2.32)$$

Such a term has proved necessary in the analysis of the infrared data for $^{32}S^{16}O_3$. Similarly, a higher order type of interaction can occur, where $\Delta\ell = \pm 4$ and $\Delta k = \pm 4$, and this was included in the analysis. This term can be expressed as

$$\langle v_t, \ell_t, k | \widetilde{H} | v_t, \ell_t \pm 4, k \pm 4 \rangle$$

$$= (W_{4,4}/8)\{(v_4 \mp \ell_4)(v_4 \pm \ell_4 + 2)(v_4 \mp \ell_4 - 2)(v_4 \pm \ell_4 + 4)\}$$

$$\cdot \{[J(J+1) - k(k \pm 1)][J(J+1) - (k \pm 1)(k \pm 2)][J(J+1) - (k \pm 2)(k \pm 3)]$$

$$\cdot [J(J+1) - (k \pm 3)(k \pm 4)]\}^{\frac{1}{2}} \qquad (2.33)$$

2.4.3.4 Fermi Resonance

In a molecule it can happen that two vibrational levels, similar in energy and having identical symmetries, interact such that the perturbation leads to the two states repelling each other. Fermi *(57)* first observed this resonance perturbation in the Raman spectrum of CO_2, where the v_1 mode of CO_2 should be intense while the $2v_2$ overtone should be weak. In fact the two Raman bands had roughly the same intensity and positions shifted in frequency. The separation of the two levels v_1 (1388.3 cm^{-1}) and $2v_2$ (1285.5 cm^{-1}) was much larger than expected based on the value of v_2 (667.3 cm^{-1}). In effect, the overtone $2v_2$, "borrows" intensity from the v_1 fundamental as a result of this resonance. This is a consequence of mixing of the eigenfunctions of the two states, a resonance interaction described as Fermi resonance.

The source of Fermi couplings between different vibrational states of the same symmetry and similar energies is the presence of cubic and quartic terms in the potential energy expression (Equation 2.4). The specific form of the cubic and quartic terms of the potential depends on the point group of the molecule and on the species of the normal coordinates involved *(58)*. Since the potential energy is invariant under all symmetry operations, only those combinations of the normal coordinates whose products are totally symmetric can appear as higher order terms. This restricts the number of possible cubic and quartic force constants and also the possibilities for Fermi resonance perturbations for a molecule.

2.5 Application to the ν_1 mode of SO_3

Considering the case for the ν_1 mode of SO_3, there are several Fermi resonance couplings possible through a cubic force constant. All overtones and combination levels of the fundamentals with an A_1' symmetry component could in theory couple with ν_1 levels. However the strongest possible Fermi resonance couplings will occur with those overtones levels most similar in energy to those of ν_1. This then reduces to two possibilities, $2\nu_4$ ($\ell = 0$) at 1060 cm^{-1} and $2\nu_2$ ($\ell = 0$) at 994 cm^{-1}, which will couple through the cubic force constants k_{144} and k_{122} respectively. Of course there are possible contributions from quartic force constants as well. However since their orders of magnitude would be significantly smaller than the cubic force constants, they were not considered in our fit of SO_3.

Aside from the Fermi resonance perturbation in the spectrum there was another direct source of perturbation to the ν_1 mode of SO_3. This occurs via the small $w_{2,2}$ interaction which can couple ν_1 ($\ell = 0$) directly to $2\nu_4$ ($\ell = \pm2$) As mentioned earlier Coriolis couplings can occur, according to Jahn's rule, only when the "product" of the vibrational species contains the species of a rotation. In the case of SO_3, D_{3h} symmetry, the rotation species are A_2' and E''. The direct product of ν_1 and the fundamentals ν_2, ν_3, and ν_4 would yield A_2'', E' and E' species respectively. As a result ν_1 cannot directly Coriolis couple with any of the fundamentals. However indirect Coriolis coupling can occur since the overtones $2\nu_2$ ($\ell = 0$) and $2\nu_4$ ($\ell = 0$), ($\ell = \pm2$) can couple to levels $\nu_2+\nu_4$ ($\ell = \pm1$) and $2\nu_4$ ($\ell = 2$) via the off-diagonal matrix elements defined by equations 2.27 and 2.29. These interactions, referred to as $W_{1,1}$ and $W_{2,2}$ for simplicity occur with the states that can directly Fermi resonate with ν_1 and their inclusion was found to be necessary in order to reproduce the experimental spectrum. Figure 2.2 illustrates these interactions.
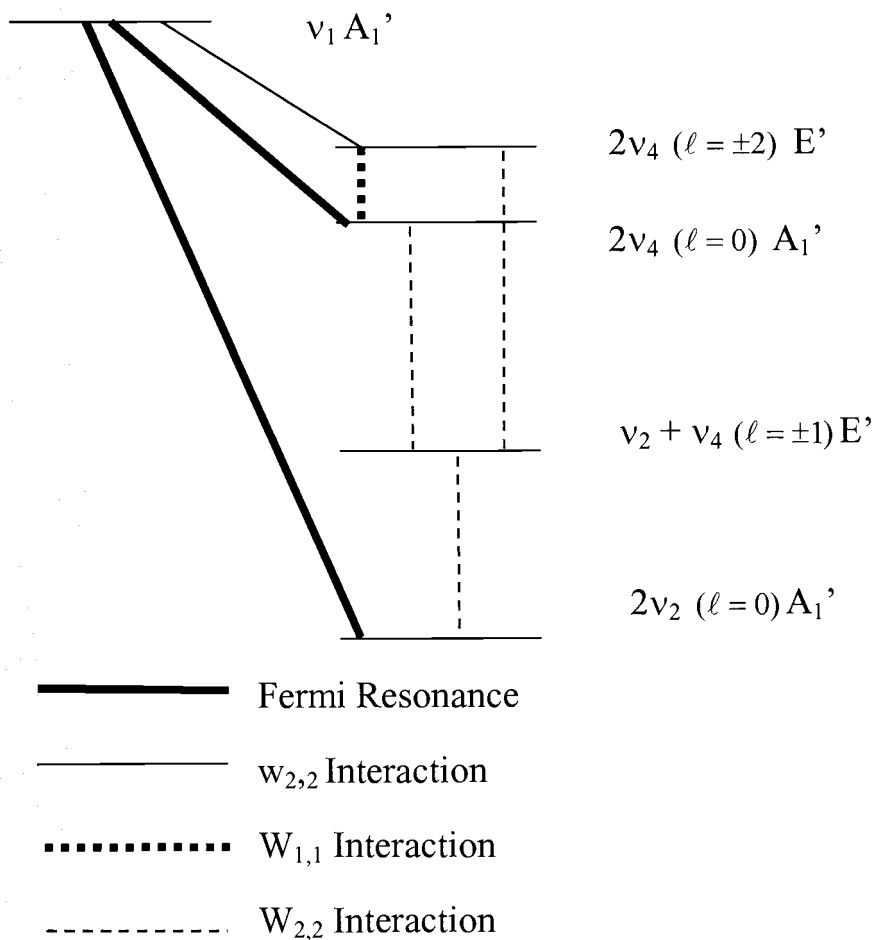
Figure 2-2 Diagrammatic representation of the sources of perturbations to the ν_1 mode. Not drawn to scale.

As a result of these couplings, the Hamiltonian matrix which represents the interactions of a ν_1 level of SO_3 is the 7 x 7 matrix, shown below in Table 2-3. Here $E_1 = \nu_1$, $E_2 = 2\nu_4$, $E_3 = \nu_2 + \nu_4$, $E_4 = 2\nu_2$ and the offdiagonal terms are as already discussed.

	v_1 ($\ell=0$)	$2v_4$ ($\ell=0$)	$2v_2$ ($\ell=0$)	$2v_4$ ($\ell=2$)	$2v_4$ ($\ell=-2$)	v_2+v_4 ($\ell=1$)	v_2+v_4 ($\ell=-1$)
v_1 ($\ell=0$)	E_1 (k,0)	½k_{144}	½k_{122}	$w_{2,2}$	$w_{2,2}$	0	0
$2v_4$ ($\ell=0$)	½k_{144}	E_2 (k,0)	0	$2^{½}W_{2,2}$	$2^{½}W_{2,2}$	$-2^{½}W_{1,1}$	$2^{½}W_{1,1}$
$2v_2$ ($\ell=0$)	½k_{122}	0	E_4 (k,0)	0	0	$2W_{1,1}$	$-2W_{1,1}$
$2v_4$ ($\ell=2$)	$w_{2,2}$	$2^{½}W_{2,2}$	0	E_2 (k+2,+2)	$W_{4,4}$	$2W_{1,1}$	0
$2v_4$ ($\ell=-2$)	$w_{2,2}$	$2^{½}W_{2,2}$	0	$W_{4,4}$	E_2 (k-2,-2)	0	$-2W_{1,1}$
v_2+v_4 ($\ell=1$)	0	$-2^{½}W_{1,1}$	$2W_{1,1}$	$2W_{1,1}$	0	E_3 (k+1,+1)	$W_{2,2}$
v_2+v_4 ($\ell=-1$)	0	$2^{½}W_{1,1}$	$-2W_{1,1}$	0	$-2W_{1,1}$	$W_{2,2}$	E_3 (k-1,-1)

Table 2-3 The Hamiltonian matrix for the v_1 mode of SO_3.

The initial difficulty involved in solving this matrix was that the parameters for most of the states that couple with v_1 were not known. The parameters for the dark or hidden states, particularly for $2v_4$, could only be determined indirectly due to their effects on v_1. However, during the course of this work, the parameters for all levels $v_2 + v_4$, $2v_2$, $2v_4$ ($\ell = 0$), and $2v_4$, ($\ell = \pm2$) became available from an analysis (in particular by Arthur Maki) of concurrent high resolution IR spectra obtained in a collaborative study with Tom Blake at Pacific Northwest National Laboratories (PNNL). (This collaboration was triggered by the CARS work.)

2.6 Application to the $\nu_1 + \nu_2$ combination band

As mentioned earlier in chapter 1, the $\nu_1 + \nu_2$ IR active combination band was also investigated in order to obtain ν_1 ro-vibrational parameters that could help understand the complexity observed in the ν_1 Raman spectra. As for the ν_1 level, there exist similar types of interactions for the $\nu_1 + \nu_2$ combination levels involved in transitions near 1565 cm^{-1}. As one might expect, the states perturbing the $\nu_1 + \nu_2$ levels involved combinations of ν_2 and ν_4. These states include $3\nu_4 (\ell = \pm 1, \pm 3)$, $\nu_1 + \nu_4 (\ell = \pm 1)$, $\nu_2 + 2\nu_4$ $(\ell = 0, \pm 2)$, $2\nu_2 + \nu_4 (\ell = \pm 1)$, and $3\nu_2$ $(\ell = 0)$. In order to correctly fit the spectrum, the interaction of these twelve nearby states must be considered. As a result a 13 x 13 Hamiltonian matrix can be written as shown on the following page. Here $E_1 = \nu_1 + \nu_4$, $E_2 = 3\nu_4$, $E_3 = \nu_1 + \nu_2$, $E_4 = \nu_2 + 2\nu_4$, $E_5 = 2\nu_2 + \nu_4$, $E_6 = 3\nu_2$ $(\ell = 0)$ and the off-diagonal elements have the same definitions as before. The use of this matrix will be discussed in chapter 4 where the $\nu_1 + \nu_2$ band is analyzed.

	$\nu_1+\nu_4$ $(\ell=1)$	$\nu_1+\nu_4$ $(\ell=-1)$	$3\nu_4$ $(\ell=1)$	$3\nu_4$ $(\ell=-1)$	$3\nu_4$ $(\ell=3)$	$3\nu_4$ $(\ell=-3)$	$\nu_1+\nu_2$ $(\ell=0)$	$\nu_2+2\nu_4$ $(\ell=0)$	$\nu_2+2\nu_4$ $(\ell=2)$	$\nu_2+2\nu_4$ $(\ell=-2)$	$2\nu_2+\nu_4$ $(\ell=1)$	$2\nu_2+\nu_4$ $(\ell=-1)$	$3\nu_2$ $(\ell=0)$
$\nu_1+\nu_4$ $(\ell=1)$	E_1 $(k+1,+1)$	$W_{2,2}$	$\frac{1}{2}^{2/3}k_{144}$	0	$w_{2,2}$	0	$2^{2/3}W_{1,1}$	0	0	0	$\frac{1}{2}k_{122}$	0	0
$\nu_1+\nu_4$ $(\ell=-1)$	$W_{2,2}$	E_1 $(k+1,-1)$	0	$\frac{1}{2}^{2/3}k_{144}$	0	$-w_{2,2}$	$-2^{2/3}W_{1,1}$	0	0	0	0	$\frac{1}{2}k_{122}$	0
$3\nu_4$ $(\ell=1)$	$\frac{1}{2}^{2/3}k_{144}$	0	E_2 $(k-1,+1)$	$2W_{2,2}$	$3^{2/3}W_{2,2}$	$3^{2/3}W_{4,4}$	$w_{1,1}$	$2W_{1,1}$	$-2^{2/3}W_{1,1}$	0	0	0	0
$3\nu_4$ $(\ell=-1)$	0	$\frac{1}{2}^{2/3}k_{144}$	$2W_{2,2}$	E_2 $(k-1,-1)$	$3^{2/3}W_{4,4}$	$3^{2/3}W_{2,2}$	$-w_{1,1}$	$-2W_{1,1}$	0	$2^{1/2}W_{1,1}$	0	0	0
$3\nu_4$ $(\ell=3)$	$w_{2,2}$	0	$3^{2/3}W_{2,2}$	$3^{2/3}W_{4,4}$	E_2 $(k+3,+3)$	0	0	0	$6^{2/3}W_{1,1}$		0	0	0
$3\nu_4$ $(\ell=-3)$	0	$-w_{2,2}$	$3^{2/3}W_{4,4}$	$3^{2/3}W_{2,2}$	0	E_2 $(k-3,-3)$	0	0	0	$-6^{2/3}W_{1,1}$	0	0	0
$\nu_1+\nu_2$ $(\ell=0)$	$2^{2/3}W_{1,1}$	$-2^{2/3}W_{1,1}$	$w_{1,1}$	$-w_{1,1}$	0	0	E_3 $(k,0)$	$\frac{1}{2}k_{144}$	0	0	0	0	$\frac{3}{4}^{2/3}k_{122}$
$\nu_2+2\nu_4$ $(\ell=0)$	0	0	$2W_{1,1}$	$-2W_{1,1}$	0	0	$\frac{1}{2}k_{144}$	E_4 $(k,0)$	$2^{2/3}W_{2,2}$	$2^{2/3}W_{2,2}$	$-2W_{1,1}$	$2W_{1,1}$	0
$\nu_2+2\nu_4$ $(\ell=2)$	0	0	$-2^{2/3}W_{1,1}$	0	$6^{2/3}W_{1,1}$	0	0	$2^{2/3}W_{2,2}$	E_4 $(k+2,+2)$	$W_{4,4}$	$8^{2/3}W_{1,1}$	0	0
$\nu_2+2\nu_4$ $(\ell=-2)$	0	0	0	$2^{2/3}W_{1,1}$	0	$-6^{2/3}W_{1,1}$	0	$2^{2/3}W_{2,2}$	$W_{4,4}$	E_4 $(k-2,-2)$	0	$-8^{2/3}W_{1,1}$	0
$2\nu_2+\nu_4$ $(\ell=1)$	$\frac{1}{2}k_{122}$	0	0	0	0	0	0	$-2W_{1,1}$	$8^{2/3}W_{1,1}$	0	E_5 $(k+1,+1)$	$W_{2,2}$	$6^{2/3}W_{1,1}$
$2\nu_2+\nu_4$ $(\ell=-1)$	0	$\frac{1}{2}k_{122}$	0	0	0	0	0	$2W_{1,1}$	0	$-8^{2/3}W_{1,1}$	$W_{2,2}$	E_5 $(k+1,-1)$	$-6^{2/3}W_{1,1}$
$3\nu_2$ $(\ell=0)$	0	0	0	0	0	0	$\frac{3}{4}^{2/3}k_{122}$	0	0	0	$6^{2/3}W_{1,1}$	$-6^{2/3}W_{1,1}$	E_6 $(k,0)$

Table 2-4 The Hamiltonian matrix for the $\nu_1+\nu_2$ mode of SO_3.

2.7 Symmetry Properties and Statistical Weights for SO_3

Given the complex interactions that proved important in SO_3, it is fortunate that due to symmetry restrictions, roughly two thirds of the energy levels cannot exist. These symmetry restrictions will now be discussed.

The total eigenfunction (ψ_T) of a molecule in the simplest approximation may be written as the product of the electronic (ψ_e), vibrational (ψ_v), rotational (ψ_r) and spin (ψ_s) wavefunctions.

$$\psi_T = \psi_e \psi_v \psi_r \psi_s \tag{2.34}$$

The nuclear spin, I, of oxygen in this molecule is zero, that is O is a boson. As a result the nuclear spin function ψ_s is symmetric and the O atom exchange operator acting upon ψ_T must yield $+\psi_T$. Since the ground electronic and vibrational functions are symmetric, the symmetry restrictions derive from the product $\psi_r \psi_v$. The symmetries of the ψ_v are known and thus only the symmetries properties of the rotational levels need to be determined. The text by Allen and Cross (24) provides a detailed treatment of such symmetry considerations, as summarized below.

The symmetry species of the rotational levels is found by considering the effect of the symmetry operations on the rotational wavefunction. The eigenfunction of the symmetric top may be written as

$$\psi_{J,K,M}(\theta,\chi,\phi) = \Theta_{J,K,M}(\theta) \cdot e^{iK\chi} \cdot e^{\pm iM\phi} \qquad (2.35)$$

where J, K, M are quantum numbers for total angular momentum (J), its projection along the molecular z-axis (K) and its projection along the laboratory fixed axis (M) respectively. θ, χ and ϕ are the Eulerian angles which relate the orientation of the molecule in its molecular coordinate system to the laboratory coordinate system. $\Theta(\theta)$ represents hypergeometric functions expressed in terms of the variable $\sin^2(\theta/2)$. Since SO_3 is an oblate symmetric top of D_{3h} symmetry, the rotational wavefunctions will have symmetries of the rotational subgroup of this molecule, i.e. that of D_3. The character table of D_3 is given in Table 2-5.

D_3	E	$2C_3$	$3C_2$
A_1	1	1	1
A_2	1	1	-1
E	2	-1	0

Table 2-5 Character Table of D_3

The problem is now reduced to investigating the behavior of the symmetric rotor eigenfunctions under the three operations of the group, E, C_3 and C_2. First consider the identity operation.

$$\psi_{J,K,M}(\theta,\chi,\phi) \xrightarrow{\ E\ } \psi_{J,K,M}(\theta,\chi,\phi) \tag{2.36}$$

Under the identity operation the rotational eigenfunction clearly remains unchanged. Thus for $K=0$ $\chi_E' = 1$ and for $|K| \neq 0$, since the levels are doubly degenerate, $\chi_E' = 2$. Next consider the effect of a C_3 operation, which changes χ to $\chi + 2\pi/3$.

$$\psi_{J,K,M}(\theta,\chi,\phi) \xrightarrow{\ C_3\ } \psi_{J,K,M}\left(\theta,\chi + \frac{2\pi}{3},\phi\right) = e^{2\pi Ki/3} \cdot \psi_{J,K,M}(\theta,\chi,\phi) \tag{2.37}$$

For a given J and M, $K \neq 0$, there are two functions $\psi_{J,K,M}$ and $\psi_{J,-K,M}$. Thus the character of the rotation is given by

$$\chi'_{C_3} = e^{2\pi iK/3} + e^{-2\pi iK/3} = 2\cos\left(\frac{2\pi K}{3}\right) \qquad \text{if } K \neq 0. \tag{2.38}$$

However if $K = 0$ or a multiple of 3, the rotational eigenfunction remains unchanged and thus $\chi_{C3}' = 1$.

Finally, consider the effect of a C_2 rotation, which is slightly more complicated. Here one must consider a two fold rotation about an axis perpendicular to the symmetry axis and making an angle α with the molecular x axis. In this case, the changes are θ to $\pi - \theta$, ϕ to $\pi + \phi$ and χ to $\pi - \chi + 2\alpha$, (22, 24) yielding

$$\psi_{J,K,M}(\theta,\chi,\varphi) \xrightarrow{\ C_2\ } \psi_{J,K,M}(\pi-\theta,\pi-\chi+2\alpha,\pi+\varphi) \approx (-1)^J \cdot \psi_{J,-K,M}(\theta,\chi,\phi) \quad (2.39)$$

Thus if $K \neq 0$, $\chi_{C2}' = 0$; if $K = 0$, $\chi_{C2}' = (-1)^J$. Table 2-6 can be constructed for the representation of D_3 formed by $\psi_{J,K,M}$.

	χ_E'	χ_{C3}'	χ_{C2}'	Symmetry
$K = 0$ J even	1	1	1	A_1
$K = 0$ J odd	1	1	-1	A_2
$|K| = 3p$	2	2	0	$A_1 + A_2$
$|K| = 3p \pm 1$	2	-1	0	E

Table 2-6 The symmetry species for the rotational eigenfunctions for SO_3.

For the rotational subgroup D_3, the eigenfunctions of the rotational levels are of the species A_1, A_2 or E. Given these symmetry possibilities for the rotational eigenfunctions, we need only to determine the symmetry of the product $\psi_r\psi_v$ for the possible vibrational states of SO_3. For the ground state, $\psi_v = A_1'$ and in order for ψ_T to be totally symmetric, ψ_r must be of A_1 symmetry as well. Thus energy levels exist only for even values of J for $K = 0$ and for $K = 3p$ (where p is an integer), that is multiples of 3. No energy levels exist for $K = 3p \pm 1$ since these are of E symmetry. Hence roughly two thirds of the energy levels in the molecule no longer exist due to symmetry considerations.

The restrictions for the A_1' ν_1 mode are identical to those of the ground state. For the ν_2 mode, $\psi_v = A_2''$ and in order for ψ_T to be totally symmetric, ψ_r must be of A_2 symmetry as well. Thus energy levels exist only for odd J values for $K = 0$ and for values such that $K = 3p$. Similar logic can be applied for ν_3 and ν_4 modes, which are of E symmetry. In order for ψ_T to be totally symmetric, hence ψ_r must have E symmetry. Thus energy levels exist only for values of K such that $K = 3p \pm 1$ (i.e. 1, 2, 4, 5,...).

The validity of these nuclear spin restrictions is beautifully demonstrated in the infrared and Raman spectra obtained in this study and, indeed, a comprehensive understanding of all these theoretical aspects of SO_3 was essential in the modeling of the Raman active ν_1 mode, described in chapter 4.

3. EXPERIMENTAL

3.1 CARS Experimental Setup

A description of the high resolution CARS apparatus has been given previously *(8)*. Figure 3-1 displays the experimental layout. Briefly, the pump laser was a 20 Hz seeded Nd-YAG laser (Continuum, custom laser) that, as operated, gave 40 ns pulses at 532 nm. The seeder temperature was adjusted so that the 532 nm output was positioned at 18788.4624(15) cm^{-1} (50% absorption on the blue side of iodine atlas *(59)* line 1111) and this was monitored to ensure that no drift occurred during measurements. A beam splitter took off part of the 532 nm output of a 100 mJ/pulse yielding two portions (each 2-4 mJ/pulse) which served as pump beams in a three-dimensional phase-matching arrangement (folded 'BOXCARS').

The remaining 532 nm energy was employed to pump three dye cells that amplified the continuous output of a tunable ring dye laser (Coherent, CR-699-29) pumped with an Ar$^+$ laser (Coherent, Innova 90, 6 W). For purpose of calibration, a small portion of the (Stokes) output from the dye laser was used to measure absorption of I$_2$ vapor. The main output from the dye laser after amplification had an energy 0.3 to 1 mJ per pulse.

This apparatus to measure coherent Raman spectra has a demonstrated *(10)* resolution of 0.001 cm^{-1} but this was degraded slightly in these measurements due to poor performance of the amplifier stages of the Nd-YAG laser and to saturation effects, as discussed later.
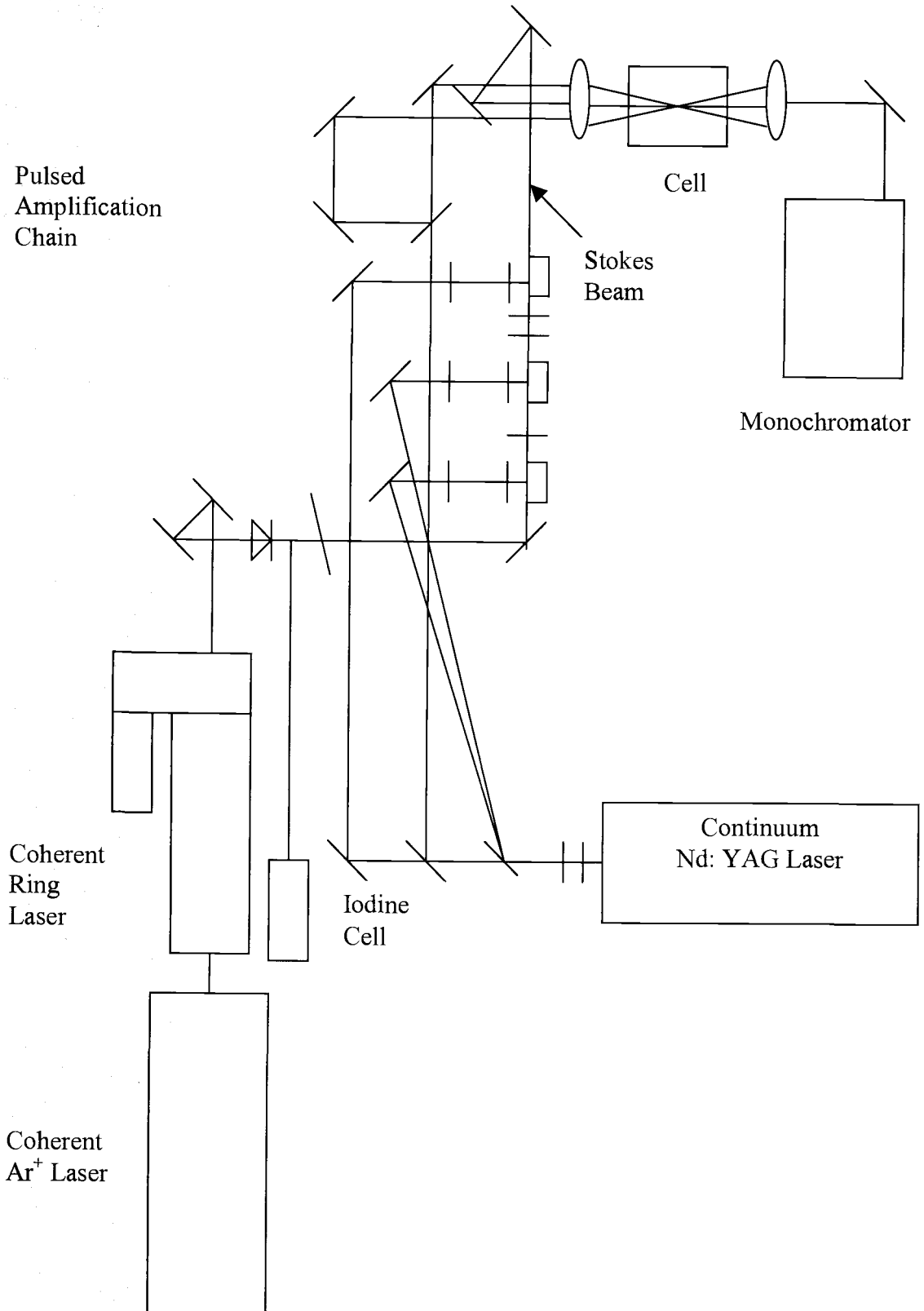
Figure 3-1 Layout for the CARS Experiment

Several problems were encountered with the custom built Continuum Nd:YAG during the course of these experiments. Due to a poor engineering design of the laser heads, leaching of the cladding material (magnesium oxide) occurred. This not only contaminated the internal cooling water supply to the heads but also deposited a thin film on the Nd:YAG rods and flashlamps, thus reducing the laser power efficiency. Continuum has since improved on their laser head design but the laser was no longer under warranty and replacement of the heads by Continuum was not financially feasible at the time. Thus with the assistance of Ted Hinke from the OSU Chemistry machine shop, new laser head housings were designed and constructed. The Nd:YAG rods were cleaned and then inserted into the housings.

The pressure broadening experiments of acetylene, as described in chapter 5, were then performed but there remained significant noise in the spectra. In an effort to determine the source of noise in the spectra the control electronics of the piezo-mounted mirror were checked along with the seeder; also the laser power supply (including all the charging and discharging capacitor circuits) were checked for any instability. Finally, after spending several months checking every fathomable aspect of the laser, the instability was determined to be due to the thermal expansion of the aluminum blocks on which the housings were mounted. Through these blocks the hot internal cooling water entered and exited the new heads. This very subtle effect led to a lack of pointing stability in the laser beam. Of course any instability in the pump beams becomes magnified in the amplification chain and ultimately in the CARS signal and hence the observed noise in the spectra. Mounting the head of the laser on ball bearing mounts in order to stabilize it solved the problem.

Also a significant portion of time was spent trying to optimize the efficiency of the dye laser amplification chain. The efficiency was improved significantly by changing the last stage from a longitudinally pumped cell to a transversely pumped cell. It was also found that significant amplification of the seed beam was achieved by carefully optimizing the concentration of the dye in the three stages of the amplification chain. The result was that the power of the amplified Stokes beam was increased by a factor of three and the pulse-to pulse stability was also improved.

The Stokes beam and two pump beams (532 nm) were then focused with a lens (focal length 400 mm) into a cell containing the gas of interest. The beam overlap was adjusted for maximum CARS signal that was optically filtered and detected with a Hamamatsu R955 photomultiplier. The output from this detector was integrated with a signal averager (Stanford Research, SR250), the analog output of which was digitized with a microcomputer that served also to scan the ring dye laser.

3.2 Preparation of Sulfur Trioxide

Sulfur trioxide $^{32}S^{16}O_3$ was collected from the distillation of fuming sulfuric acid. It was also prepared by the oxidation of sulfur with $^{16}O_2$ at 450°C in the presence of platinum foil serving as a catalyst.

$$2^X S + 3^Y O_2 \xrightarrow{450°C, Pt} 2^X S^Y O_3 \qquad (3.1)$$

Platinum foil and 0.09 g of sulfur were added to a 175 mL glass reaction vessel sealed with Teflon fittings. This vessel was heated to 60 °C while pumping in order to remove any water that may have been present in the sulfur. The reaction cell was then attached to a vacuum line and an excess of oxygen (620 Torr) was added. The reaction vessel was sealed and heated for 48 hours at 450 °C. The vessel was attached to the vacuum line again, placed in a dewar of liquid nitrogen, and any unreacted oxygen was pumped off. It was then placed in a dewar containing a mixture of methanol and nitrogen at about – 60 to – 70 °C. Any sulfur dioxide produced was pumped off. The yield was approximately 80%. This method was used with $^{18}O_2$ (Isotec, 98.3%), $^{16}O_2$, ^{32}S and ^{34}S (Cambridge Isotope Laboratories, 98.8%) to prepare all of the isotopomers $^{32}S^{18}O_3$, $^{34}S^{18}O_3$ and $^{34}S^{16}O_3$ as well.

3.3 CARS Experiments on Sulfur Trioxide

Sulfur trioxide is very difficult gas with which to work due to its great reactivity with water and its very corrosive nature. It attacks the o-rings on the cell windows after several hours, thus only when measurements are to be made was it transferred to the cell. It also attacked the Validyne AP-10 pressure sensor employed, making pressure readings somewhat unreliable. As a result an ice bath was used to control the vapor pressure of SO_3. An excess of SO_3 was sublimed into the cell and the vapor pressure was taken to be that of the γ-form at 0 °C, e.g. 6 Torr. Some variability in the pressure

is expected, due to difficulties in controlling the temperature of a freeze out tip on the cell but pressures of 6-10 Torr are believed to apply for most recorded spectra.

3.4 CARS Experiments on Acetylene

Pressure broadening experiments were performed on commercially available acetylene (Air Liquide, 99.6%). Pressures were measured with a Validyne AP-10 pressure sensor with an estimated accuracy of 0.2 Torr. CARS spectra were obtained for the well-resolved odd-J lines of acetylene from $J = 7$ up to $J = 15$ for a pressure range of 5 - 160 Torr.

4. RESULTS AND ANALYSIS OF SO₃ SPECTRA

4.1 CARS Spectral Results for the Isotopomers of SO₃

4.1.1 $^{32}S^{16}O_3$

The first isotopomer of sulfur trioxide investigated was that of $^{32}S^{16}O_3$. As part of the routine procedure for obtaining the sample spectra, iodine spectra were concomitantly obtained. This was necessary in order to obtain an absolute frequency measurement of the dye laser ω_2 value, and hence of the Raman shift ω_1 (18788.4624) - ω_2. A frequency calibration correction was made to every single spectrum by fitting the iodine absorption lines obtained and comparing them with values from the standard iodine atlas *(59)*. The SO₃ spectra were generally obtained after an equilibrium was established between the excess solid SO₃ and its vapor pressure at 0 °C. This corresponded to a vapor pressure of the γ-form of 6 Torr.

The spectra were unchanged for SO₃ samples prepared by different methods. To establish scan reproducibility several spectra of the sample were obtained on different days as shown in Figure 4-1. As can be observed, the patterns are reproducible although there are small variations in the relative intensities and linwidths from scan to scan. This can be attributed to variation in sample pressure and, more important, to laser fluctuations in power and position, which have amplified effect in nonlinear forms of spectroscopy like CARS. Accordingly these spectra were normalized and averaged together to obtain a composite spectrum of $^{32}S^{16}O_3$.
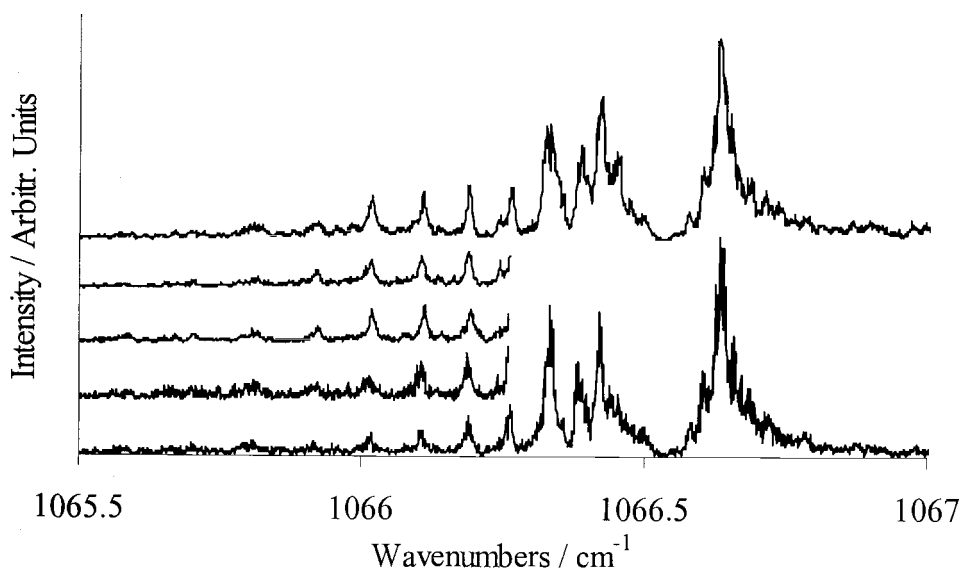
Figure 4-1 Sample of CARS spectra for $^{32}S^{16}O_3$.

This composite spectrum, shown in Figure 4-2, appears to consist of two intense Q-branch-like regions of almost equal intensity, separated by about 0.2 cm^{-1}. There is significant structure shaded to the red wavenumber side of the lower feature, a pattern like that expected for a normal single Q-branch for an oblate top. It should be noted that none of this structure was discerned in previous Raman studies *(9)*, which were at 5 cm^{-1} resolution. In the following sections we describe our somewhat torturous efforts to understand this "simple" spectrum.
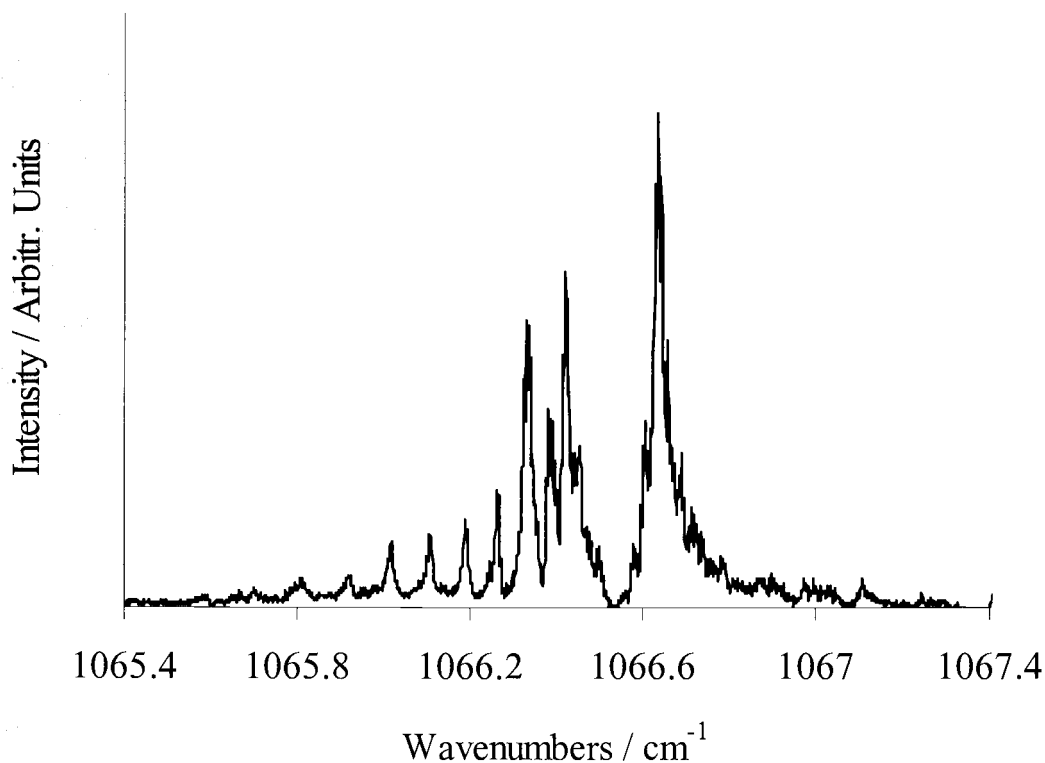
Figure 4-2 Composite CARS spectrum of $^{32}S^{16}O_3$ formed from an average of five scans as detailed in Excel File Composite3216.xls.

The observation of two Q-bands in this spectral region is puzzling. Only a simple single Q-branch is expected for a parallel band in an oblate top and no distortion in Q-line structure is expected since by symmetry no first order or second-order Coriolis interactions are allowed for v_1. None of the possible impurities such as SO_2 or O_2 have features in this region and the sample pressure is too low for appreciable contributions by the known trimer $(SO_3)_3$. Assignment of one Q-branch as a hot band transition originating from $v = 1$ levels of v_2 and v_4 bending modes was considered. However the nearly comparable intensity of the two Q-bands is inconsistent with this choice because

the relevant Boltzmann factors (squared) are 2.8 x 10^{-5} and 5.6 x 10^{-5} respectively. The only remaining assignment seemed to us to be that the bands arose from an allowed $\nu_1/2\nu_4$ Fermi-resonance, with the lower member of a slightly more integrated intensity believed to be of greater ν_1 character. Approximate values of the band origins would then be estimated at 1066.5 and 1066.7 cm^{-1} respectively.

In order to test this hypothesis, ν_1 spectra for the other isotopomers of SO_3 would be useful since the relative positions of the ν_1 and $2\nu_4$ will change. To estimate the isotopic shifts, a normal coordinate calculation was done using literature values for ν_2, ν_3, ν_4, and our value of 1066.5 cm^{-1} for ν_1. The relevant results are summarized in Table 4-1. Maximum interaction is expected when ν_1 - $2\nu_4$ = 0.

Isotopomers	ν_1 / cm^{-1}	ν_4 / cm^{-1}	ν_1-$2\nu_4$/ cm^{-1}	Δ (ν_1-$2\nu_4$) / cm^{-1}
$^{32}S^{16}O_3$	1066.5	530.1	6.3	
$^{32}S^{18}O_3$	1005.76	504.1	-2.5	8.8
$^{34}S^{16}O_3$	1066.92	527.9	11.1	-4.8
$^{34}S^{18}O_3$	1005.76	501.9	1.9	4.4

Table 4-1 Results from the harmonic force field analysis for the different isotopomers of sulfur trioxide.

However since anharmonicity effects are not taken into account in these calculations, the last column Δ (ν_1-$2\nu_4$) differences perhaps gives a better indication of how one might expect the Fermi resonance condition to change on isotopic substitution.

Assuming the "best" $\sim 50 - 50$ mixing occurs for $^{32}S^{16}O_3$, this predicts a reduced interaction for the other isotopomers, especially for $^{32}S^{18}O_3$.

4.1.2 $^{32}S^{18}O_3$

Accordingly the $^{32}S^{18}O_3$ and other isotopomers of SO_3 were synthesized, as described in chapter 3. An expanded view of a composite Q-branch spectrum of $^{32}S^{18}O_3$ is shown in Figure 4-3.
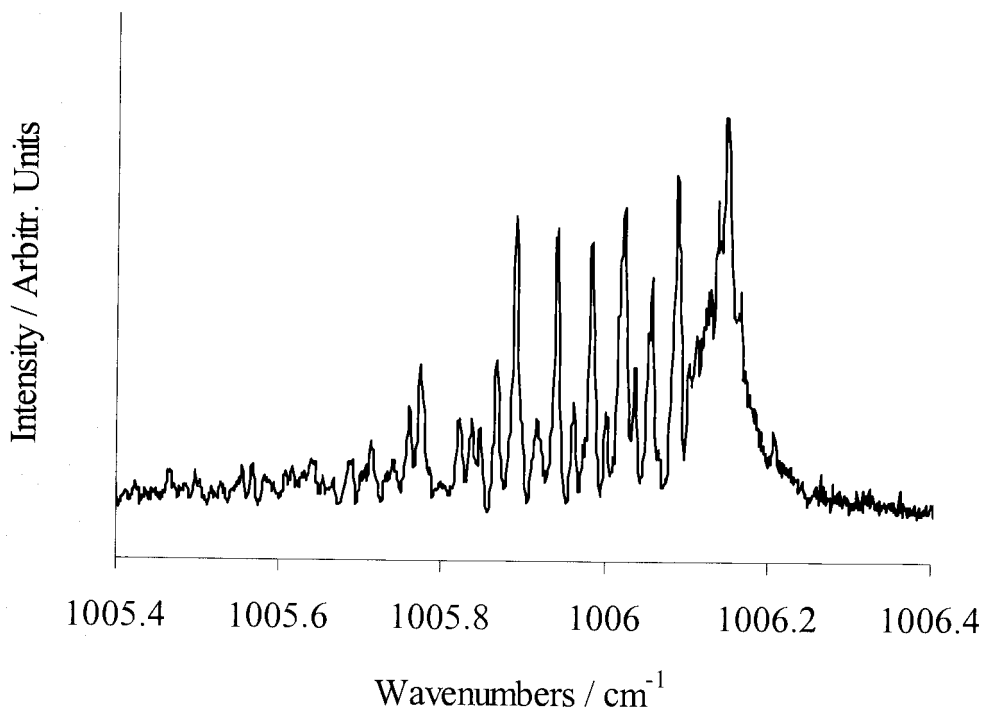
Figure 4-3 CARS spectrum of $^{32}S^{18}O_3$.

We note that the spectrum exhibits considerable structure, which one could hope to fit as a single Q-band. This result suggests that the resonance condition is indeed not as favorable for $^{32}S^{18}O_3$ so that the $2v_4$ intensity is reduced. An approximate band origin position on the blue side is at about 1006.2 cm^{-1}, in reasonable accord with the harmonic oscillator prediction of 1005.8 cm^{-1}. Note that, since the sulfur atom does not move in the v_1 vibration, the frequency ratio is just the mass factor $(16/18)^{1/2} = 0.94$. The corresponding ratio of $2v_4$ is less than this since the antisymmetric stretch does involve the sulfur atom movement.

The synthesis of $S^{18}O_3$ also produced appreciable amounts of the mixed isotopic combinations of SO_3, probably due to exchange with residual $H_2^{16}O$ in the cell and vacuum system.
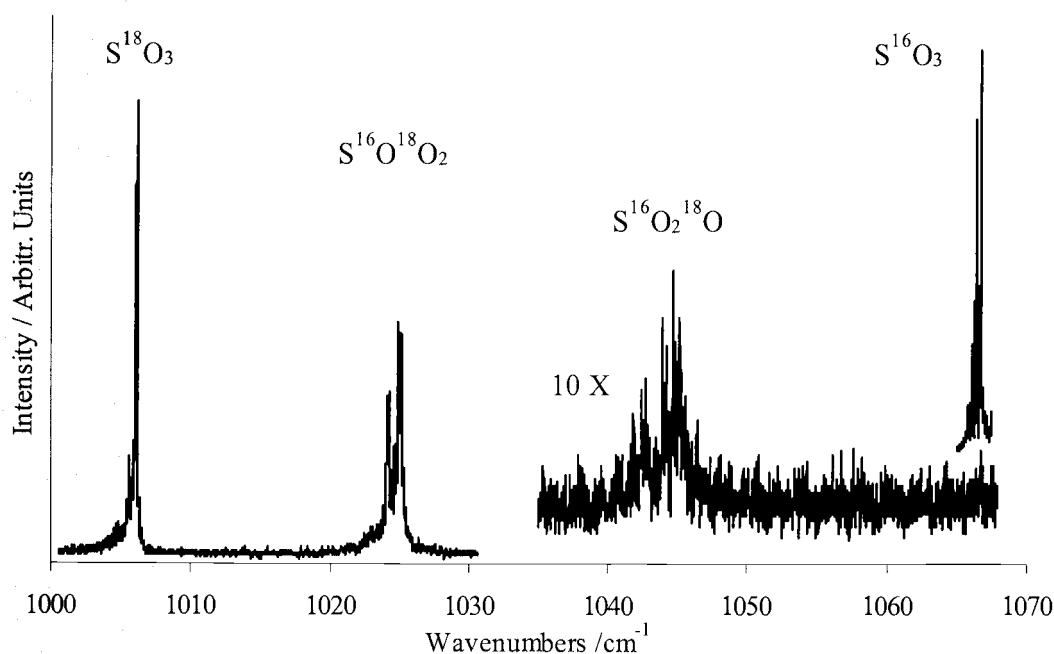
Figure 4-4 CARS spectra of ^{16}O and ^{18}O labeled spectra of SO_3. Also inserted is the Q-branch spectrum for $^{32}S^{16}O_3$ near 1066 cm^{-1}.

Figure 4-4 displays a broad scan of the ν_1 region and shows Q branches for these mixed isotopes $S^{16}O^{18}O_2$ and $S^{16}O_2^{18}O$, which were located at 1025.1 cm^{-1} and 1044.6 cm^{-1} respectively. These frequencies proved useful as added input for harmonic force field calculations, which aided us in the prediction of the frequencies for the fundamentals of the other various mixed isotopes of sulfur trioxide. These show that all ν_1 bands of the different isotopomers are isolated, with no overlapping regions. From the relative intensities in Figure 4-4 the ^{18}O composition was estimated at about 70 %. (In subsequent syntheses more care was taken and the ^{18}O content is estimated at > 90 %).

4.1.3 $^{34}S^{16}O_3$ and $^{34}S^{18}O_3$

Using the harmonic frequencies from the force field calculations as a guide to the spectral region to be scanned, the CARS spectra of the other symmetric isotopomers, $^{34}S^{16}O_3$ and $^{34}S^{18}O_3$, were obtained. Figure 4-5 shows that the spectrum of $^{34}S^{16}O_3$ consists of two apparent overlapping Q-bands, shifted down by approximately 0.5 cm^{-1} from the ν_1 region of $^{32}S^{16}O_3$. This shift is surprising since one would expect that the ν_1 frequency of $^{34}S^{16}O_3$ should not move at all relative to the ν_1 frequency of $^{32}S^{16}O_3$. However, ignoring this, one could imagine that the $2\nu_4$ component has dropped slightly to produce a maximum in the midst of the (spread out) ν_1 Q-branch spectrum. The loss of structure due to this overlap and the overall pattern is not inconsistent with the idea of a reduced Fermi-resonance for this isotopomer.
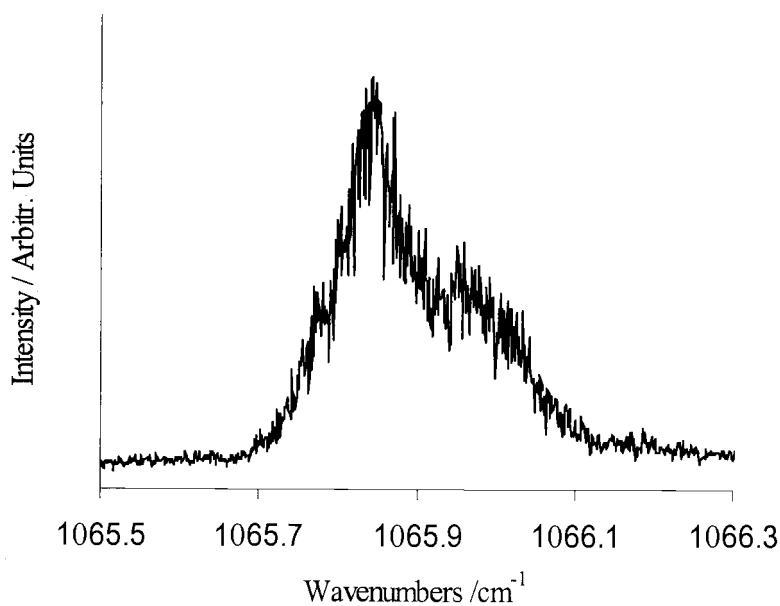
Figure 4-5 CARS spectrum of $^{34}S^{16}O_3$.

More puzzling is the ν_1 mode of $^{34}S^{18}O_3$, Figure 4-6. Here the spectrum is remarkably complex and spread out over 4 cm^{-1}, a much greater extent than in any of the other isotopomers.
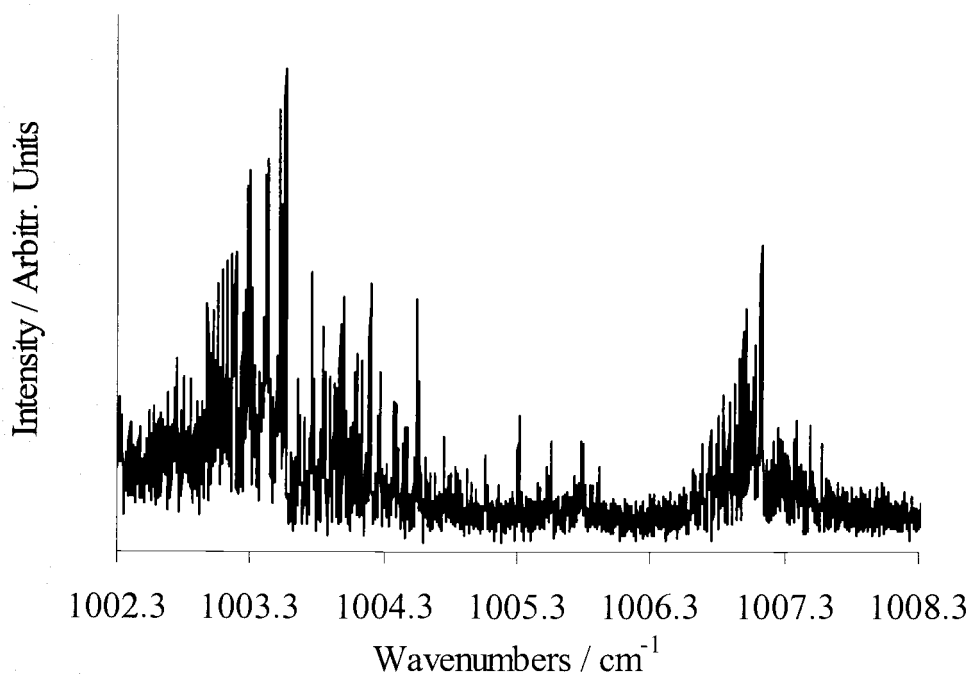
Figure 4-6 CARS spectrum of $^{34}S^{18}O_3$.

While not inconsistent with a Fermi-resonance model, this complexity, and indeed, that of all the CARS spectra, made their modeling a formidable challenge. This task has not been completed as yet, although, as to be discussed for the $^{32}S^{16}O_3$ isotopomer, significant progress has been made.

4.2 Modeling of the CARS spectrum of $^{32}S^{16}O_3$

As outlined in the theoretical section of this thesis (chapter 2), two Fermi resonance possibilities exist for ν_1: $\nu_1/2\nu_4$ and $\nu_1/2\nu_2$. Of these the $\nu_1/2\nu_4$ resonance was considered more important since $2\nu_4$ is much closer in energy to ν_1 than is $2\nu_2$. We

thus chose to model the spectrum as two separate bands, with the somewhat weaker, higher frequency Q-branch taken to be the $2\nu_4$ component and the lower band with more resolved structure treated as the ν_1 component. The Q-branches were modeled using the non rigid rotor oblate symmetric top relations below.

$$E(J,K) = BJ(J + 1) + (C - B)K^2 - D_J[J(J + 1)]^2 - D_{JK}J(J + 1)K^2 - D_K K^4 \qquad (4.1)$$

$$Q(J,K) = \nu_0 - \alpha_1^B J(J + 1) + (\alpha_1^B - \alpha_1^C)K^2 - (D_J' - D_J'')[J(J + 1)]^2$$
$$- (D_{JK}' - D_{JK}'')J(J + 1)K^2 - (D_K' - D_K'')K^4 \qquad (4.2)$$

This CARS modeling process was somewhat involved due to the nonlinear CARS dependence on χ^2, which introduces line interference effects not present in ordinary Raman spectroscopy (*1-2, 61-62*). Initially we entered a reasonable guess for a set of parameters such as the band origin (ν_1), the vibration rotation constants, ($\alpha_1^B = B'' - B'$, $\alpha_1^C = C'-C'$) and centrifugal distortion constants. Using these constants, and equations (4.1 and 4.2) we predicted frequencies as well as intensities (using the relevant Boltzmann and degeneracy factors) for the allowed Q-branch transitions. This stick spectrum was then used as input to the OSU CARS program, which is a modified version of that from Sandia National Laboratories. Assigning a reasonable Lorentzian linewidth to all the transitions, the stick spectrum was convoluted to properly include the cross terms of χ and χ_{nr} along with a Doppler linewidth convolution as well.
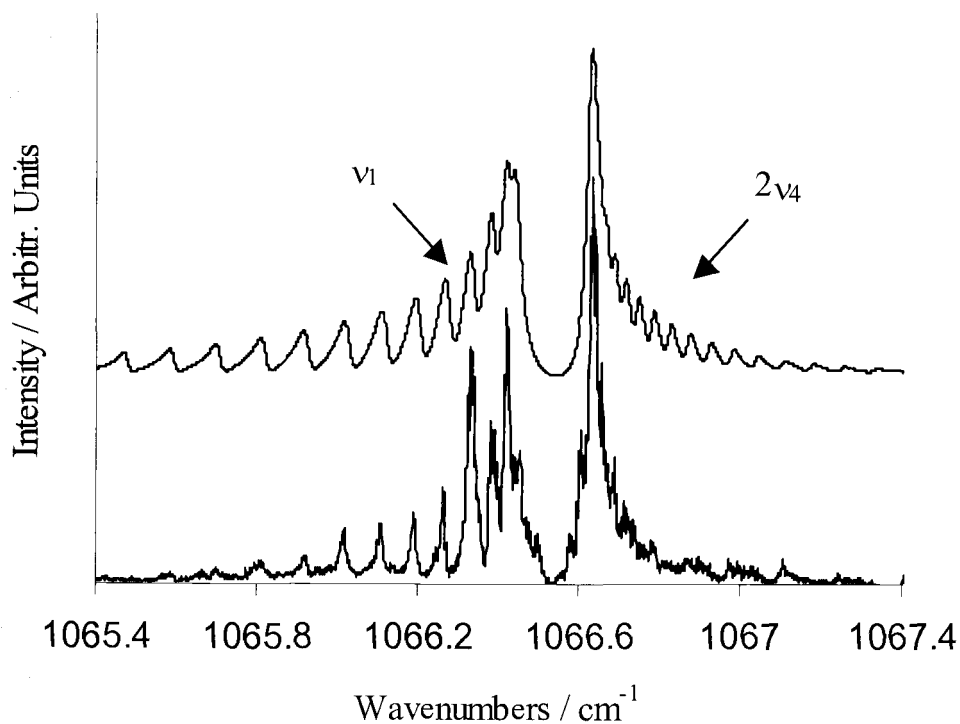
Figure 4-7 Simple model of $^{32}S^{16}O_3$ CARS spectrum. Top trace represents the model, and the lower trace, the experimental.

The resultant "best fit" is shown as the top trace in Figure 4-7 and the rovibrational parameters are in Table 4.2. It is seen that the general features of the spectrum are reproduced but the structural details are not well represented.

It is interesting that, around the time of this analysis of sulfur trioxide, a theoretical paper by Martin (*51*) appeared in which an anharmonic force field potential was obtained from a high-level "*ab initio*" quantum calculation. This predicted a set of molecular parameters for $^{32}S^{16}O_3$ which are included for comparison in Table 4-2. The agreement is not good between our parameters and the theoretical results from Martin.

Parameter	Our analysis		Martin (51)	
	v_1 band	$2v_4$ band	v_1 band	$2v_4$ band
Origin / cm^{-1}	1066.4513	1066.6315	1067.058	1055.041
α^B / cm^{-1}	2.8×10^{-5}	8.0×10^{-6}	8.1×10^{-4}	-1×10^{-3}
α^C / cm^{-1}	7.9×10^{-4}	-2.7×10^{-4}	4.1×10^{-4}	3×10^{-4}
$D_J'-D_J''$/ cm^{-1}	1.2×10^{-8}			
$D_{JK}'-D_{JK}''$ / cm^{-1}	-4.3×10^{-8}			
$D_K'-D_K''$ / cm^{-1}	-6.7×10^{-8}			

Table 4-2 Comparison of rovibrational parameters obtained for $^{32}S^{16}O_3$ using a model of two independent bands, v_1 and $2v_4$, with theoretical results from Martin (51).
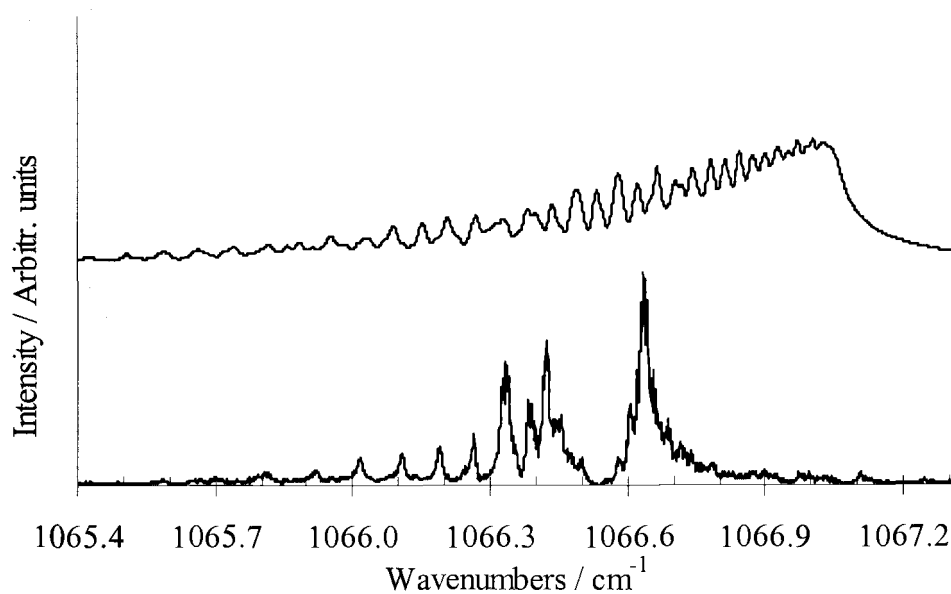
Figure 4-8 Model generated using the parameters from Martin's *ab initio* calculation.

It is also seen in Figure 4-8 that Martin's parameters do not reproduce the experimental spectrum at all.

Despite further modeling effort involving systematic variation of all parameters in equation 4.2, it was found that, although the general pattern of the spectra could be reproduced, we could never obtain a detailed match nor a set of molecular parameters for sulfur trioxide judged reliable. Moreover, we were troubled that the assumption of two separate Fermi-resonant bands seemed to require unusual anharmonicity behaviour for SO_3. In particular, $2\nu_4$ would be expected to be located at roughly 1060 cm^{-1} (530 cm^{-1} x 2); however from the fit it is predicted to be ~7 cm^{-1} higher at 1066.6 cm^{-1}. This implies that the x_{44} anharmonicity constant is positive, whereas a negative value is much more common for stretching modes. Also from Martin's anharmonic calculations, the predicted position for $2\nu_4$ was even lower, at 1055 cm^{-1}, and x_{44} was much smaller, -0.011 cm^{-1}.

Finally, the very small ν_1, $2\nu_4$ splitting (~0.2 cm^{-1}) implied by this Fermi resonance interpretation of the spectrum suggested an unusually small value for the k_{144} anharmonic potential term that produces the mixing. For comparison, in the classic case of Fermi resonance in CO_2, where the ν_1 symmetric stretch and the overtone of the ν_2 bend are nearly resonant, the observed splitting of the levels is more than 100 cm^{-1}. It seemed unlikely that this term could be so small for SO_3 and indeed Martin's calculations predicted a value of 1.56 cm^{-1}. Thus reluctantly, we were forced to consider more carefully some of the more subtle off-diagonal interaction possibilities outlined in chapter 2. This analysis drew heavily on the results of concurrent IR studies, as described below.

4.3 Details of the Modeling Process

Modeling of the spectrum was quite involved and Figure 4-9 is a schematic indicating the sequence of steps followed.

J and K quantum numbers of representative transitions in resolved Q_K features and in IR spectra assigned

Least squares fit of the 7 x 7 matrix for each J' K' level

Frequencies, computed intensities for v_1 from the eigenvector matrix imported into the CARS program

CARS convolution of stick spectrum, including χ_{nr}, cross terms of χ along with Lorentzian and Doppler linewidths

Visual comparison of observed and calculated CARS spectrum, modification of assignments

Figure 4-9 Flow chart indicating the sequence of steps taken to model the spectrum of $^{32}S^{16}O_3$.

The aim of this modeling exercise was to determine the rovibrational parameters for v_1 by accounting for coupling of the v_1 levels with $2v_4$, $v_2 + v_4$ and $2v_2$. As described in chapter 2, this analysis required the parameters for $2v_4 (\ell = 0)$, $(\ell = \pm 2)$, $2v_2$ $(\ell = 0)$, and $v_2+v_4 (\ell = \pm 1)$, which were not initially known. However, as a result of our collaboration with PNNL and Arthur Maki, triggered by our v_1 spectra, detailed analysis of the fundamentals, v_2 and v_4, and the hot bands, $2v_2-v_2$, $(v_2+v_4)-v_4$ were achieved. Using our preliminary v_1 rovibrational data, Maki was then able to analyze in detail the $2v_4 (\ell = 0)-v_4$, $2v_4 (\ell = 2)-v_4$, $(v_2+v_4)-v_2$ and $2v_2-v_2$ hot bands. Then, with these new improved parameters, we attempted to more accurately fit our v_1 spectrum. The difficulty involved here was that the resolution of our data was such that individual J, K lines were not distinguished, as they are in the IR data. However J stacks with common K were resolved and the models predicted that for J = K transitions, the intensities were a maximum. Accordingly we assigned peak maxima in the spectrum as individual J = K lines. Doing this, the best results obtained thus far are shown on the next page in Figure 4-10 where the top spectrum represents the model calculation.

It is obvious that significant improvement has been made in reproducing this complex spectrum, compared to our previous model in Figure 4-7. However the fit is not perfect and more work was undertaken to obtain improved v_1 parameters by using IR data from combination bands such as $(v_1+ v_2)$, as will be discussed later.
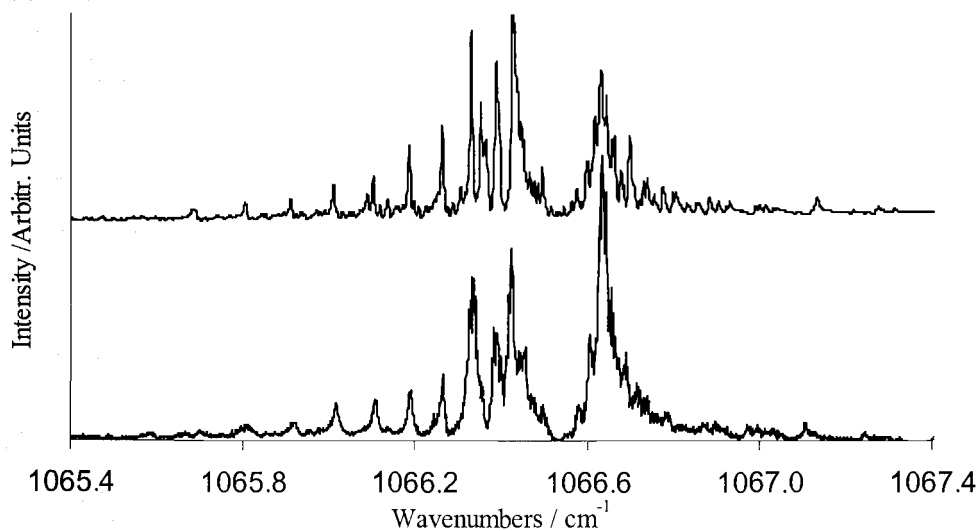
Figure 4-10 Model of $^{32}S^{16}O_3$ CARS spectrum using IR data. Top trace represents the model, and the lower trace, the experimental.

To understand the complexity of the spectrum, it is useful to examine the eigenvector matrix of the coupled states v_1, $2v_4$, $v_2 + v_4$ and $2v_2$. Diagonalization of this matrix not only gives the levels but also the component of v_1 in each level. From this information one can generate reduced energy diagrams, which serve to indicate when level crossings occur in the interacting states. One type of a reduced energy diagram is a plot of the energy difference between the state of interest and the ground state $((E'(J,K)-E''(J,K))$ versus the $J''(J''+1)$ quantum number.
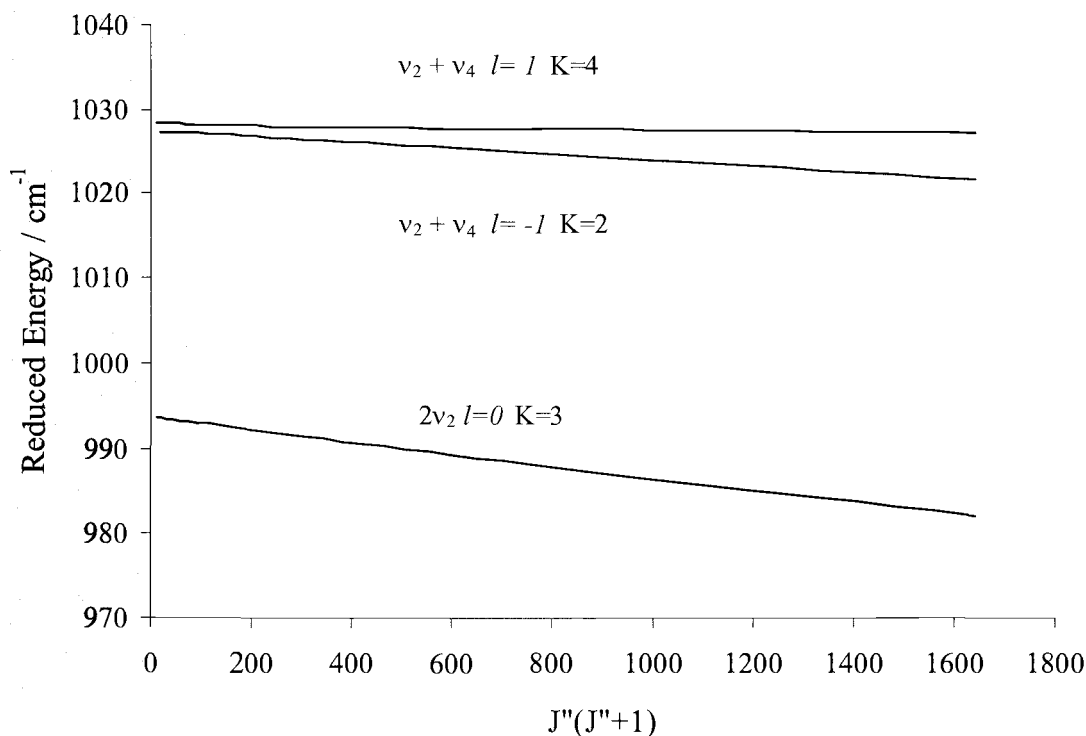
Figure 4-11 Reduced energy diagram for $\nu_2+\nu_4$ ($\ell = \pm 1$) and $2\nu_2$ modes.

Using the parameters (Appendix A) generated from the fit in Figure 4-10, the reduced energy diagram in Figure 4-11 was generated for the states $2\nu_2$ and $\nu_2 + \nu_4$ ($\ell = \pm 1$) coupled to the levels $K = 3$ levels of ν_1. As can be observed there is a simple linear dependence of the reduced energy versus $J(J+1)$. This indicates that the interaction of these levels with ν_1 is weak and there are no energy level crossings occurring for these states. However such is not the case for the interactions of $2\nu_4$ ($\ell = 0, \pm 2$) with ν_1, K=3. Figure 4-12 reveals a marked nonlinearity, indicating level crossings for K=3 at $J(J+1)$ values of about 600, where ν_1 and $2\nu_4$ ($\ell = -2$) are equally mixed and at 1100, where $2\nu_4$ ($\ell = 0$) takes on the dominant ν_1 character.
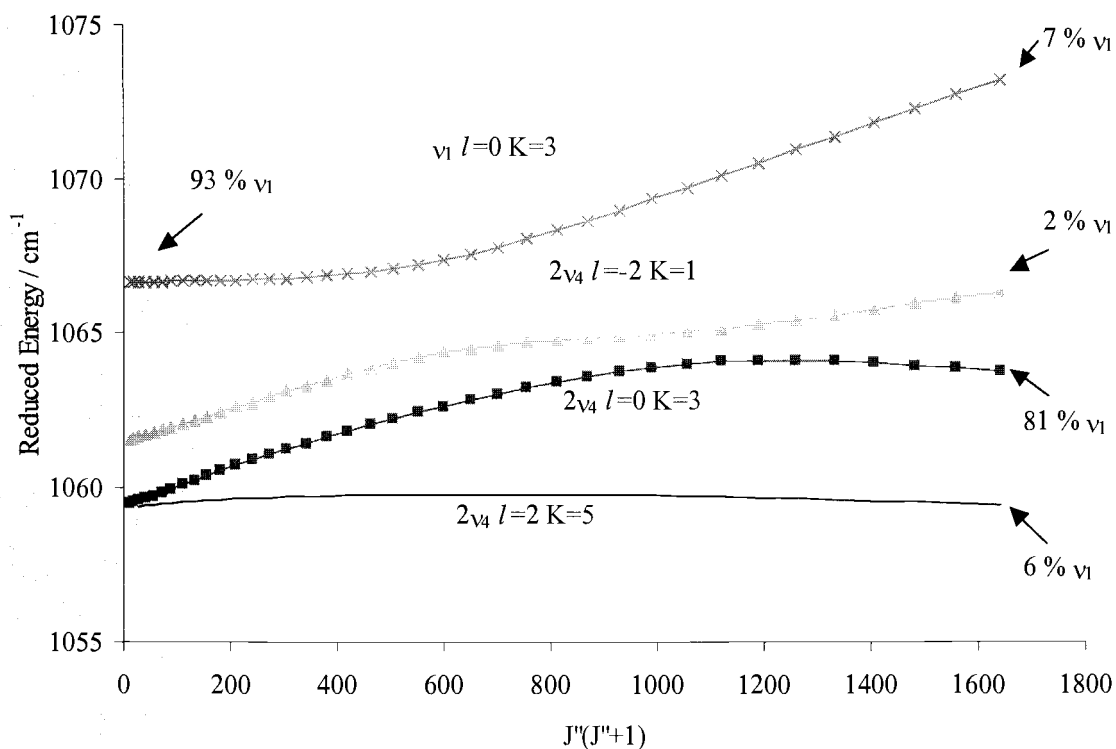
Figure 4-12 Reduced energy level diagram for ν_1 and its closest perturbing states. Indicated as well are the percentage composition of ν_1 at two extreme values of J", J"=0 and J"= 40.

Such diagrams could also be generated for other values of K, however one is sufficient to indicate the extent to which subtle mixing occurs among these level. In view of this, it can be seen why simpler models do not reproduce the CARS spectrum for $^{32}S^{16}O_3$. The mixing has been incorporated in obtaining Figure 4-10 and yields the parameters of Table 4-3 for the $^{32}S^{16}O_3$.

The ν_1 molecular parameters obtained from the fit are now in remarkably good agreement with those obtained from the high level *ab initio* calculation performed by Martin, except for the band origin of ν_1. This is expected since in his calculation,

Martin did not consider the possibility of a Fermi resonance interaction and thus his ν_1 value cannot be directly compared to ours. Exact agreement of calculated and observed ν_1 spectra has not been achieved however, and this led us next to consider other ways to determine the ro-vibrational parameters of ν_1.

Parameter	$^{32}S^{16}O_3$	Martin (theoretical)
ν_1 (cm$^{-1)}$)	1064.59(1)	1067.06
k_{144} (cm^{-1})	-2.898(4)	-1.56
α_B (cm^{-1})	0.000818(2)	0.00081
α_C (cm^{-1})	0.000329(5)	0.00041
B_e (cm^{-1})	0.349600(6)	0.34962
r_e (Å)	1.41768(12)	1.4176
C_e (cm^{-1})	0.1748(5)	
r_e (Å)	1.41749(14)	

Table 4-3 The molecular parameters obtained for ν_1 along with estimated uncertainties (in parentheses).

4.4 Analysis of the IR $\nu_1 + \nu_2$ combination band

As mentioned earlier, in order to obtain additional information on the molecular parameters of the ν_1 mode, the IR active difference and combination bands of ν_1 could be investigated. The $\nu_1 - \nu_2$ and $\nu_1 - \nu_4$ difference bands are buried in the ν_2; ν_4 bands

and have not been identified. However significant progress was made in the analysis of

the $v_1 + v_2$ combination band and thus will be discussed in detail here. Survey scans of

both $v_1 + v_4$ and $v_1 + v_2$ combination bands and the resultant calculated spectrum are

shown below in Figure 4-13. The large peaks in the spectrum are due to the presence of

water in the spectrometer and were ignored in the analysis.
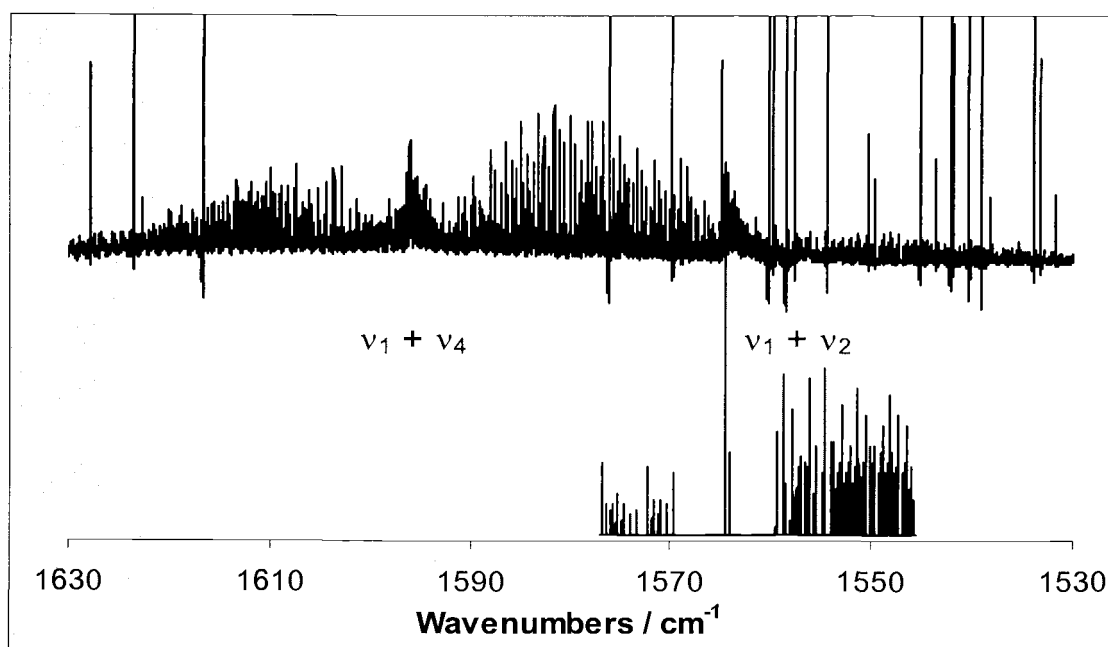
Figure 4-13 Survey scans of $v_1 + v_4$ and $v_1 + v_2$ in the top trace and the calculated spectrum in the bottom trace.

An expanded view of the spectral region from 1546 - 1550 cm^{-1} is displayed in

Figure 4-14. This is interesting since it clearly reveals a regular pattern of lines, which

could be assigned as shown on the following page.
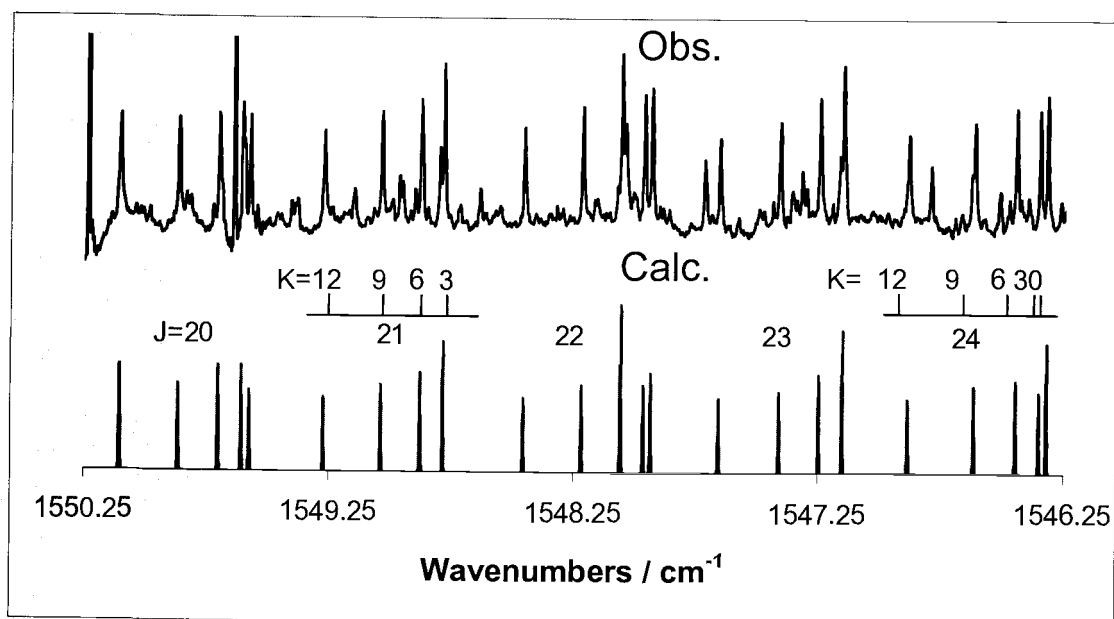
Figure 4-14 Expanded view of some of the assigned P-branch lines, top trace, along with the calculated spectrum, bottom trace.

The pattern consists of alternating groups of four and five lines. The groups are consistent with a progression of J lines corresponding to different K quantum numbers, increasing in J as one marches away from the central Q-branch at 1565 cm^{-1}. The fact that the groups consist of alternating groups of four and five lines was a striking result of the nuclear spin statistics discussed earlier in chapter two. The ground state consists of energy levels such that for the K = 0 stack, only even J energy levels exist. Thus only even J lines will contain the K = 0 transition in the progression. An assignment of the individual transitions was thus possible and an analysis was made using the transitions in Table 4-4.

Frequency	Residual	J'	K'	L'	J"	K"	L"
				Assignment			
1545.56547	0.00228	24	3	0	25	3	0
1545.66488	0.00078	24	6	0	25	6	0
1545.84567	-0.00014	24	9	0	25	9	0
1546.14097	0.00076	24	12	0	25	12	0
1546.31947	0.00120	23	0	0	24	0	0
1546.34989	0.00043	23	3	0	24	3	0
1546.44505	-0.00052	23	6	0	24	6	0
1546.61470	-0.00062	23	9	0	24	9	0
1546.88160	0.00019	23	12	0	24	12	0
1547.14993	-0.00098	22	3	0	23	3	0
1547.24422	-0.00050	22	6	0	23	6	0
1547.40653	-0.00124	22	9	0	23	9	0
1547.65443	-0.00034	22	12	0	23	12	0
1547.93284	-0.00012	21	0	0	22	0	0
1547.96303	-0.00054	21	3	0	22	3	0
1548.05547	-0.00142	21	6	0	22	6	0
1548.21608	-0.00137	21	9	0	22	9	0
1548.45457	-0.00019	21	12	0	22	12	0
1548.78288	-0.00090	20	3	0	21	3	0
1548.87698	-0.00095	20	6	0	21	6	0
1549.03794	-0.00107	20	9	0	21	9	0
1549.27357	-0.00032	20	12	0	21	12	0
1549.57721	0.00013	19	0	0	20	0	0
1549.60819	-0.00044	19	3	0	20	3	0
1549.70377	-0.00065	19	6	0	20	6	0
1549.86733	-0.00058	19	9	0	20	9	0
1550.10503	0.00001	19	12	0	20	12	0
1550.43570	0.00010	18	3	0	19	3	0
1550.53398	0.00043	18	6	0	19	6	0
1550.70049	-0.00009	18	9	0	19	9	0
1550.94252	0.00000	18	12	0	19	12	0
1551.22985	0.00016	17	0	0	18	0	0
1551.36359	0.00050	17	6	0	18	6	0
1551.53475	0.00052	17	9	0	18	9	0
1551.78277	0.00051	17	12	0	18	12	0
1552.08909	0.00069	16	3	0	17	3	0
1551.53475	0.00052	17	9	0	18	9	0
1551.78277	0.00051	17	12	0	18	12	0
1552.08909	0.00069	16	3	0	17	3	0
1552.19154	0.00030	16	6	0	17	6	0
1552.36721	0.00048	16	9	0	17	9	0

Table 4-4 The assignment of transitions for the $\nu_1 + \nu_2$ combination band.

Frequency	Residual	J'	K'	L'	J"	K"	L"
				Assignment			
1552.62155	0.00022	16	12	0	17	12	0
1552.87752	0.00099	15	0	0	16	0	0
1552.91176	0.00053	15	3	0	16	3	0
1553.01723	0.00066	15	6	0	16	6	0
1553.19695	0.00055	15	9	0	16	9	0
1553.45766	0.00005	15	12	0	16	12	0
1553.73073	0.00062	14	3	0	15	3	0
1553.83839	0.00051	14	6	0	15	6	0
1554.02233	0.00038	14	9	0	15	9	0
1554.50827	0.00041	13	0	0	14	0	0
1554.54500	0.00089	13	3	0	14	3	0
1554.65454	0.00033	13	6	0	14	6	0
1554.84349	0.00116	13	9	0	14	9	0
1555.35295	0.00051	12	3	0	13	3	0
1555.46485	0.00011	12	6	0	13	6	0
1555.65634	-0.00032	12	9	0	13	9	0
1556.11671	-0.00007	11	0	0	12	0	0
1556.15538	0.00096	11	3	0	12	3	0
1556.26831	-0.00046	11	6	0	12	6	0
1556.46408	-0.00016	11	9	0	12	9	0
1556.94921	-0.00026	10	3	0	11	3	0
1557.06600	0.00029	10	6	0	11	6	0
1557.69771	-0.00054	9	0	0	10	0	0
1557.73598	-0.00110	9	3	0	10	3	0
1559.28669	-0.00160	7	3	0	8	3	0
1569.70249	-0.00122	7	0	0	6	0	0
1570.36405	-0.00186	8	3	0	7	3	0
1570.93858	-0.00216	9	0	0	8	0	0
1570.97844	-0.00133	9	3	0	8	3	0
1571.09762	-0.00069	9	6	0	8	6	0
1571.58516	-0.00044	10	3	0	9	3	0
1572.14622	0.00025	11	0	0	10	0	0
1572.18370	-0.00014	11	3	0	10	3	0
1572.29889	0.00002	11	6	0	10	6	0
1573.36024	0.00066	13	3	0	12	3	0
1574.04751	0.00057	14	6	0	13	6	0
1574.61839	0.00019	15	6	0	14	6	0
1574.80047	0.00091	15	9	0	14	9	0
1575.18607	0.00085	16	6	0	15	6	0
1575.36335	0.00102	16	9	0	15	9	0
1575.64885	0.00107	17	3	0	16	3	0

Table 4-4 (cont'd) The assignment of transitions for the $\nu_1 + \nu_2$ combination band.

Frequency	Residual	J'	K'	Assignment L'	J"	K"	L"
1575.92174	-0.00029	17	9	0	16	9	0
1576.31223	0.00078	18	6	0	17	6	0
1576.74535	0.00033	19	0	0	18	0	0
1576.77627	-0.00067	19	3	0	18	3	0
1577.03864	-0.00066	19	9	0	18	9	0

Table 4-4 (cont'd) The assignment of transitions for the $v_1 + v_2$ combination band

This analysis included the full 13 x 13 coupled matrix described in Table 2-4 with estimates of the hidden (dark) states made from the v_2, v_4 parameters of Appendix A. The good quality of the fit is apparent from the very small magnitudes of the residuals. This fit was not possible if the effects of the nearby perturbing states in Table 2-4 were ignored. The resultant ro-vibrational parameters are shown in Appendix B. As part of the future work more transitions will have to be assigned, in particular in the $v_1 + v_4$ part of the spectrum. As one can observe from the broad survey scan in Figure 4-11, this region is somewhat intense and complicated by the presence of the R lines for the $v_1 + v_2$ combination band however we believe that such an assignment is possible and have begun a preliminary analysis.

A comparison of the v_1 parameters obtained thus far from the $v_1 + v_2$ analysis is given in Table 4-5 below.

Mode	ν_n / cm^{-1}	α^B / cm^{-1}	α^C / cm^{-1}
ν_2 (Maki)	497.56773(1)	7.99(4) x 10^{-4}	-1.2783(5) x 10^{-4}
$\nu_1 + \nu_2$	1559.3760(7)	3(1) x 10^{-4}	1.82(5) x 10^{-4}
ν_1 (from $\nu_1 + \nu_2$)[a]	1061.8082(7)	3.10(5) x 10^{-4}	1.14(1) x 10^{-4}
ν_1 (from ν_1)	1064.59(1)	8.81(2) x 10^{-4}	3.29(5) x 10^{-4}
ν_1 (Martin)	1067.06	8.1 x 10^{-4}	4.1 x 10^{-4}

Table 4-5 Molecular parameters for the ν_1 mode from the combination band $\nu_1 + \nu_2$. [a]Here the assumption is that the parameters for ν_1 are simply the difference between the parameters obtained for $\nu_1 + \nu_2$ and ν_2.

Table 4-5 provides a comparison of the key molecular parameters ν_1, α_1^B, α_1^C obtained in different ways. The ν_1 parameter determined from the combination band is assumed to be a linear combination of the ν_1 and ν_2 values. There is no real reason to expect this to be true since anharmonicity is ignored in this addition. In fact, the difference $(\nu_1 + \nu_2) - \nu_1 - \nu_2 = 2.78$ cm^{-1} implies an anharmonicity constant $-x_{12}$ of half this, 1.39 cm^{-1}, in reasonable accord with Martin's "ab initio" value of 1.11 cm^{-1}. The α_1^B, α_1^C vibrational-rotational constants are all of reasonable magnitudes. Our values from the ν_1 analysis are in good accord with Martin's theoretical predicition, but are quite different from the $\nu_1 + \nu_2$ band analysis. This is believed to be due to neglect of proper incorporation of the $\nu_1 + \nu_4$ transitions, a task that remains for future work.

Also reserved for future work is the detection and analysis of the $\nu_1 - \nu_2$ and $\nu_1 - \nu_4$ hot bands. These are of particular interest since they directly sample the upper state ν_1

levels that we sense in the ν_1 CARS spectra. One would thus expect exact agreement for parameters obtained from analysis of these difference bands and of the ν_1 spectrum. This analysis is very challenging since these ν_1-ν_2 and ν_1-ν_4 transitions occur in the middle of the ν_2 and ν_4 regions along with other hot bands. The intensities of the difference transitions are inherently weak so it is difficult to find and assign lines. Some progress has been made however and this effort will continue.

In summary, our CARS spectra have revealed for the first time an unanticipated complexity in the Raman spectrum of sulfur trioxide whose analysis proved to be a complicated task involving many of the fine details of spectroscopy. Good progress has been made towards understanding the complex $^{32}S^{16}O_3$ spectrum and, for the first time, experimental molecular parameters have been obtained for this mode. The success in modeling this spectrum has involved new infrared data obtained from collaboration with Tom Blake at PNNL and a more detailed theoretical analysis of the fundamental modes in collaboration with Arthur Maki. The stage has been set for completion of the full analysis of all $^{32}S^{16}O_3$ bands and for similar treatment of the other isotopomers. In chapter 6 we include some specific recommendations for future work.

5. COLLISIONAL BROADENING OF THE ν_2 Q-BRANCH OF ACETYLENE

5.1 Introduction

This chapter is a slightly modified version of a journal article published in the Journal of Raman Spectroscopy, vol. 31, 719-723 (2000). The article presents linewidth and line shift measurements for acetylene as measured by the OSU CARS apparatus.

Quantitative linewidth measurements of Raman spectra were performed as early as 1950, where Stoicheff (62) measured the broadening of the rotational lines of nitrogen. There he observed that the broadening of the rotational lines was linear with pressure up to 25 atm. Since the advent of lasers and improved spectral resolution, considerable effort has been devoted to the study of spectral line broadening of Raman-active transitions (63-68). This work has given detailed information about the effect of density, temperature and collisional partner on shape, width and shift of spectral lines for various molecules. Such studies can improve our knowledge about intermolecular interactions and associated processes of collisional perturbation of molecular motion.

In a practical vein, linewidth data is essential in applying sophisticated optical diagnostic techniques for accurate measurements of temperature, concentration and velocity in combustion, plasma and CVD reactor systems (69-71). Acetylene is an important constituent in such systems and the aim of the current study was to measure broadening coefficients for lines of the Q-branch spectrum of C_2H_2 at room temperature in the pressure region where the rotational structure is still resolved. For this purpose, the high-resolution CARS spectrometer at Oregon State University was used.

5.2 Experimental

A description of the CARS apparatus used for this investigation was given in detail in Chapter 3. All spectra were obtained at room temperature. Care was taken to keep the laser power low at the higher pressures since the windows of the cell tended to burn very easily, leaving deposits of carbon due to the decomposition of acetylene. As with the sulfur trioxide, spectra were calibrated against iodine in order to obtain absolute frequency measurements.

5.3 Theory of Line Broadening Factors

Several models exist to explain the broadening of Raman lines over a wide range of pressures and temperature. These range from semi-classical approaches for molecular scattering (72) to a fully quantum formalism (73-75). Also several fitting laws have been used to model state-to-state rotationally inelastic rates, which are then summed to yield the total rate out of a particular rotational state. It is this total outward rate that determines the width of the corresponding Q-branch lines and is based on several energy gap models (76 - 79).

In our studies a much simpler approach can be used since the spectra obtained were of isolated lines and at low pressures. At low pressures (1-10 Torr), the profiles of individual J-lines are primarily broadened inhomogeneously due to the Doppler effect. For an individual Q-branch transition at $\nu_R = \nu_1 - \nu_2$, the Doppler half-width at half maximum for spontaneous Raman scattering in the forward direction is:

$$\Gamma_{DR} \text{ (HWHM)} = \nu_R/c \, (2kT \ln 2 \,/m)^{\frac{1}{2}}. \tag{5.1}$$

Here c is the velocity of light, k the Boltzmann constant, T the temperature and m the molecular mass. In the case of collinear CARS, one obtains a quasi-Gaussian profile with a half-width equal to about 1.2 times Γ_{DR} (*80, 81*). In addition, for the ~2° crossing of the ν_1, ν_2 beams in our BOXCARS sampling arrangement, Γ_{DR} increases slightly by an angular factor *(82)* of 1.04, yielding for CARS an expected Gaussian FWHM value of $\Gamma_{DC} = 0.0030$ cm^{-1} for acetylene at 295 K. As discussed later, an additional contribution Γ_{INST}, assumed to be Gaussian, is expected from the experimental instrument function.

The corresponding homogeneous half-width Γ inside the Doppler profile is determined by collisions, which are responsible for relaxation of translational Γ_t, rotational Γ_r, and vibrational Γ_v degrees of freedoms. Assuming that collisional relaxational mechanisms are statistically independent:

$$\Gamma = \Gamma_t + \Gamma_r + \Gamma_v. \tag{5.2}$$

Owing to all of these collisional mechanisms, the corresponding contributions to the line-broadening will increase linearly with increasing density:

$$\Gamma_{t,r,v} = (N_L \, \sigma_{t,r,v} \, <\!v\!>) \, N. \tag{5.3}$$

Here Loschmidt's number (N_L = 2.687 x 10^{19} cm^{-3}) is used to express the number density N in amagat units and $<v> = (16\, kT/\pi m)^{\frac{1}{2}}$ is the average relative molecular velocity. σ_t is the cross-section for collisions responsible for changing the projection of molecular velocity on the direction of the wave vector $\mathbf{q} = \mathbf{k}_1 - \mathbf{k}_2$. σ_r is the cross-section for collisions, which change the value of rotational momentum of molecules. We note that the depolarisation ratio ρ is 0.03 for lines of the ν_2 Q-branch of C_2H_2 (83) so the anisotropic component is negligible. Thus the scattering is due to the isotropic (spherical) part of the polarizability and collisional orientational relaxation (collisions changing only the direction of the rotational moment vector J) does not influence the width of Q-lines. Finally, σ_v is the cross-section for collisions providing vibrational dephasing of oscillators. For many molecules $\sigma_t \geq \sigma_r >> \sigma_v$.

Of special interest is the region of density where collisions changing the projection of molecular velocity are sufficiently frequent that $\Gamma_t \approx \Gamma_{DC}$. Further increases in density can then lead to a decrease in the translational contribution to the linewidth:

$$\Gamma_t = C\, /\, N,\qquad\qquad\qquad (5.4)$$

where $C = 4\pi c \delta^2_D/N_L\sigma_t<v>$, and $\delta_D = \nu_R/c\, (kT/m)^{1/2}$ (67). This narrowing phenomenon, termed the Dicke effect or motional narrowing, has been studied extensively by Raman spectra for the molecules D_2 and H_2 (84-87), for which σ_t is large compared to σ_r. For most other molecules the cross-sections σ_t and $\sigma_{r+v} = \sigma_r + \sigma_v$ are comparable and one obtains a homogeneous Lorentzian profile with HWHM

$$\Gamma = \Gamma_t + \Gamma_{r+v} = C / N + (N_L \sigma_{r+v} <v>) N. \tag{5.5}$$

The expectation then is that the limiting linewidth at zero pressure will be $(\Gamma^2_{DC} + \Gamma^2_{inst})^{1/2}$ and this will initially decrease as one passes through the "suppressed" region where $\Gamma_t \approx \Gamma_{DC}$ and motional narrowing occurs. Beyond this pressure, the increasing contribution of Γ_{r+v} dominates and a linear increase with density is expected, mainly due to rotational relaxation. One of the objectives of the present study then was to determine whether linewidth vs. density measurements could permit the separate determination of σ_t and σ_{r+v}.

For this study, the pressure range was chosen such that most J components of the Q-branch are well resolved and the distances between them exceed their homogeneous widths. In this case, the spectrum is given by the following expression:

$$S \propto \left| \sum_J A_J \frac{\Delta_J + i\Gamma_J}{\Delta_J^2 + \Gamma_J^2} + \chi^{NR} \right|^2 \tag{5.6}$$

Here $\Delta_J = \nu_J - (\nu_1 - \nu_2)$ and $\nu_J = \nu_o - \alpha J(J+1) - \beta J^2(J+1)^2$, with ν_o, α, β the vibrational-rotational constants for the ν_2 mode of the linear C_2H_2 molecule (88). The relative intensity factor for the dominant isotropic component of the scattering is $A_J = g_J (2J+1) \exp[-E_J/kT]$, where E_J is the rotational energy of the J'th level of the ground state and the nuclear statistical weight is either $g_J = 3$ (J odd) or $g_J = 1$ (J even). Γ_J is the homogeneous collisional HWHM and χ^{NR} is the nonresonant nonlinear susceptibility

$\chi^{(3)NR}$ originating from far electronic resonances and neighbouring vibrational-rotational lines.

5.4 Results and Discussion

With use of the spectrometer described above, CARS spectra of separate lines of the ν_2 Q-branch were obtained at room temperature for pure acetylene pressures from 5-160 Torr. The spectra shown in Figure 5-1 for 5 and 130 Torr pressure demonstrate the transformation of the line shapes with increase of density of pure acetylene gas.
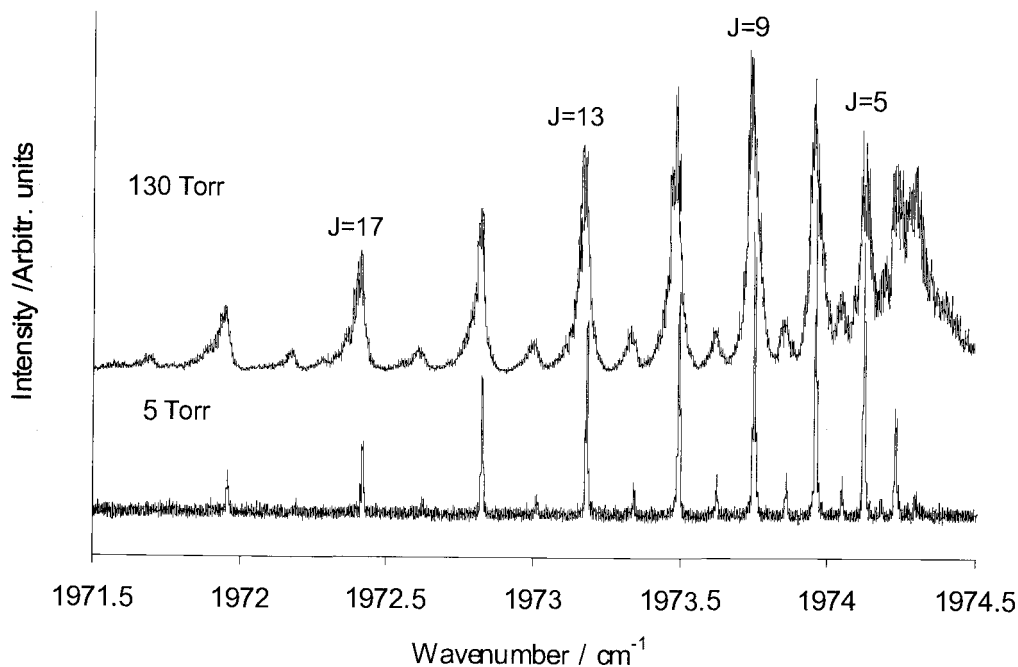
Figure 5-1 Examples of experimental CARS spectra of acetylene at room temperature.

To examine the effect of density on linewidth and position, measurements were made for the more intense and well-resolved odd-J lines from J = 7 up to J = 15. As an example, an experimental spectrum for the J = 7 Q-branch line of acetylene at 5 Torr is given in Figure 5-2. Also shown is the best fit curve calculated for a Lorentzian half-width of 0.0020 cm^{-1} convoluted by a single Gaussian, taken as 0.00304 cm^{-1} (the rms value of the Doppler (0.0030 cm^{-1}) and instrumental (0.0005 cm^{-1}) half-widths). The (small) interference contributions of all other transitions were included in the sum of Equation (5.1) and χ^{NR} and an experimental baseline were also varied for best least squares fit.
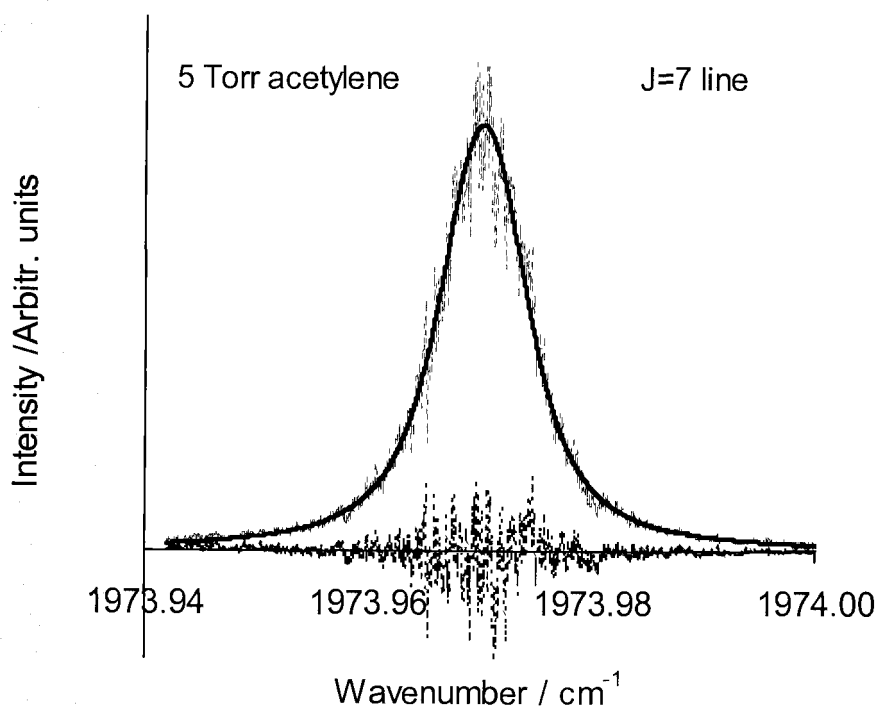
Figure 5-2 Shape of the Q-branch line J = 7 in the CARS spectrum of acetylene at 5 Torr. The obs. − calc. residual is shown at the bottom; as for any CARS spectrum, the absolute value of the noise is greatest when the CARS signal is strongest.

It is noteworthy that, even at this low pressure, the total half-width was well in excess of the Doppler width and, indeed, no decrease in linewidth was seen as the pressure was increased. In the process of fitting spectra of other lines at different pressures, there were further suggestions that the Gaussian component was larger than expected and that perhaps the instrumental contribution was underestimated due to saturation of ac-Stark broadening caused by the high laser intensities at the focal volume of the sample. This was examined experimentally for one of the narrowest lines, Q_{15} of acetylene, at 5 Torr and Figure 5-3 shows the half-width variation for (total) green pulse energies from 2 to 16 mJ per pulse.
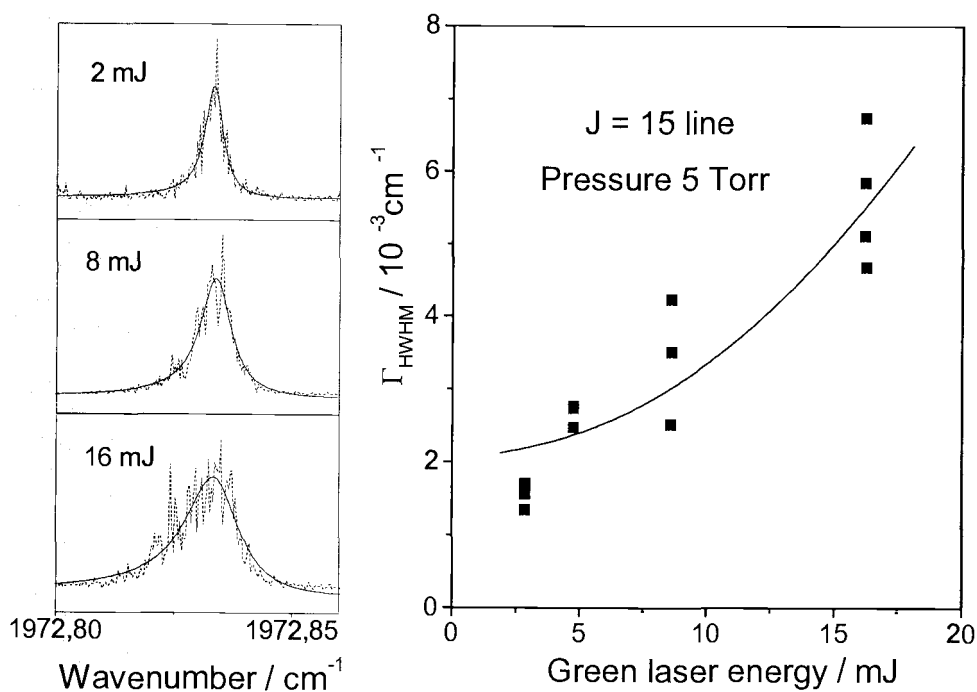
Figure 5-3. Spectrum of individual J=15 line showing saturation effects at different green laser energies (left). The transition maximum at low pressure and laser energy is 1972.833 cm^{-1}. Directly measured linewidth versus green laser energy is shown to the right. The energy of red laser was kept at 0.3 mJ.

As seen in the figure, over this energy range the half-width of this line varied from 0.0024 to 0.0060 cm^{-1}; at 8 mJ green pulse energy the observed half-width increase over the extrapolated zero energy value was about 0.001 cm^{-1}. These observations are in reasonable accord with estimates of saturation and Stark-effect broadening made as described in the literature (*89 – 92*). Under the conditions of our experiments, where the width of 532 nm laser pulse was 40 ns and the focusing length was 300 mm, the corresponding intensities were 10 GW/cm^2 for 8 mJ green laser energy and 0.4 GW/cm^2 for 0.3 mJ red laser energy. For these intensities we calculate that saturation broadening would increase the half-width by 0.0025 cm^{-1}, a value somewhat larger than that measured. A calculation for Stark broadening indicates that the corresponding half-width increase would be 0.001 cm^{-1}. These estimates show that the broadening is primarily due to saturation and they predict a half-width increase from 0.0007 to 0.005 cm^{-1} as the green pulse energy ranges from 2 to 16 mJ. It should be noted that these results of experimental and calculated broadening are in a good agreement with CARS studies of saturation broadening in C_2H_2 by Duncan et al. (*93*).

From the above considerations, it was concluded that some extent of saturation occurred for most of the linewidth experiments, where the energy of green pump laser was about 4-5 mJ and that of the red Stokes laser was 0.3 mJ. This saturation will depend on laser amplitude fluctuations and on spatial jitter in the beam overlap, variables which are difficult to control. It will have greatest effect at low pressures and, at a given power, the saturation contribution would decrease with density according to the relation

$$\Gamma_{HWHM} \cong kN\left[1 + \frac{G}{(kN)^2}\right] \tag{5.7}$$

where $k = d\Gamma/dN$, G is the saturation parameter (*89*), and N is the gaseous density.

Although this saturation effect prevented the detection of motional narrowing at low densities, accurate line broadening and line shift coefficients were determinable from the higher density measurements. For this purpose, a simplified lineshape analysis procedure was adopted in which the best effective Gaussian half-width, representing both Doppler and all instrumental contributions, was determined for a series of pressure measurements for each line. The saturation contribution was assumed to have the density dependence shown in Equation (5.3). At the first step the experimental contour was fitted as a Lorentzian shape with nonresonant background and baseline varied for best fit. This width was taken as the "experimental" width but it is clear that this fitting procedure becomes incorrect at low pressures where a Voigt profile is expected. Accordingly, this was taken into account by introducing the simplified Voigt formula:

$$\Gamma = \sqrt{\Gamma_L^2 A(\Gamma_G + B(\Gamma_G)} \tag{5.8}$$

where $A(\Gamma_G)$ and $B(\Gamma_G)$ are functions of Gaussian parameter Γ_G determined from modeling of Voigt profiles. In these model calculations, it was found that this procedure served to determine the Γ parameters with sufficient accuracy (2-3 %).

Using this relation and an assumed linear dependence with density of the Lorentzian contribution, for each pressure series a single limiting Γ_G for zero pressure was obtained. As illustration, Figure 5-4a shows the resultant fit for the J = 9 line.
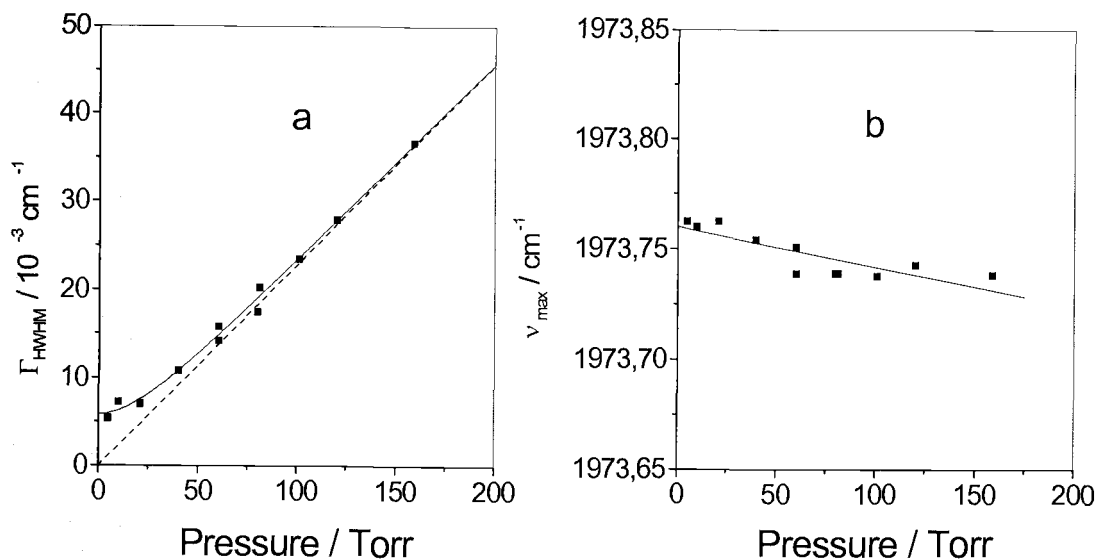
Figure 5-4. Pressure dependencies of linewidth (a) and line shift (b) for J=9.
a) Symbols - directly measured Γ_{HWHM} ; Solid line – fit of data taking into account nonresonant background, Lorentzian (collisional broadening) contribution and Gaussian (Doppler broadening and instrument function) contribution; dashed line - Lorentzian contribution Γ_r, caused by rotationally inelastic collisions . Corresponding broadening coefficient is $k_{J=9}= d\Gamma/dp = -21.6 \times 10^{-5}$ $cm^{-1}/Torr$. b) Symbols - positions of line maxima; solid line – fit of data assuming a linear dependence on pressure. Corresponding shift coefficient is $\delta_{J=9} = dv_J/dp = -18 \times 10^{-5}$ $cm^{-1}/Torr$.

Displayed are the directly measured half-widths (symbols), the approximation of the data obtained using the above-described procedure (solid line) and the deduced homogeneous Lorentzian half-widths (dashed line) at various pressures. Taking the Doppler half-width as 0.003 cm^{-1}, the fitted parameter Γ_G = 0.0045 cm^{-1} implies an instrumental contribution of 0.0033 cm^{-1}, significantly larger than the 0.0005 cm^{-1} seen

for this CARS spectrometer in other studies but consistent with the saturation discussed above. It should be noted that there was some variation in Γ_G values obtained for different J-lines (0.0040 cm^{-1} for J=7, 0.0032 cm^{-1} for J=11 and 0.0038 cm^{-1} for J=15), variability that is attributed to slightly different laser powers and imaging conditions in each series of measurements. It is also seen that, within the scatter of the data of Figure 5-4a, the assumption of a linear increase with density for Γ_L is justified and the effect of Dicke narrowing is not apparent. The dominant broadening is believed to arise from rotationally inelastic collisions ($\sigma_{r+v} \approx \sigma_r$ in Equation. 5.1).

In the manner described above, the homogeneous Lorentzian contributions Γ_r were determined for lines J = 7-15 in the pressure range 5-160 Torr, yielding the pressure broadening coefficients k_J and tabulated in Table 5-1 shown in Figure 5-5.

Gas	J number	$d\Gamma_{r+v}/dN \cdot 10^3$ (cm^{-1}/amagat)	$\sigma_{r+v} \cdot 10^{16}$ (cm^2)	$\sigma_0 \cdot 10^{16}$ (cm^2)
C_2H_2	7	145	147	76
	9	164	166	
	11	137	139	
	13	130	132	
	15	121	122	
D_2	2	2.3	0.94	20
N_2	10-18	40	44	40

Table 5-1 Broadening coefficients and cross-sections.
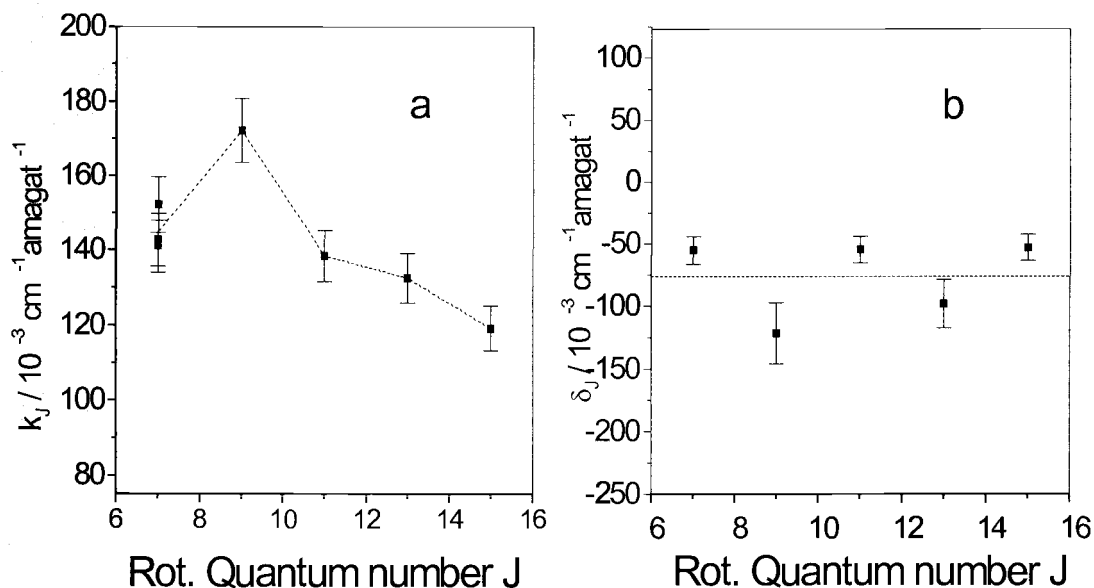
Figure 5-5 J-dependence of line broadening (a) and line shift (b) coefficient.
a) Symbols - collisional broadening coefficients; dashed line is just to connect experimental points.   b) Symbols - lineshift coefficients; dashed line represents "average" value for all measured lines $\langle\delta\rangle = -76 \times 10^{-3}$ cm^{-1} amagat^{-1}.

As seen for other molecules, the broadening coefficient decreases slightly for higher J lines, in accord with the lower probability of inelastic rotational relaxation as the rotational energy level spacing increases at high J.   The maximum occurs for J = 9, corresponding to the level calculated to have the greatest population at room temperature and to the Q-line of greatest intensity in Figure 5-1.   For J = 15, it may be noted that the cross section for rotational relaxation σ_r (obtained from our measured k_r = 121 cm^{-1}/amagat) is equal to 122 Å^2, somewhat larger than the gas-kinetic cross section σ_t = 76 Å^2 calculated from viscosity data.   It is this near equality of these cross sections that makes it difficult to observe Dicke narrowing for acetylene.   In contrast, in the case

of the D_2 molecule, where such narrowing is easily observed, σ_r (0.94 $Å^2$) (67) is 130 times smaller than for acetylene whereas $\sigma_t = 21$ $Å^2$ is only reduced by about a factor of four. It is also interesting that the value of σ_r for C_2H_2 is about three times that of N_2, indicating much more efficient rotational relaxation in the former molecule. In part this can be attributed to smaller rotational spacing ($B[C_2H_2]/B[N_2] = 0.59$) but this also may be a consequence of a stronger intermolecular coupling due to hydrogen bonding between the terminal hydrogens and the π electrons of the triple bond.

The measurements also yielded frequency shifts of the maxima of the Q-branch lines, as illustrated for J=9 in Figure 5-4a. These shifts were all linear, within experimental error, and the line shift coefficients $\delta_J = d\nu_J/dp$ that were deduced are displayed in Figure5-4b. All δ_J are negative and, within the experimental uncertainty, no J dependence is apparent. The average value $<\delta_J> = -0.075$ cm^{-1}/amagat can be compared with similar J averages of -0.005 and -0.003 cm^{-1}/amagat reported for N_2 (77) and O_2 (78), respectively. The negative sign in each case is consistent with a weakening of the relevant bond due to the long-range attractive part of the intermolecular potential and the larger magnitude of the weakening for C_2H_2 is again a likely consequence of a hydrogen-bonding interaction.

Although absolute values of the Q transitions at zero pressure were not the focus of this work, it was found that the Q_0 band origin agreed within 0.01 cm^{-1} with that calculated from the parameters deduced from high resolution infrared data, as reported recently (88):

$$Q_J \text{ (cm}^{-1}) = 1974.3160 - 0.006181 \, J(J+1) + 6.7 \times 10^{-9} \, J^2(J+1)^2 \qquad (5.9)$$

This expression also reproduced the relative positions of all the measured odd J maxima to within ± 0.002 cm^{-1}.

5.5 Conclusion

Line broadening and shifts for odd lines $J = 7 \div 15$ of the ν_2 Q-branch of acetylene were investigated in the pressure range 5 to 160 Torr using high-resolution CARS-spectroscopy. Evidence was seen for power broadening of the lines at low pressures and the extent of this is in agreement with estimates for saturation effects. The Lorentzian linewidth contributions caused by rotationally inelastic collisions were separated from Doppler and instrumental contributions and the corresponding broadening coefficients for these lines were determined. The precision of the linewidth measurements (mostly limited by saturation broadening) did not permit distinction of motional narrowing caused by translational relaxation. The shifts of Q-line maxima with pressure were studied and the shift coefficients were determined.

6 CONCLUSIONS

This thesis has highlighted two of the major fundamental applications of high resolution spectroscopy; (a) the measurement of accurate frequencies of transitions and the determination of molecular parameters from these, and (b) the measurement of transition linewidths as a function of pressure and the elucidation of collisional mechanisms that produce line broadening.

In particular the study of sulfur trioxide gave unique spectral information on the v_1 mode through the use of CARS spectroscopy. Previous Raman spectral data on this mode for $^{32}S^{16}O_3$ was only at 5 cm^{-1} resolution; and our high resolution CARS measurements have improved this by a factor of 5000. Although expected to be a simple spectrum, in order to model it with moderate success it proved necessary to incorporate all the various esoteric sources of perturbations encountered in spectroscopy. Particular effort has been employed to model the spectrum of $^{32}S^{16}O_3$ since this is key to future analysis of data for the other isotopomers. The v_1 modes of all the symmetric isotopic forms were observed for the first time. This work has stimulated collaboration with several other groups to obtain high resolution infrared data in order to fill the gap in the existing body of knowledge for sulfur trioxide.

In future work additional information about the rovibrational parameters for the v_1 levels could be obtained from the IR data analysis of difference and sum bands such as $v_1 \pm v_2$ and $v_1 \pm v_4$. Such an effort has been initiated for $v_1 + v_2$ for $^{32}S^{16}O_3$, as discussed in chapter 4. For the difference bands, the transitions are expected to be weak and to occur in the midst of the v_2 and v_4 spectra, along with their hot bands. The major advantage of the difference band analysis is that there would be sufficient resolution to

unambiguously make assignments involving specific J, K levels that are common to the v_1 transitions. The sum bands v_1+v_2 and v_1+v_4 do not connect directly to the same v_1 levels, hence yield the v_1 rovibrational parameters only indirectly. However the bands occur in an uncluttered region and the band assignments appear to be more feasible as was demonstrated by the analysis of v_1+v_2. Further analysis effort on all these bands appears warranted.

The studies of the collisional linewidths of acetylene at low pressures have demonstrated that simple models can be used to understand the linewidth effects caused by collisions. Throughout this investigation, the strength and weaknesses of CARS as a routine analysis technique became apparent. Its strength lies in its ability to observe symmetric modes, which are often invisible in the IR, and its sensitivity in detecting species at low pressures. However its weakness lies in the fact that the CARS signals can saturate, leading to anomalous relative intensities, as well as power broadening effects, which in both cases, increase the linewidths of the transitions under investigation. This was a particular problem at low pressures where the linewidth is expected to be limited by its inherent Doppler width. Despite this, at higher pressures, we were able to obtain accurate line broadening coefficients for acetylene. This information adds to the body of knowledge on collisional broadening in polyatomic molecules, a significant contribution since most previous Raman linewidth studies (90 %) have been limited to studies of nonpolar diatomics such as hydrogen and nitrogen.

BIBLIOGRAPHY

1. J. W. Nibler and G. V. Knighten, in Raman Spectroscopy of Gases and Liquids, edited by A. Weber (Springer-Verlag, Berlin, Heidelberg, New York, 1979), Chap. 7.

2. J. W. Nibler and G. A. Pubanz, in Advances in Non-Linear Spectroscopy, edited by R. J. H. Clark and R. E. Hester (John Wiley & Sons Ltd., Chichester, 1988), Vol.15, Chap. 1.

3. D. M. Guthals, K. P. Gross and J. W. Nibler, *J. Chem. Phys.,* **70**, 2393-2398 (1979).

4. N. E. Triggs, M. Zahedi, J. W. Nibler, P. DeBarber, and J. J. Valentini, *J. Chem. Phys.*, **96**, 1822-1831 (1992).

5. K. W. Brown, N. H. Rich, and J. W. Nibler, *J. Mol. Spectrosc.*, **151**, 482-492 (1992).

6. K. H. Lee, K. W. Brown, N. E. Triggs, A. D. Richardson, N.H. Rich, and J. W. Nibler, *J. Chem. Phys.*, **98**, 10100-10101 (1993).

7. K. H. Lee, N. E. Triggs, and J. W. Nibler, *J. Phys. Chem.*, **98**, 4382-4388 (1994).

8. M. L. Orlov, J. F. Ogilvie and J. W. Nibler, *J. Mol. Spectrosc.*, **185**, 128-141 (1997).

9. S.-Y. Tang, and C. W. Brown, *J. Raman. Spectrosc.,* **3**, 387-390 (1975).

10. M. Leuchs, M. Crew, J. Harrison, M. F. Hineman and J. W. Nibler, *J. Chem. Phys.*, **105**, 4885-4888 (1996).

11. D. A. Greenhalgh, in Advances in Nonlinear Spectroscopy, edited by R.J.H. Clark and R.E. Hester (John Wiley & Sons Ltd., Chichester, 1988), Vol. 15, Chap. 5.

12. M. Péalat, J. P. Taran, and F. Moya, *Opt. Laser Technol.* **12**, 21 (1980).

13. J. W. Nibler, J. R. Mac Donald and A. B. Harvey, *Opt. Commun.*, **18**, 371-373 (1976).

14. G. Fanjoux, G. Millot, R. Saint-Loup, R. Chaux, and L. Rosenmann, *J.Chem. Phys.*, **101 (2)**, 1061-1071 (1994).

15. D. A. Russell and W. B. Roh, *J. Mol. Spectrosc.*, **124**, 240-242 (1987).

16. K. A. Vereschagin, V. V. Smirnov, E. t. H. Chrysostom and J. W. Nibler, *J. Raman Spectrosc.*, **31**, 719-723 (2000).

17. C. V. Raman and K. S. Krishnan, *Nature* **121**, 501 (1928).

18. A. Smekal, *Natusiss.* **11**, 873 (1923).

19. A. Weber, in Handbook on Vibrational Spectroscopy, (to be published).

20. A. C. Eckbreth, *Appl. Phys. Lett.* **32(7)**, 421-423 (1978).

21. G. Herzberg, "Molecular Spectra and Molecular Structure: Infrared and Raman Spectra of Polyatomic Molecules", Van Nostrand Co., Inc., Princeton, N. J. (1945).

22. E. B. Wilson, Jr., J. Decius, and P. C.Cross, "Molecular Vibrations", Dover, New York (1980).

23. P. F. Bernath, "Spectra of Atoms and Molecules", Oxford, New York (1995).

24. H. C. Allen Jr., and, P. C.Cross, "Molecular Vib-Rotors", John Wiley & Sons, Inc., New York (1963).

25. D. Papousek, and M. R. Aliev, "Molecular Vibrational-Rotational Spectra", Elsevier, Amsterdam (1982).

26. P. W. Schenk, and R. Steudel, "Inorganic Sulphur Chemistry" edited by G. Nickless, Elsevier, Amsterdam, (1968).

27. T. Moeller, "Inorganic Chemistry", John Wiley and Sons Inc., 1963.

28. H. von Gerding, W. J. Nijveld, and G. J. Muller, *Z. Physik Chem.* **B (35)**, 193-215 (1937).

29. H. von Gerding, and J. Lecomte, *Physica* **6**, 737-763 (1939).

30. S.-H. Jou., M.-Y. Shen, C.-H. Yu,, and Y.-P. Lee, *J. Chem. Phys.* **104(15)**, 5745-53 (1996).

31. V. B. Laptev, A. A. Makarov, L. M. Tumanova, and E. A. Ryabov, *Spectrochim. Acta, Part A*, **54A(3)**, 491-494 (1998).

32. R. W. Lovejoy, J. H. Colwell, D. F. Eggers, Jr., and G.D. Halsey, Jr., *J. Chem. Phys.*, **36(3)**, 612-17 (1962).

33. K. Von Stopperka,, *Z. Chem.*, **6**, 153-154 (1966).

34. V. E. Bondybey, and J. H. English, *J. Mol. Spectrosc.*, **109(2)**, 221-8 (1985) .

35. R. Bent, and W. R. Ladner, *Spectrochim. Acta*, **19**, 931-935 (1963).

36. B. Krakow, and R. C. Lord, *J. Chem. Phys.*, **44**, 3640 (1966).

37. R. K. Thomas, , and H. W. Thompson, *Proc. Roy. Soc.,Ser. A*, **314(1518)**, 329-39 (1969).

38. A. Kaldor, A. G. Maki, A. J. Dorney, and I. M. Mills, *J. Mol. Spectrosc.*, **45(2)**, 247-52 (1973).

39. J. Ortigoso, R. Escribano, A. G. Maki, *J. Mol. Spectrosc.*, **138(2)**, 602-13 (1989).

40. J. B. Milne, and A. Ruoff, *J. Mol. Spectrosc.*, **23(4)**, 408-15 (1967).

41. A. Kaldor, and A. G. Maki, *J. Mol. Struct.*, **15(1)**, 123-30 (1973).

42. N. F. Henfrey, and B. A. Thrush, *Chem. Phys. Lett.*, **102 (2-3)**, 135-8 (1983).

43. H. von Gerding, W. J. Nijveld, *Rec.Trav.Chim.*, **59**,1206-1219 (1940).

44. G. E. Walrafen, *J. Chem. Phys.*, **40(8)**, 2326-2341 (1964).

45. N. J. Brassington, H. G. M. Edwards, D. W. Farwell, D. A. Long, and H. R. Mansour, *J. Raman Spectrosc.*, **7(3)**, 154-7 (1978).

46. V. Meyer, D. H. Sutter, H. Dreizler, *Z. Naturforsch., A: Phys. Sci.*, **46(8)**, 710-14 (1991).

47. M. R. Aliev, and V. M. Mikhailov, *Opt. Spektrosk.*, **35(2)**, 251-9 (1973).

48. J. K. G.Watson, *J. Mol. Spectrosc.*, **40(3)**, 536-44 (1971).

49. J. Duncan, *J. Mol. Spectrosc.*, **60**, 225-238 (1976).

50. A. J. Dorney, A. R. Hoy, and I. M. Mills, *J. Mol. Spectrosc.*, **45(2)**, 253-60 (1973).

51. J. M. L. Martin, *Spectrochim. Acta, Part A*, **55A(3)**, 709-718 (1999).

52. E. B. Wilson Jr., and J. B. Howard, *J. Chem.Phys.*, **4**, 260-268 (1936).

53. J. K. G. Watson, *Mol. Phys.*, **15**, 479-490(1968).

54. I. M. Mills in Molecular Spectroscopy: Modern Research edited by Roa Narahari K., Mathews C.W. (Academic Press, New York 1972).

55. C. Di Lauro, and I. M. Mills, *J. Mol. Spectrosc.*, **21**, 386-413 (1966).

56. G. J. Cartwright, and I. M. Mills, J. *Mol. Spectrosc.*, **34(3)**, 415-39 (1970).

57. E. Fermi, *Z. Physik*, **71**, 250 (1931).

58. J. Pliva, *J. Mol. Spectrosc.*, **139**, 278-285 (1990).

59. S. Gerstenkern and P. Luc, *Atlas du Spectra d'Absorption de la Molecule d'Iode*, Centre National de la Recherche Scientifique, Paris, France, (1978).

60. G. L. Eesley, "Coherent Raman Spectroscopy", Pergammon Press, (1981).

61. K. H. Lee, Ph.D. Thesis, Oregon State University (1991).

62. B. P. Stoicheff, Ph.D. Thesis, University of Toronto (1950).

63. A.Weber (ed) Raman spectroscopy of Gases and Liquids, Vol. 11 Springer:Berlin, 1979.

64. L. Galatry, *Phys.Rev.*, **122**, 1218-1223 (1961).

65. S.G. Rautian and I.I. Sobel'man, *Usp.Fiz.Nauk* **90**, 209-236 (1966) [*Sov.Phys.Usph.* **9**, 701(1967).

66. L.A. Rahn, R.L. Farrow and G.J. Rosasco, *Phys.Rev A*, **v.43, N11,** 6075-6088 (1991).

67. D.N. Kozlov, V.V. Smirnov and S.Yu.Volkov, *Appl. Phys. B*, **B48(3)**, 273-283 (1989).

68. J.W. Forsman, J. Bonamy, D. Robert, J.P. Berger, R. Saint-Loup and H. Berger, *Phys.Rev.*, **A 52**, 2652-2663 (1995).

69. A.C. Eckbreth, *Laser Diagnostics for Combustion Temperature and Species* pp. 220 - 300, Abacus, Cambridge, Mass. (1988).

70. D.A. Greenhalgh Quantitative CARS spectroscopy. in *Advances in Nonlinear Spectroscopy,* ed. by R.J.H. Clark and R.E. Hester. John Wiley& Sons, Chichester, (1988).

71. N. Herlin, M. Lefebvre, M. Péalat, and J. Perrin: *J.Phys.Chem.* **96**, 7063-7072 (1992).

72. P. W. Anderson, Phys. Rev. **76**, 647-661 (1949).

73. M. Baranger, Phys. Rev. **111**, 481-493 (1958).

74. M. Baranger, Phys. Rev. **111**, 494-504 (1958).

75. M. Baranger, Phys. Rev. **112**, 855-865 (1958).

76. L. A. Rahn, R. E.Palmer, M. L. Koszykowski, and D.A. Greenhalgh, Chem. Phys. Lett., **133(3)**, 513-516 (1987).

77. L. Bonamy, J. Bonamy, J.; D. Robert, B. Lavorel, R. Saint-Loup, R. Chaux, J. Santos and H. Berger, *J. Chem. Phys.* **89**, 5568-5577 (1988).

78. G. Millot, R. Saint-Loup, J. Santos, R. Chaux, H. Berger, J. Bonamy, *J. Chem. Phys.,* **96,** 961-971 (1992).

79. P. M. Sinclair, J. W. Forsman, J. R. Drummond, and A.D. May, Phys. Rev. *A* **48**, 3030-3035 (1993).

80. R. L. Byer and M. A. Henesian : U.S. NTIS, AD Rep. P.20 (1977).

81. J. O. Bjarnason, B. S. Hudson and H.C. Andersen, *J. Chem. Phys.* **70**, 4130-4148 (1979).

82. A. Weber, "High resolution Raman studies of gases" in *The Raman Effect*, ed. by A. Anderson, V.2, 543, Dekker, New York (1973).

83. W. F. Murphy, W. Holzer and J. J. Berstein, *Appl. Spectroscopy*, **23**, 211-218 (1969).

84. P. Lallemand and P. Simova, *J.Mol.Spectrosc.* **26**, 262-276 (1968).

85. V.G. Cooper, A.D.May and B.K.Gupta, *Canad. J. Phys.* **48**, 725-729 (1970).

86. M.A. Henesian, L.A. Kulevsky and R.L. Byer, *Opt. Commun.* **18**, 225 (1976).

87. B.B. Krynetsky, L.A. Kulevsky, V.A. Mishin, A.M. Prokhorov, A.D. Savel'ev and V.V. Smirnov, *Opt.Commun.* **21**, 225-228 (1977).

88. Y. Kabbadj, M. Herman, G. Di Lonardo, L. Fusina and J.W.C. Johns, *J. Mol. Spectrosc.* **150**, 535-565 (1991).

89. D.N. Kozlov, V.V. Smirnov and V.I. Fabelinsky, *Dokl.Akad.Nauk.USSR*, **246**, 304-307 (1979) [*Soviet Phys. - Doklady* **24**, 369 (1979)].

90. L.A. Rahn, R.L. Farrow, M.L. Koszykowski and P.L Mattern, *Phys Rev.Letters,* **45**, 620-623 (1980).

91. A.M. Brodnikovsky, V.N. Zadkov, M.G. Karimov and N.I. Koroteev, *Opt. Spectrosk.* **54**, 385-388 (1983) [*Opt. Apectrosc.(USSR)* **54**, 227 (1983)].

92. M. Pealat, M. Lefevre, J.-P. Taran and P.L. Kelly, *Phys. Rev.,* **38,** 1948-1965 (1988).

93. M.D. Duncan, Oesterlin, F. Koenig and R.L. Byer: *Chem. Phys. Lett.* **80**, 253-256 (1981).

APPENDICES

APPENDIX A. MOLECULAR PARAMETERS REQUIRED TO FIT THE ν_1 MODE

Molecular Parameter		Value cm^{-1}	Std. Error	Vibrational State Identifiers									
C"	Const.(1)	1.73988143E-01	2.1E-08	0	1	2	0	0	0	0	0	0	0
B"	Const.(2)	3.48543351E-01	4.1E-08	1	1	0	0	0	0	0	0	0	0
-D"$_J$	Const.(3)	-3.10795707E-07	3.2E-11	2	1	0	0	0	0	0	0	0	0
-D"$_{JK}$	Const.(4)	5.49126798E-07	3.9E-11	1	1	2	0	0	0	0	0	0	0
-D"$_K$	Const.(5)	-2.56825239E-07	2.0E-11	0	1	4	0	0	0	0	0	0	0
H"$_J$	Const.(6)	6.72634462E-13	6.7E-15	3	1	0	0	0	0	0	0	0	0
H"$_{JK}$	Const.(7)	-2.63431391E-12	1.5E-14	2	1	2	0	0	0	0	0	0	0
H"$_{KJ}$	Const.(8)	3.26150320E-12	2.1E-14	1	1	4	0	0	0	0	0	0	0
H"$_K$	Const.(9)	-1.30104010E-12	1.4E-14	0	1	6	0	0	0	0	0	0	0
h"$_3$	Const.(10)	-1.26510254E-14	6.5E-16	0	1	21	0	0	0	0	0	0	0
ν_3	Const.(11)	1.39152024E+03	1.2E-05	0	2	0	0	0	1	0	0	0	0
Cζ'	Const.(12)	8.35292109E-02	1.7E-07	0	2	1	1	0	1	0	0	0	0
$\eta_{J'}$	Const.(13)	-1.82803344E-08	2.1E-10	0	2	3	1	0	1	0	0	0	0
$\eta_{K'}$	Const.(14)	6.37174111E-08	1.9E-10	1	2	1	1	0	1	0	0	0	0
η_{H9}'	Const.(15)	-4.05657510E-24		2	2	1	1	0	1	0	0	0	0
q$_{DJ}$	Const.(16)	6.84888331E-05	6.2E-08	0	2	0	0	0	1	2	2	0	0
q$_{HJ}$	Const.(17)	9.77579169E-10	4.0E-11	1	2	0	0	0	1	2	2	0	0
δq$_{J2}$	Const.(18)	4.82011116E-14	6.1E-15	2	2	0	0	0	1	2	2	0	0
h$_2$	Const.(19)	2.06332873E-09	3.4E-12	0	2	11	0	0	1	0	0	0	0
C'	Const.(20)	1.73388888E-01	2.9E-08	0	2	2	0	0	1	0	0	0	0
B'	Const.(21)	3.47412871E-01	4.8E-08	1	2	0	0	0	1	0	0	0	0
-D'$_J$	Const.(22)	-3.11234721E-07	3.4E-11	2	2	0	0	0	1	0	0	0	0
-D'$_{JK}$	Const.(23)	5.50002676E-07	4.6E-11	1	2	2	0	0	1	0	0	0	0
-D'$_K$	Const.(24)	-2.57290158E-07	2.6E-11	0	2	4	0	0	1	0	0	0	0
H'$_J$	Const.(25)	6.87534332E-13	6.5E-15	3	2	0	0	0	1	0	0	0	0
H'$_{JK}$	Const.(26)	-2.66936393E-12	1.5E-14	2	2	2	0	0	1	0	0	0	0
H'$_{KJ}$	Const.(27)	3.27143932E-12	2.3E-14	1	2	4	0	0	1	0	0	0	0
H'$_K$	Const.(28)	-1.29398871E-12	1.5E-14	0	2	6	0	0	1	0	0	0	0
ν_2	Const.(29)	4.97567732E+02	1.4E-05	0	3	0	0	0	0	0	0	0	0
C'	Const.(30)	1.74115969E-01	4.2E-08	0	3	2	0	0	0	0	0	0	0
B'	Const.(31)	3.48543351E-01		1	3	0	0	2	0	0	0	0	0
$-\alpha_{B2'}$	Const.(32)	7.99012524E-04	4.2E-06	1	3	0	0	0	0	0	0	0	0
-D'$_J$	Const.(33)	-3.12622623E-07	4.3E-11	2	3	0	0	0	0	0	0	0	0
-D'$_{JK}$	Const.(34)	5.51435202E-07	8.3E-11	1	3	2	0	0	0	0	0	0	0
-D'$_K$	Const.(35)	-2.57445582E-07	5.4E-11	0	3	4	0	0	0	0	0	0	0

Table A-1 Molecular Parameters required to fit ν_1.

	Molecular Parameter	Value cm^{-1}	Std. Error	Vibrational State Identifiers									
H'_J	Const.(36)	5.99887275E-13	8.2E-15	3	3	0	0	0	0	0	0	0	0
H'_{JK}	Const.(37)	-2.33635342E-12	2.3E-14	2	3	2	0	0	0	0	0	0	0
H'_{KJ}	Const.(38)	2.84054602E-12	3.0E-14	1	3	4	0	0	0	0	0	0	0
H'_K	Const.(39)	-1.10337365E-12	1.6E-14	0	3	6	0	0	0	0	0	0	0
h'_3	Const.(40)	1.93699264E-14	3.3E-15	0	3	21	0	0	0	0	0	0	0
ν_4	Const.(41)	5.30086423E+02	1.2E-05	0	3	0	0	0	1	0	0	0	0
B'	Const.(42)	1.73830873E-01	3.3E-08	0	3	2	0	0	1	0	0	0	0
C'	Const.(43)	3.48543351E-01		1	3	0	0	2	1	0	0	0	0
$-\alpha_{B4'}$	Const.(44)	-7.27695003E-05	2.1E-06	1	3	0	0	0	1	0	0	0	0
$-D'_J$	Const.(45)	-3.11891339E-07	4.4E-11	2	3	0	0	0	1	0	0	0	0
$-D'_{JK}$	Const.(46)	5.53001472E-07	7.1E-11	1	3	2	0	0	1	0	0	0	0
$-D'_K$	Const.(47)	-2.59665889E-07	4.1E-11	0	3	4	0	0	1	0	0	0	0
H'_J	Const.(48)	7.32584299E-13	9.5E-15	3	3	0	0	0	1	0	0	0	0
H'_{JK}	Const.(49)	-2.88254179E-12	2.5E-14	2	3	2	0	0	1	0	0	0	0
H'_{KJ}	Const.(50)	3.60449789E-12	3.0E-14	1	3	4	0	0	1	0	0	0	0
H'_K	Const.(51)	-1.45405128E-12	1.7E-14	0	3	6	0	0	1	0	0	0	0
q	Const.(52)	2.28337532E-04	2.1E-06	0	3	0	0	0	1	2	2	0	0
q_J	Const.(53)	-4.17546360E-21		1	3	0	0	0	1	2	2	0	0
$C\zeta'$	Const.(54)	-8.51962215E-02	9.1E-07	0	3	1	1	0	1	0	0	0	0
$\eta_{J'}$	Const.(55)	-8.92103951E-07	1.2E-08	1	3	1	1	0	1	0	0	0	0
$\eta_{K'}$	Const.(56)	8.55245802E-07	1.2E-08	0	3	3	1	0	1	0	0	0	0
$2^{1/2}B\zeta'$	Const.(57)	2.83508410E-01	1.2E-04	0	3	0	0	0	1	1	1	0	0
η_{BJ}'	Const.(58)	-7.04856273E-07	3.8E-09	1	3	0	0	0	1	1	1	0	0
η_{BK}'	Const.(59)	4.75342145E-07	1.4E-09	0	3	2	0	0	1	1	1	0	0
h'_2	Const.(60)	9.98992437E-11	1.0E-11	0	3	11	0	0	1	0	0	0	0
ν_1	Const.(61)	1.06451542E+03	1.3E-03	0	99	0	0	0	0	0	0	0	0
C'	Const.(62)	1.73988143E-01		0	99	2	0	1	0	0	0	0	0
$-\alpha_{C1'}$	Const.(63)	-3.73510211E-04	3.9E-06	0	99	2	0	0	0	0	0	0	0
B'	Const.(64)	3.4854335E-01		1	99	0	0	2	0	0	0	0	0
$-\alpha_{B1'}$	Const.(65)	-7.33356233E-04	2.6E-06	1	99	0	0	0	0	0	0	0	0
$-D'_J$	Const.(66)	-3.84094561E-07	1.5E-09	2	99	0	0	0	0	0	0	0	0
$-D'_{JK}$	Const.(67)	6.71330210E-07	3.3E-09	1	99	2	0	0	0	0	0	0	0
$-D'_K$	Const.(68)	-3.12694236E-07	1.9E-09	0	99	4	0	0	0	0	0	0	0
H'_J	Const.(69)	6.77123010E-13		3	99	0	0	0	0	0	0	0	0
H'_{JK}	Const.(70)	-2.63651690E-12		2	99	2	0	0	0	0	0	0	0
H'_{KJ}	Const.(71)	3.24996000E-12		1	99	4	0	0	0	0	0	0	0
H'_K	Const.(72)	-1.28773830E-12		0	99	6	0	0	0	0	0	0	0
$\frac{1}{2}k_{144}$	Const.(73)	-1.46516E+00	1.9E-03	0	99	0	0	0	0	0	0	0	1

Table A-1 (Cont'd) Molecular Parameters required to fit ν_1.

Molecular Parameter		Value cm^{-1}	Std. Error	Vibrational State Identifiers									
$k_{144K'}$	Const.(74)	1.733074E-15		0	99	2	0	0	0	0	0	0	1
$k_{144J'}$	Const.(75)	-3.204548E-07	1.0E-06	1	99	0	0	0	0	0	0	0	1
$\frac{1}{2}k_{122}$	Const.(76)	1.135000E+01		0	99	0	0	0	0	0	0	0	3
$k_{122K'}$	Const.(77)	1.630434E-05	1.3E-05	0	99	2	0	0	0	0	0	0	3
q	Const.(78)	-2.71097E-05	7.2E-07	0	99	0	0	0	0	2	2	0	1
ν_1 $2\nu_4(l=0)$ -	Const.(79)	1.064515E+03		0	99	0	0	61	0	0	0	1	0
ν_1	Const.(80)	-4.72757E+00	1.9E-03	0	99	0	0	0	0	0	0	1	0
C'	Const.(81)	1.736694E-01	4.8E-07	0	99	2	0	0	0	0	0	1	0
B'	Const.(82)	3.486568E-01	2.3E-06	1	99	0	0	0	0	0	0	1	0
$-\alpha B_4'$	Const.(83)	-7.27695E-05		1	99	0	0	44	0	0	0	1	0
$-\alpha B_4'$	Const.(84)	-7.27695E-05		1	99	0	0	44	0	0	0	1	0
$-D'_J$	Const.(85)	-3.19799E-07	3.4E-10	2	99	0	0	0	0	0	0	1	0
$-D'_{JK}$	Const.(86)	5.647200E-07	6.1E-10	1	99	2	0	0	0	0	0	1	0
$-D'_K$	Const.(87)	-2.62889E-07	3.6E-10	0	99	4	0	0	0	0	0	1	0
H'_J	Const.(88)	8.784673E-13	1.4E-13	3	99	0	0	0	0	0	0	1	0
H'_{JK}	Const.(89)	-5.47673E-12	4.6E-13	2	99	2	0	0	0	0	0	1	0
H'_{KJ}	Const.(90)	9.527199E-12	5.0E-13	1	99	4	0	0	0	0	0	1	0
H'_K	Const.(91)	-5.06744E-12	1.8E-13	0	99	6	0	0	0	0	0	1	0
q	Const.(92)	2.371400E-04	3.3E-06	0	99	0	0	0	0	2	2	1	0
c_{44}	Const.(93)	1.575765E-08	3.7E-10	0	99	0	0	0	0	4	4	1	0
$B\zeta'$	Const.(94)	2.809795E-01	1.3E-04	0	99	0	0	0	0	1	1	1	1
η_{BJ}'	Const.(95)	-8.04249E-08	1.2E-08	1	99	0	0	0	0	1	1	1	1
η_{BK}'	Const.(96)	1.703543E-17		0	99	2	0	0	0	1	1	1	1
ν_1 $2\nu_4(l=0)$ -	Const.(97)	1.064515E+03		0	99	0	0	61	2	0	0	1	0
ν_1 $\delta(2\nu_4$	Const.(98)	-4.72757E+00		0	99	0	0	80	2	0	0	1	0
$(l=2))$ -$\nu_1)$	Const.(99)	6.648380E-01	8.3E-04	0	99	0	0	0	2	0	0	1	0
$C\zeta'$	Const.(100)	-8.50528E-02	1.1E-06	0	99	1	1	0	2	0	0	1	0
$\eta_{J'}$	Const.(101)	5.384242E-07	1.2E-08	0	99	3	1	0	2	0	0	1	0
$\eta_{K'}$	Const.(102)	-5.780948E-07	1.2E-08	1	99	1	1	0	2	0	0	1	0
C'	Const.(103)	1.736723E-01	9.1E-08	0	99	2	0	0	2	0	0	1	0
B'	Const.(104)	3.486529E-01	2.4E-06	1	99	0	0	0	2	0	0	1	0
$-\alpha_{B4}'$	Const.(105)	-7.276950E-05		1	99	0	0	44	2	0	0	1	0
$-\alpha_{B4}'$	Const.(106)	-7.276950E-05		1	99	0	0	44	2	0	0	1	0
$-D'_J$	Const.(107)	-3.197987E-07		2	99	0	0	85	2	0	0	1	0
$-D'_{JK}$	Const.(108)	5.6471999E-0		1	99	2	0	86	2	0	0	1	0
$-D'_K$	Const.(109)	-2.6288945E-0		0	99	4	0	87	2	0	0	1	0
H'_J	Const.(110)	8.784674E-13		3	99	0	0	88	2	0	0	1	0

Table A-1 (Cont'd) Molecular Parameters required to fit ν_1.

Molecular Parameter		Value cm^{-1}	Std Error	Vibrational State Identifiers									
H'$_{JK}$	Const.(111)	-5.476729E-12		2	99	2	0	89	2	0	0	1	0
H'$_{KJ}$	Const.(112)	9.527199E-12		1	99	4	0	90	2	0	0	1	0
H'$_K$	Const.(113)	-5.067435E-12		0	99	6	0	91	2	0	0	1	0
h$_4$	Const.(114)	-1.343517E-06	1.5E-07	0	99	31	0	0	2	0	0	1	0
q	Const.(115)	1.950719E-04	2.0E-06	0	99	0	0	0	1	2	2	2	0
$\nu_2+\nu_4$	Const.(116)	1.0279023E+03	2.1E-05	0	99	0	0	0	1	0	0	2	0
Cζ'	Const.(117)	-8.4875691E-02	2.9E-06	0	99	1	1	0	1	0	0	2	0
$\eta_{J'}$	Const.(118)	-8.9506825E-07	1.2E-08	1	99	1	1	0	1	0	0	2	0
$\eta_{K'}$	Const.(119)	8.55245802E-07		0	99	3	1	56	1	0	0	2	0
C'	Const.(120)	1.73958647E-01	9.8E-08	0	99	2	0	0	1	0	0	2	0
B'	Const.(121)	3.48460853E-01	2.5E-06	1	99	0	0	0	1	0	0	2	0
$-\alpha_{B4'}$	Const.(122)	-7.2769500E-05		1	99	0	0	44	1	0	0	2	0
$-\alpha_{B2'}$	Const.(123)	7.99012524E-04		1	99	0	0	32	1	0	0	2	0
-D'$_J$	Const.(124)	-2.9603132E-07	4.9E-10	2	99	0	0	0	1	0	0	2	0
-D'$_{JK}$	Const.(125)	5.20548151E-07	7.2E-10	1	99	2	0	0	1	0	0	2	0
-D'$_K$	Const.(126)	-2.4312932E-07	3.2E-10	0	99	4	0	0	1	0	0	2	0
Bζ'	Const.(127)	2.82591637E-01	1.3E-04	0	99	0	0	0	1	1	1	2	1
η_{BJ}'	Const.(128)	-5.6811328E-07	1.2E-08	1	99	0	0	0	1	1	1	2	1
η_{BK}'	Const.(129)	4.75342145E-07		0	99	2	0	59	1	1	1	2	1
H'$_J$	Const.(130)	1.73131300E-12	1.0E-13	3	99	0	0	0	1	0	0	2	0
H'$_{JK}$	Const.(131)	-4.1601582E-12	3.3E-13	2	99	2	0	0	1	0	0	2	0
H'$_{KJ}$	Const.(132)	2.69568138E-12	3.6E-13	1	99	4	0	0	1	0	0	2	0
H'$_K$	Const.(133)	-2.5463728E-13	1.3E-13	0	99	6	0	0	1	0	0	2	0
h'$_2$	Const.(134)	-3.7852042E-11	6.5E-11	0	99	11	0	0	1	0	0	2	0
2ν_2	Const.(135)	9.95448901E+02	4.9E-05	0	99	0	0	0	0	0	0	3	0
h'$_3$	Const.(136)	-5.0123640E-14	1.4E-14	0	99	21	0	0	0	0	0	3	0
C'	Const.(137)	1.74256751E-01	4.2E-06	0	99	2	0	0	0	0	0	3	0
B'	Const.(138)	3.48422194E-01	2.7E-06	1	99	0	0	0	0	0	0	3	0
$-\alpha_{B2'}$	Const.(139)	7.99012524E-04		1	99	0	0	32	0	0	0	3	0
$-\alpha_{B2'}$	Const.(140)	7.99012524E-04		1	99	0	0	32	0	0	0	3	0
-D'$_J$	Const.(141)	-3.0476172E-07	4.7E-10	2	99	0	0	0	0	0	0	3	0
-D'$_{JK}$	Const.(142)	5.38902662E-07	6.2E-10	1	99	2	0	0	0	0	0	3	0
-D'$_K$	Const.(143)	-2.5254097E-07	3.7E-10	0	99	4	0	0	0	0	0	3	0
H'$_J$	Const.(144)	-1.7862384E-12	7.1E-14	3	99	0	0	0	0	0	0	3	0
H'$_{JK}$	Const.(145)	4.58607038E-12	2.3E-13	2	99	2	0	0	0	0	0	3	0
H'$_{KJ}$	Const.(146)	-4.0048886E-12	2.9E-13	1	99	4	0	0	0	0	0	3	0
H'$_K$	Const.(147)	1.20064838E-12	1.4E-13	0	99	6	0	0	0	0	0	3	0

Table A-1 (Cont'd) Molecular Parameters required to fit ν_1.

APPENDIX B. MOLECULAR PARAMETERS REQUIRED TO FIT THE $\nu_1 + \nu_2$ MODE

Molecular Parameter		Value cm^{-1}	Std. Error	Vibrational State Identifiers									
C"	Const.(1)	1.739881E-01		0	1	2	0	0	0	0	0	0	0
B"	Const.(2)	3.485434E-01		1	1	0	0	0	0	0	0	0	0
-D"$_J$	Const.(3)	-3.108148E-07		2	1	0	0	0	0	0	0	0	0
-D"$_{JK}$	Const.(4)	5.491522E-07		1	1	2	0	0	0	0	0	0	0
-D"$_K$	Const.(5)	-2.568389E-07		0	1	4	0	0	0	0	0	0	0
H"$_J$	Const.(6)	6.771230E-13		3	1	0	0	0	0	0	0	0	0
H"$_{JK}$	Const.(7)	-2.636517E-12		2	1	2	0	0	0	0	0	0	0
H"$_{KJ}$	Const.(8)	3.249960E-12		1	1	4	0	0	0	0	0	0	0
H"$_K$	Const.(9)	-1.287738E-12		0	1	6	0	0	0	0	0	0	0
h"$_3$	Const.(10)	-1.264699E-14		0	1	21	0	0	0	0	0	0	0
q	Const.(11)	2.001897E-04		0	97	0	0	0	1	2	2	0	0
$\nu_1+\nu_4$	Const.(12)	1.591802E+03	1.38E-2	0	97	0	0	0	1	0	0	0	0
Cζ'	Const.(13)	-8.069662E-02	7.74E-4	0	97	1	1	0	1	0	0	0	0
$\eta_{J'}$	Const.(14)	-8.865765E-07		1	97	1	1	0	1	0	0	0	0
$\eta_{K'}$	Const.(15)	8.693766E-07		0	97	3	1	0	1	0	0	0	0
C'	Const.(16)	1.742600E-01	3.91E-5	0	97	2	0	0	1	0	0	0	0
B'	Const.(17)	3.484311E-01		1	97	0	0	0	1	0	0	0	0
-$\alpha_{B14'}$	Const.(18)	2.912194E-04	9.35E-5	1	97	0	0	0	1	0	0	0	0
-D'$_J$	Const.(19)	-2.956968E-07		2	97	0	0	0	1	0	0	0	0
-D'$_{JK}$	Const.(20)	5.206764E-07		1	97	2	0	0	1	0	0	0	0
-D'$_K$	Const.(21)	-2.435990E-07		0	97	4	0	0	1	0	0	0	0
$2^{\frac{1}{2}}$Bζ'	Const.(22)	2.696440E-01	2.83E-3	0	97	0	0	0	1	1	1	0	2
$\eta_{BJ'}$	Const.(23)	-6.678065E-07		1	97	0	0	0	1	1	1	0	2
$\eta_{BK'}$	Const.(24)	4.754928E-07		0	97	2	0	0	1	1	1	0	2
$\frac{1}{2}^{\frac{1}{2}}k_{144}$	Const.(25)	-2.113900		0	97	0	0	0	1	0	0	0	1
$\frac{1}{2}^{\frac{1}{2}}k_{144}$	Const.(26)	1.733074E-15		0	97	2	0	0	1	0	0	0	1
$\frac{1}{2}^{\frac{1}{2}}k_{144}$	Const.(27)	2.600400E-05		1	97	0	0	0	1	0	0	0	1
$\frac{1}{2}$k$_{122}$	Const.(28)	1.135000E+01		0	97	0	0	0	1	0	0	0	4
$\frac{1}{2}$k$_{122}$	Const.(29)	-1.600151E-04		0	97	2	0	0	1	0	0	0	4
H'$_J$	Const.(30)	1.943139E-12		3	97	0	0	0	1	0	0	0	0
H'$_{JK}$	Const.(31)	-5.723017E-12		2	97	2	0	0	1	0	0	0	0
H'$_{KJ}$	Const.(32)	5.305027E-12		1	97	4	0	0	1	0	0	0	0
H'$_K$	Const.(33)	-1.516646E-12		0	97	6	0	0	1	0	0	0	0
h'$_2$	Const.(34)	-6.048856E-11		0	97	11	0	0	1	0	0	0	0
3ν_4 *(l=0)*	Const.(35)	1.589792E+03		0	97	0	0	0	1	0	0	1	0

Table B-1 Molecular Parameters required to fit $\nu_1 + \nu_2$.

Molecular Parameter		Value cm^{-1}	Std. Error	Vibrational State Identifiers									
C'	Const.(36)	1.735119E-01		0	97	2	0	0	1	0	0	1	0
B'	Const.(37)	3.486873E-01		1	97	0	0	0	1	0	0	1	0
$-\alpha_{B4'}$	Const.(38)	-7.546076E-05	4.80E-5	1	97	0	0	0	1	0	0	1	0
$-\alpha_{B4'}$	Const.(39)	-7.546076E-05	-2.75E-5	1	97	0	0	0	1	0	0	1	0
$-\alpha_{B4'}$	Const.(40)	-7.546076E-05		1	97	0	0	0	1	0	0	1	0
$-D'_J$	Const.(41)	-3.191280E-07		2	97	0	0	0	1	0	0	1	0
$-D'_{JK}$	Const.(42)	5.633046E-07		1	97	2	0	0	1	0	0	1	0
$-D'_K$	Const.(43)	-2.623160E-07		0	97	4	0	0	1	0	0	1	0
H'_J	Const.(44)	5.023671E-13		3	97	0	0	0	1	0	0	1	0
H'_{JK}	Const.(45)	-3.440269E-12		2	97	2	0	0	1	0	0	1	0
H'_{KJ}	Const.(46)	6.237321E-12		1	97	4	0	0	1	0	0	1	0
H'_K	Const.(47)	-3.394162E-12		0	97	6	0	0	1	0	0	1	0
q	Const.(48)	2.137422E-04		0	97	0	0	0	1	2	2	1	0
C_{44}	Const.(49)	1.594398E-08		0	97	0	0	0	1	4	4	1	0
w_{11}	Const.(50)	2.802198E-04		0	97	0	0	0	1	1	1	1	1
$B\zeta'$	Const.(51)	2.822474E-01		0	97	0	0	0	1	1	1	1	2
$\eta_{BJ'}$	Const.(52)	-6.678065E-07		1	97	0	0	0	1	1	1	1	2
$\eta_{BK'}$	Const.(53)	4.754928E-07		0	97	2	0	0	1	1	1	1	2
$3\nu_4\, l=3$	Const.(54)	1.591099E+03		0	97	0	0	0	3	0	0	1	0
$C\zeta'$	Const.(55)	-8.492170E-02		0	97	1	1	0	3	0	0	1	0
$\eta_{J'}$	Const.(56)	4.618863E-07		0	97	3	1	0	3	0	0	1	0
$\eta_{K'}$	Const.(57)	-5.020339E-07		1	97	1	1	0	3	0	0	1	0
C·	Const.(58)	1.735119E-01		0	97	2	0	0	3	0	0	1	0
B'	Const.(59)	3.486766E-01		1	97	0	0	0	3	0	0	1	0
$-\alpha_{B4'}$	Const.(60)	-7.546076E-05		1	97	0	0	0	3	0	0	1	0
$-\alpha_{B4'}$	Const.(61)	-7.546076E-05		1	97	0	0	0	3	0	0	1	0
$-\alpha_{B4'}$	Const.(62)	-7.546076E-05		1	97	0	0	0	3	0	0	1	0
$-D'_J$	Const.(63)	-3.191280E-07		2	97	0	0	0	3	0	0	1	0
$-D'_{JK}$	Const.(64)	5.633046E-07		1	97	2	0	0	3	0	0	1	0
$-D'_K$	Const.(65)	-2.623160E-07		0	97	4	0	0	3	0	0	1	0
H'_J	Const.(66)	5.023671E-13		3	97	0	0	0	3	0	0	1	0
H'_{JK}	Const.(67)	-3.440269E-12		2	97	2	0	0	3	0	0	1	0
H'_{KJ}	Const.(68)	6.237321E-12		1	97	4	0	0	3	0	0	1	0
H'_K	Const.(69)	-3.394162E-12		0	97	6	0	0	3	0	0	1	0
h'_4	Const.(70)	-1.332837E-06		0	97	31	0	0	3	0	0	1	0
$\nu_1+\nu_2$	Const.(71)	1.559376E+03	7.22E-4	0	97	0	0	0	0	0	0	2	0
C'	Const.(72)	1.739881E-01		0	97	2	0	1	0	0	0	2	0
$-\alpha_{C12'}$	Const.(73)	-1.824798E-04	5.45E-6	0	97	2	0	0	0	0	0	2	0
B'	Const.(74)	3.485434E-01		1	97	0	0	2	0	0	0	2	0

Table B-1 (cont'd) Molecular Parameters required to fit $\nu_1+\nu_2$.

Molecular Parameter		Value cm^{-1}	Std. Error	Vibrational State Identifiers									
$-\alpha_{B12'}$	Const.(75)	-3.451160E-04	1.16E-4	1	97	0	0	0	0 0	0	2	0
$-D'_J$	Const.(76)	-3.721233E-07		2	97	0	0	0	0 0	0	2	0
$-D'_{JK}$	Const.(77)	7.157727E-07		1	97	2	0	0	0 0	0	2	0
$-D'_K$	Const.(78)	-3.645396E-07		0	97	4	0	0	0 0	0	2	0
H'_J	Const.(79)	6.771230E-13		3	97	0	0	0	0 0	0	2	0
H'_{JK}	Const.(80)	-2.636517E-12		2	97	2	0	0	0 0	0	2	0
H'_{KJ}	Const.(81)	3.249960E-12		1	97	4	0	0	0 0	0	2	0
H'_K	Const.(82)	-1.287738E-12		0	97	6	0	0	0 0	0	2	0
$\frac{1}{2}k_{144}$	Const.(83)	-1.494780		0	97	0	0	0	0 0	0	2	1
$k_{144K'}$	Const.(84)	1.733074E-15		0	97	2	0	0	0 0	0	2	1
$k_{144J'}$	Const.(85)	1.838802E-05		1	97	0	0	0	0 0	0	2	1
$\frac{1}{2}^{\frac{1}{2}}k_{122}$	Const.(86)	1.966000E+01		0	97	0	0	0	0 0	0	2	3
$k_{122K'}$	Const.(87)	-2.770000E-04		0	97	2	0	0	0 0	0	2	3
$2\nu_4+\nu_2$ ($l=0$)	Const.(88)	1.557767E+03	1.53E-2	0	97	0	0	0	0 0	0	3	0
C	Const.(89)	1.738017E-01		0	97	2	0	0	0 0	0	3	0
B'	Const.(90)	3.486873E-01		1	97	0	0	0	0 0	0	3	0
$-\alpha_{B4'}$	Const.(91)	-7.546076E-05		1	97	0	0	0	0 0	0	3	0
$-\alpha_{B4'}$	Const.(92)	-7.546076E-05		1	97	0	0	0	0 0	0	3	0
$-\alpha_{B2'}$	Const.(93)	7.609014E-04		1	97	0	0	0	0 0	0	3	0
$-D'_J$	Const.(94)	-3.191280E-07		2	97	0	0	0	0 0	0	3	0
$-D'_{JK}$	Const.(95)	5.633046E-07		1	97	2	0	0	0 0	0	3	0
$-D'_K$	Const.(96)	-2.623160E-07		0	97	4	0	0	0 0	0	3	0
H'_J	Const.(97)	5.023671E-13		3	97	0	0	0	0 0	0	3	0
H'_{JK}	Const.(98)	-3.440269E-12		2	97	2	0	0	0 0	0	3	0
H'_{KJ}	Const.(99)	6.237321E-12		1	97	4	0	0	0 0	0	3	0
H'_K	Const.(100)	-3.394162E-12		0	97	6	0	0	0 0	0	3	0
q	Const.(101)	2.137422E-04		0	97	0	0	0	0 2	2	3	0
C_{44}	Const.(102)	1.739881E-01		0	97	2	0	1	0 0	0	2	0
$B\zeta'$	Const.(103)	-1.824798E-04	5.45E-6	0	97	2	0	0	0 0	0	2	0
$\eta_{BJ'}$	Const.(104)	3.485434E-01		1	97	0	0	2	0 0	0	2	0
$\eta_{BK'}$	Const.(105)	-3.451160E-04	1.16E-4	1	97	0	0	0	0 0	0	2	0
$2\nu_4+\nu_2$ ($l=0$)	Const.(106)	1.557767E+03		0	97	0	0	88	2 0	0	3	0
$l=0$ - $l=2$	Const.(107)	6.540000E-01		0	97	0	0	0	2 0	0	3	0
$C\zeta'$	Const.(108)	-8.474820E-02		0	97	1	1	0	2 0	0	3	0
$\eta_{J'}$	Const.(109)	4.618863E-07		0	97	3	1	0	2 0	0	3	0
$\eta_{K'}$	Const.(110)	-5.020339E-07		1	97	1	1	0	2 0	0	3	0
C'	Const.(111)	1.738017E-01		0	97	2	0	0	2 0	0	3	0

Table B-1 (cont'd) Molecular Parameters required to fit $\nu_1+\nu_2$.

Molecular Parameter		Value cm^{-1}	Std. Error	Vibrational State Identifiers									
B'	Const.(112)	3.486766E-01	1	97	0	0	0	2	0	0	3	0
-αB_4'	Const.(113)	-7.546076E-05	1	97	0	0	0	2	0	0	3	0
-αB_4'	Const.(114)	-7.546076E-05	1	97	0	0	0	2	0	0	3	0
-αB_2'	Const.(115)	7.609014E-04	1	97	0	0	0	2	0	0	3	0
-D'$_J$	Const.(116)	-3.191280E-07	2	97	0	0	0	2	0	0	3	0
-D'$_{JK}$	Const.(117)	5.633046E-07	1	97	2	0	0	2	0	0	3	0
-D'$_K$	Const.(118)	-2.623160E-07	0	97	4	0	0	2	0	0	3	0
H'$_J$	Const.(119)	5.023671E-13	3	97	0	0	0	2	0	0	3	0
H'$_{JK}$	Const.(120)	-3.440269E-12	2	97	2	0	0	2	0	0	3	0
H'$_{KJ}$	Const.(121)	6.237321E-12	1	97	4	0	0	2	0	0	3	0
H'$_K$	Const.(122)	-3.394162E-12	0	97	6	0	0	2	0	0	3	0
h'$_4$	Const.(123)	-1.332837E-06	0	97	31	0	0	2	0	0	3	0
q	Const.(124)	2.001897E-04	0	97	0	0	0	1	2	2	4	0
$2v_2+v_4$ (l=1)	Const.(125)	1.526031E+03	0	97	0	0	0	1	0	0	4	0
Cζ'	Const.(126)	-8.457470E-02	0	97	1	1	0	1	0	0	4	0
$\eta_{J'}$	Const.(127)	-8.865765E-07	1	97	1	1	0	1	0	0	4	0
$\eta_{K'}$	Const.(128)	8.693766E-07	0	97	3	1	0	1	0	0	4	0
C'	Const.(129)	1.740456E-01	0	97	2	0	0	1	0	0	4	0
B'	Const.(130)	3.484311E-01	1	97	0	0	0	1	0	0	4	0
-αB_4'	Const.(131)	-7.546076E-05	1	97	0	0	0	1	0	0	4	0
-αB_2'	Const.(132)	7.609014E-04	1	97	0	0	0	1	0	0	4	0
-αB_2'	Const.(133)	7.609014E-04	1	97	0	0	0	1	0	0	4	0
-D'$_J$	Const.(134)	-2.956968E-07	2	97	0	0	0	1	0	0	4	0
-D'$_{JK}$	Const.(135)	5.206764E-07	1	97	2	0	0	1	0	0	4	0
-D'$_K$	Const.(136)	-2.435990E-07	0	97	4	0	0	1	0	0	4	0
Bζ'	Const.(137)	2.822474E-01	0	97	0	0	0	1	1	1	4	1
$\eta_{BJ'}$	Const.(138)	-6.678065E-07	1	97	0	0	0	1	1	1	4	1
$\eta_{BK'}$	Const.(139)	4.754928E-07	0	97	2	0	0	1	1	1	4	1
H'$_J$	Const.(140)	1.943139E-12	3	97	0	0	0	1	0	0	4	0
H'$_{JK}$	Const.(141)	-5.723017E-12	2	97	2	0	0	1	0	0	4	0
H'$_{KJ}$	Const.(142)	5.305027E-12	1	97	4	0	0	1	0	0	4	0
H'$_K$	Const.(143)	-1.516646E-12	0	97	6	0	0	1	0	0	4	0
h'$_2$	Const.(144)	-6.048856E-11	0	97	11	0	0	1	0	0	4	0
$3v_2$	Const.(145)	1.493641E+03	0	97	0	0	0	0	0	0	5	0
h'$_3$	Const.(146)	-4.492624E-14	0	97	21	0	0	0	0	0	5	0
C'	Const.(147)	1.743102E-01	0	97	2	0	0	0	0	0	5	0
B'	Const.(148)	3.485434E-01	1	97	0	0	0	0	0	0	5	0
-α_{B2}'	Const.(149)	7.609014E-04	1	97	0	0	0	0	0	0	5	0

Table B-1 (cont'd) Molecular Parameters required to fit $v_1+ v_2$.

Molecular Parameter		Value cm^{-1}	Std. Error	Vibrational State Identifiers									
-α_{B2}'	Const.(150)	7.609014E-04	1	97	0	0	0	0	0	0	5	0
-α_{B2}'	Const.(151)	7.609014E-04	1	97	0	0	0	0	0	0	5	0
-D_J'	Const.(152)	-3.068127E-07	2	97	0	0	0	0	0	0	5	0
-D_{JK}'	Const.(153)	5.505088E-07	1	97	2	0	0	0	0	0	5	0
-D_K'	Const.(154)	-2.622031E-07	0	97	4	0	0	0	0	0	5	0
H_J'	Const.(155)	3.787743E-13	3	97	0	0	0	0	0	0	5	0
H_{JK}'	Const.(156)	-2.795830E-12	2	97	2	0	0	0	0	0	5	0
H_{KJ}'	Const.(157)	4.530304E-12	1	97	4	0	0	0	0	0	5	0
H_K'	Const.(158)	-2.115103E-12	0	97	6	0	0	0	0	0	5	0

Table B-1 (cont'd) Molecular Parameters required to fit $\nu_1 + \nu_2$.